GLM Flash Data Trends during Tropical Cyclone Intensification Changes

by

David J. PeQueen, B.S.

A Thesis

In

Atmospheric Science

Submitted to the Graduate Faculty
of Texas Tech University in
Partial Fulfillment of
the Requirements for
the Degree of

MASTER OF SCIENCE

Approved

Eric C. Bruning
Chair of the Committee

Stephanie N. Stevenson

John L. Schroeder

Mark Sheridan
Dean of the Graduate School

December, 2021

ACKNOWLEDGMENTS

Completing my master's degree at Texas Tech would not have been possible without the support of my family, friends, and colleagues. I would like to specifically thank my advisor, Dr. Eric Bruning, for the extensive support, discussions, and feedback throughout my thesis work; my committee members, Dr. Stephanie Stevenson and Dr. John Schroeder, for both bringing their expertise to my Defense and making meaningful suggestions for improvement; my fellow Atmospheric Science students; my wife, Cynthia; my parents, Carol and Jeff; my brothers, Danny and Will; and the many, many unnamed people who have helped me to reach this milestone in my education.

TABLE OF CONTENTS

ACKNOWLEDGMENTS ……... ii

ABSTRACT …….. v

LIST OF TABLES……... vi

LIST OF FIGURES ……... vii

1. INTRODUCTION ……... 1

2. LITERATURE REVIEW ……... 5

a. Inner-Core Flashes Preceding or During Intensification ……..... 7

b. Inner-Core Flashes Preceding or During Weakening …… 11

c. Inner-Core Flashes Relative to the RMW ……..... 12

d. RMW Observations ……... 14

e. GLM Instrument ……..... 15

f. Synopsis …… 18

3. METHODOLOGY …… 19

4. RESULTS …… 26

a. Alvin (2019 ENP) …… 26

b. Barbara (2019 ENP) ……... 27

c. Erick (2019 ENP) …… 28

d. Juliette (2019 ENP) …… 29

e. Kiko (2019 ENP) …… 30

f. Lorena (2019 ENP) …… 32

g. Raymond (2019 ENP) …… 33

h. Alberto (2018 NA) …….. 34

i. Chris (2018 NA) …… 34

j. Michael (2018 NA) …….. 36

k. Barry (2019 NA) ……..... 37

l. Dorian (2019 NA) …… 38

m. Humberto (2019 NA) ……..…… 41

n. Jerry (2019 NA) …….. 42

o. Multi-Storm Analysis ……. 43

p. GLM Flash Characteristic Trends …… 56

5. CONCLUSIONS ……..... 60

REFERENCES ……... 64

APPENDIX …… 71

ABSTRACT

Using lightning as an indicator for tropical cyclone (TC) intensity change has been a subject of investigation for more than 25 years. While the general TC radial flash distribution is well-characterized in the literature, the position of inner-core lightning bursts (ICLB) relative to the radius of maximum wind (RMW) as an instructive factor in forecasting 24-hour storm intensity change is a recent development. The Geostationary Lightning Mapper (GLM) aboard the Geostationary Operational Environmental Satellite (GOES) has added continuous coverage of intracloud and cloud-to-ground flashes for tens of TCs in both the eastern north Pacific (ENP, observed by GOES-17) and north Atlantic (NA, observed by GOES-16) ocean basins. This analysis will provide an overview of 194 two-hour ICLB activity periods in non-landfalling conditions from 14 TCs (seven from 2018-2019 NA TCs; seven from 2019 ENP TCs) and explore the joint distribution of flash rate, area, and energy properties as a function of TC intensity change, radial distance, and time.

This GLM dataset supports several previous conclusions in the TC literature, including that NA TCs tend to have greater flash density than ENP TCs, weaker TCs tend to have more flashes than stronger TCs, the presence of an ICLB alone is not sufficient to inform intensity change forecasts, and lightning in any given TC is episodic. Interior to the RMW, ICLBs preceded an average 24-hour strengthening of +9.07 kts. Extending outside the RMW, ICLBs preceded a slight preference for 24-hour weakening between 1 and 1.5 RMW (-2.84 kt) and a stronger preference for 24-hour weakening beyond 1.5 RMW (-9.04 kt). Upcoming periods of rapid intensification were better predicted by the RMW relationship established in the literature than upcoming rapid weakening. Additionally, three TCs produced extended, long-duration (>15 hour) periods of nearly continuous flashes approximately at the RMW. Slight variations in the range of lightning during these times implies the potential to use lightning as another indicator of RMW variability.

LIST OF TABLES

4.1 Dorian Higher Precision Coordinates ……. 40

4.2 24-Hour Intensity Change Averages Following ICLB ……... 49

4.3 RI and RW Comparison to S18 …….. 52

LIST OF FIGURES

1.1 Stevenson et al. (2018) IC vs. r/RMW …… 13

3.1 Minimum Detected Energy: Barbara (2019) ……... 20

3.2 Minimum Detected Energy: Dorian (2019) …… 20

3.3 Minimum Detected Energy: Isaias (2020) …….. 21

3.4 Bahama Bar: Florence (2020) ……. 22

3.5 Dorian D-Values ……. 23

3.6 Dorian Wind Speed using D-Value as TC Center …….. 24

4.1 RMW Location vs. ICLB-TC Center Distance, All Periods …….. 45

4.2 RMW Location vs. ICLB-TC Center Distance, Modified Inner-Core ……... 46

4.3 ICLB Distribution Histograms …… 47

4.4 24-Hour Intensity Change vs. r/RMW, Strengthening / Weakening …….. 50

4.5 24-Hour Intensity Change vs. r/RMW, Continuous / Non-continuous …….. 52

4.6 24-Hour Intensity Change vs. r/RMW, NA / ENP ……. 54

4.7 24-Hour Intensity Change vs. r/RMW, Distance from TC Center ……. 55

4.8 24-Hour Intensity Change vs. r/RMW, Wind Speed …….. 56

A.1 Alvin Flashes, Distance from Center vs. Time ……... 72

A.2 Alvin Joint Histogram, AFA vs. FED ……. 73

A.3 Alvin Joint Histogram, AFA vs. TOE ……. 74

A.4 Barbara Flashes, Distance from Center vs. Time ……..... 75

A.5 Barbara Joint Histogram, AFA vs. FED ……. 76

A.6 Barbara Joint Histogram, AFA vs. TOE ……. 77

A.7 Erick Flashes, Distance from Center vs. Time ……..... 78

A.8 Erick Joint Histogram, AFA vs. FED ……. 79

A.9 Erick Joint Histogram, AFA vs. TOE ……. 80

A.10 Juliette Flashes, Distance from Center vs. Time ……. 81

A.11 Juliette Joint Histogram, AFA vs. FED …….. 82

A.12 Juliette Joint Histogram, AFA vs. TOE …….. 83
A.13 Kiko Flashes, Distance from Center vs. Time …… 84
A.14 Kiko Joint Histogram, AFA vs. FED …….. 85
A.15 Kiko Joint Histogram, AFA vs. TOE …….. 86
A.16 Lorena Flashes, Distance from Center vs. Time …… 87
A.17 Lorena Joint Histogram, AFA vs. FED ……... 88
A.18 Lorena Joint Histogram, AFA vs. TOE ……... 89
A.19 Raymond Flashes, Distance from Center vs. Time …… 90
A.20 Raymond Joint Histogram, AFA vs. FED …….. 91
A.21 Raymond Joint Histogram, AFA vs. TOE …….. 92
A.22 Alberto Flashes, Distance from Center vs. Time ……..... 93
A.23 Alberto Joint Histogram, AFA vs. FED …… 94
A.24 Alberto Joint Histogram, AFA vs. TOE …… 95
A.25 Chris Flashes, Distance from Center vs. Time ……... 96
A.26 Chris Joint Histogram, AFA vs. FED ……..... 97
A.27 Chris Joint Histogram, AFA vs. TOE ……..... 98
A.28 Michael Flashes, Distance from Center vs. Time ……... 99
A.29 Michael Joint Histogram, AFA vs. FED ……... 100
A.30 Michael Joint Histogram, AFA vs. TOE ……... 101
A.31 Barry Flashes, Distance from Center vs. Time …… 102
A.32 Barry Joint Histogram, AFA vs. FED ……... 103
A.33 Barry Joint Histogram, AFA vs. TOE ……... 104
A.34 Dorian (NHC) Flashes, Distance from Center vs. Time ……... 105
A.35 Dorian (NHC) Joint Histogram, AFA vs. FED …… 106
A.36 Dorian (NHC) Joint Histogram, AFA vs. TOE …… 107
A.37 Dorian (Non-NHC) Flashes, Distance from Center vs. Time ……... 108
A.38 Dorian (Non-NHC) Joint Histogram, AFA vs. FED …… 109
A.39 Dorian (Non-NHC) Joint Histogram, AFA vs. TOE …… 110

A.40 Humberto Flashes, Distance from Center vs. Time …….. 111

A.41 Humberto Joint Histogram, AFA vs. FED …… 112

A.42 Humberto Joint Histogram, AFA vs. TOE ……... 113

A.43 Jerry Flashes, Distance from Center vs. Time …….. 114

A.44 Jerry Joint Histogram, AFA vs. FED …… 115

A.45 Jerry Joint Histogram, AFA vs. TOE …… 116

CHAPTER 1

INTRODUCTION

The latest growth in available global lightning data has enabled atmospheric scientists to gain greater insight into many different types of atmospheric phenomena. Lightning in tropical cyclones (TCs), low-pressure systems with multi-day lifespans that can traverse thousands of kilometers, had traditionally only been observed with ground-based detection networks as a TC nears coastlines. The World Wide Lightning Location Network (WWLLN) advanced this detection capability to provide global coverage with very low-frequency (VLF, 3 – 30 kHz) electromagnetic pulse observations emitted by lightning discharges. The propagation path of VLF in the Earth-ionosphere waveguide permits long-range detection to have a range greater than 1000 km (Lay et al. 2007; Price et al. 2009). The recent rise of satellite-based detection networks has complemented this pioneering oceanic lightning detection capability with unprecedented spatiotemporal resolution of lightning within TCs from the earliest storm development, through peak intensity, and eventual weakening and dissipation. One of these new satellite-based instruments is the Geostationary Lightning Mapper (GLM) aboard two of the Geostationary Operational Environmental Satellite (GOES) series missions: GOES-16 (East, 75.2° W) and GOES-17 (West, 137.2° W) (Goodman et al. 2013; Rudlosky & Virts 2021).

While TC intensity forecasts have improved at a rate that is statistically significant in the 2000s (DeMaria et al. 2014), TC geographic tracks have consistently proven to be more reliably and accurately forecasted than future storm intensity. Numerous previous publications in the literature confirm that the general lightning

distribution in TCs, while episodic, is well understood. The TC lightning community focus has now primarily shifted to TC storm dynamics, physical insights into storm evolution, and the possibility of using lightning as a meaningful diagnostic tool in predicting TC intensification changes, in particular periods of rapid intensification (RI). Kaplan and DeMaria (2003) proposed a definition of RI based on the 95th percentile of all 24-hour over-water North Atlantic (NA) TC intensity changes from 1989 – 2000. This equates to a 30 kt (15.4 m s^{-1}) increase in maximum sustained wind speed over 24 hours. For the 163 TCs in their sample, these authors report that 63% of all hurricanes, 83% of all major hurricanes, and every Category 4 and 5 storm on the Saffir-Simpson Hurricane Wind Scale (SSHWS) underwent RI at least once in their lifespan, where SSHWS is a 1 to 5 scale that classifies a TC according to its maximum sustained wind speed. This 30 kt or greater wind speed increase in a 24-hour period has been adopted throughout the literature as the standard RI definition.

Conversely, the literature contains a few different definitions for over-water rapid weakening (RW). DeMaria et al. (2012) implemented a RW criterion of a 20 kt or greater decrease in 24 hours, and Xu et al. (2017) utilized a weaker RW limit of 15 kt or greater decrease. Wood and Ritchie (2015) took data from the Statistical Hurricane Intensity Prediction Scheme (SHIPS) archive covering more than three decades of TCs (1982 – 2013), excluding any time periods in which a TC underwent an eyewall replacement cycle, came within 50 km of a coastline, or became extratropical. They reported percentile intensity decreases for both the NA and eastern North Pacific (ENP) ocean basins for 25, 30, and 35 kt delineations. To align with the 95th percentile NA definition for RI, the RW definition was likewise chosen based on the NA intensity decrease at the

95th percentile. This work will use the Wood and Ritchie (2015) selection of a 30 kt or greater decrease in a 24-hour period as the RW definition.

Stevenson et al. (2018) utilized the ground-based WWLLN to conduct a 10-year survey, 2005 – 2014, over both the NA and ENP ocean basins. Their study identified that the radial position of TC inner-core lightning bursts (ICLBs) relative to the radius of maximum wind (RMW) frequently provided insight into the subsequent 24-hour intensity change of the storm. Here inner-core refers to the radial region within 100 km of the TC center, which is generally accepted as the standard throughout the literature, though Stevenson et al. (2016) suggests that 100 km may not be sufficient to capture all inner-core flashes for storms with large RMW, especially weaker TCs (tropical depressions and tropical storms). The RMW is measured through in-situ observations or remote sensing and is another approximate indicator of storm intensity, as it is generally larger in weaker TCs and contracts with intensification (Shapiro & Willoughby 1982; Willoughby 1990).

This study investigates if the ICLB position trend relative to the RMW is likewise detected in several GLM-observed TCs, utilizing storms measured by GOES-East and GOES-West in the NA basin in 2018-2019 and the ENP basin in 2019, respectively. This work will also analyze the major GLM-provided lightning statistics, including flash extent density (FED), average flash area (AFA), and total optical energy (TOE), for these TCs as a function of time, radial distance, and storm intensity change.

Chapter 2 of this work contains an overview of the current TC lightning literature that investigates changing TC storm intensity, RMW measurements, and more details about GLM. The focus of this investigation is to understand the usefulness of GLM signals for operational intelligence related to intensity change, rather than a direct

physical processes study. Chapter 3 contains a description of the methodology for storm analysis and RMW determination. Chapter 4 provides a summary of results obtained from the GLM data, beginning with storm-by-storm writeups, with more complete intensity information, RMW estimations, scatter plots of radial flash distribution, and flash statistic joint histograms provided in the Appendix. Chapter 5 summarizes the analysis and conclusions.

CHAPTER 2

LITERATURE REVIEW

Lightning is a high-current electrical discharge in the atmosphere. Thunderstorm flashes occur primarily within a cloud or from cloud-to-ground (DeMaria et al. 2012). In order to create a flash, there needs to be separate regions of opposite electrical charge. Many studies have investigated the mechanisms that create this charge transfer, but collisions between supercooled liquid water droplets and ice crystals are crucial in separating positive and negative ions. In thunderstorms, strong updrafts carry the positive charge to the top of the cloud, leaving the middle of the cloud negatively charged and a mixture of charges in the lower portion of the cloud (Ahrens 2013). In TCs, updraft strength is much weaker than in regular convective thunderstorms, rarely exceeding 10 m s^{-1} even for very intense TCs, and downdrafts are only 1-3 m s^{-1} (Jorgensen et al. 1985), which explains why inner-core TC lightning is somewhat rare.

Both satellite observations and Doppler radar imagery show that outbursts of intense eyewall convection are more common in intensifying TCs than in constant intensity cases (Steranka et al. 1986; Rogers et al. 2013). Cloud top heights are usually greatest in the TC eyewall (Jorgensen 1984). Griffin (2017) found that rapidly intensifying TCs have more overshooting tops than either slowly intensifying or constant intensity TCs.

Strong TCs will often undergo an eyewall replacement cycle that induces a pause in strengthening or begins TC weakening. Shapiro & Willoughby (1982) discussed the circularly symmetric, convective rings seen in strong TCs. This eyewall cycle occurs as the initial eyewall moves inward and a secondary eyewall forms outside of the first. This

secondary wind maximum contracts and replaces the previous eyewall, independently of the horizontal spatial scale in which it occurs (Willoughby et al. 1982).

Molinari et al. (1994) used the National Lightning Detection Network (NLDN) in one of the earliest studies on lightning in TCs. They studied the cloud-to-ground radial lightning distribution of NA basin Hurricane Andrew (1992). The NLDN observed three distinct periods of eyewall lightning within 40 km of the storm center, all occurring during periods of storm intensification, that lasted a few hours in duration and then ceased. This single system study was followed by Molinari et al. (1999), which examined NLDN data from four moderate strength or greater hurricanes and found that eyewall lightning outbreaks again occurred at the beginning of or during times of intensification.

The other major conclusion from Molinari et al. (1994, 1999) was the occurrence of three common regions of flash frequency radially distributed from the storm center. Their examination of nine NA TCs confirmed similar results to what occurred in Hurricane Andrew. Traveling outward from the storm center, the TC eyewall region contains a small maximum in flash count, followed by a distinct minimum in flash activity 80 – 100 km outside the eyewall, and finally a large maximum in the outer rainbands 210 – 290 km from the center.

Multiple subsequent studies agreed with these findings, though with some disparity in the reported distances. Abarca et al. (2011) distinguished between a narrower, more distinct region of weak activity between 60 – 120 km radii in hurricanes, with non-hurricane TCs exhibiting a broader 40 – 180 km range of fewer flashes. In contrast, Xu et al. (2017) found that eyewall flash density exceeded outer rainband flash density by a factor of three, and outer rainband flash density also exceeded the inner rainband flash

density by a factor of three. However, intensifying TCs were found to have substantially lower inner-core flash density than weakening and neutral TCs. Radial distance divisions were dependent on storm intensity, meaning stronger systems had more tightly contracted activity bands.

a. Inner-Core Flashes Preceding or During Intensification

Several studies have utilized WWLLN data to probe lightning activity in TCs. Price et al. (2009) collected data for all Category 4 and stronger TCs globally (58 TCs in total) over a three-year period, 2005 – 2007, and 56 of those TCs showed "statistically significant positive correlations between lightning activity and maximum sustained winds." The most common time from peak lightning activity to maximum winds, by both mean and median, was 30 hours for this dataset. However, DeMaria et al. (2012) noted that using a fixed lag between peak lightning activity and maximum winds, rather than an optimal lag, made the correlations not nearly as high.

Pan et al. (2010) limited their WWLLN domain to the northwest Pacific, in which seven super typhoons developed from 2005 to 2008. Each typhoon produced eyewall lightning several hours prior to or just before it reached maximum intensity. The authors noted that less than 1% of flashes occurred within 100 km of storm center for these TCs, which is a smaller ratio than NA basin storms, where Molinari et al. (1999) found 4.3% of flashes occurred within 80 km. Pan et al. (2010) found minimal or no lightning in the typhoon centers during weakening. Nearly all such flashes occurred while the TCs were still intensifying.

Pan et al. (2014) continued and expanded on their earlier study by considering WWLLN data for 69 typhoons over the northwest Pacific Ocean from 2005 to 2009, a subset from 133 TCs. In comparison to weak typhoons, the inner-core average lightning density for super typhoons was more than twice as large. However, both of these classifications exhibited the same near-monotonic decrease in flash density with radius, which agrees with the findings of DeMaria et al. (2012) in the NA and ENP basins. Note that averaging storms of all intensities together smooths out the apparent minimum in activity outside the eyewall that is visible when looking at an individual TC. Considering a similar time lag measurement as Price et al. (2009), Pan et al. (2014) found that lightning activity peaked before maximum wind intensity in 56% of weak typhoons and 78% of super typhoons, but with geometric mean lags of 30 hours for the super typhoons and a much longer 60 hours for weak typhoons. Accounting for the Price et al. (2009) critique from DeMaria et al. (2012) to use a fixed time lag, Pan et al. (2014) found that 37 of their 69 typhoons (54%) showed a positive correlation between flash and wind peaks (constant 24-hour lag).

Zhang et al. (2015) also looked at WWLLN data for TCs over the northwest Pacific Ocean from 2005 to 2009, a set of 116 TCs, finding that lightning density was greater in the inner-core for cases of RI than for cases of RW, which contrasts with the findings of DeMaria et al. (2012) for Atlantic basin storms. As DeMaria et al. (2012) described, strong sea surface temperature gradients could account for the different physical responses by TCs observed across the different basins, implying a single relationship between lightning activity and storm intensity change is unlikely to be sufficient for all locations.

WWLLN data was employed again with Abarca et al. (2011), which considered the 24 NA basin TCs that approached the continental United States within 400 km from 2004 – 2007. This group also made use of NLDN (high detection efficiency, limited coverage) to assess WWLLN's suitability for TC observations, since it was a network with low detection efficiency (preferentially detecting strokes with the largest peak currents) but greater oceanic coverage. Using a method proposed by Jacobson et al. (2006), the authors reported a strong spatial correlation that verifies the relevant lightning activity is well captured by WWLLN. For strong flashes in non-hurricanes, Abarca et al. (2011) reported the inner-core and outer band flash densities were comparable, whereas in hurricanes, the inner-core exhibited only half the flash density of the outer band. This distinction was not apparent for weaker WWLLN-observed flashes.

Another important study involving WWLLN that has been referenced already is DeMaria et al. (2012), which considered the flash densities and associated intensity changes of all NA and ENP TCs from 2005 – 2010. This work neatly summarized several of the general TC literature conclusions to date and included graphical comparisons of TC lightning activity between the NA and ENP basins. Broadly, DeMaria et al. (2012) found that average lightning density decreases with increasing distance from the storm center, weaker TCs tend to have more lightning than stronger TCs, intensifying TCs tend to have greater lightning density than weakening TCs, and lightning in any given TC is episodic. In the cross-basin comparisons, NA TCs exhibited nearly twice the flash density of ENP TCs.

Fierro et al. (2018) used early GLM data to probe Hurricane Maria, a 2017 NA basin storm that underwent RI and reached Category 5 status on the SSHWS. Maria had

an increase in inner-core flashes near the end of the original phase of intensification. A land interaction with the island of Barbuda led to a brief 6-hour interval of TC weakening and increased lightning activity, but Maria quickly restrengthened to a Category 5, during which time inner-core flashes continued but were most prominent early before noticeably declining. The storm then gradually weakened, during which time the inner-core lightning virtually ceased and outer region flashes rapidly increased. Despite a concern for location errors in the provisional GLM data of an average 17 km for the domain considered, all of these described inner-core flashes occurred within 50 km of the TC center.

Zawislak et al. (2016) conducted a thorough investigation into the 2014 NA basin storm Edouard, including the use of WWLLN data. The lightning time series indicated deep convective pulses with a burst of inner-core flashes around 0000 UTC 13 September, which preceded a period of intensification.

Stevenson et al. (2014) examined WWLLN data of 2010 NA basin storm Earl, which underwent RI after an ICLB interior to the RMW. With microwave and lightning data for the same storm, Susca-Lopata et al. (2015) estimated the radial distribution of intense convection and found it preferentially within the 8 km altitude RMW during RI. They did, however, note some ambiguity with the location of intense convection relative to the 2 km altitude RMW, especially when Earl was vertically misaligned early in its development.

b. Inner-Core Flashes Preceding or During Weakening

There are several examples of TC studies that seem to contrast with the general inner-core lightning implications discussed so far. From WWLLN observations of 2005 NA TCs Emily, Katrina, and Rita, Thomas et al. (2010) found that the relative number of positive cloud-to-ground (CG) flashes in the inner-core increased prior to and during TC weakening.

Using Tropical Rainfall Measuring Mission (TRMM) data from 1997 to 2008, Jiang and Ramirez (2013) determined the values of several parameters necessary for RI to occur, including total volumetric rain, near-surface radar reflectivity, and brightness temperatures. In their dataset, only 7% of RI storms produced lightning in the inner-core, less than the other intensity change categories. The reverse relationship was seen in the outer rainbands. 37% of TCs that underwent RI contained rainband flashes, contrasted with only 20% of weakening TCs.

Another important finding by DeMaria et al. (2012) was that spikes in inner-core lightning activity were often signals for the end of an intensification period. This team reported that NA TCs that underwent RW in the subsequent 24 hours had larger inner-core flash density than those that underwent RI. They hypothesized that this could be the result of two processes, depending on storm strength. For weaker TCs, the interaction between the vertical shear and storm circulation potential vorticity column could present as intense asymmetric convection. In stronger TCs, a secondary eyewall formation could account for the increase in inner-core flash density.

Xu et al. (2017) considered TRMM overpass storm data over six ocean basins (NA, ENP, northwest Pacific, southwest Pacific, northern Indian, and southern Indian)

from 1998-2013, keeping only the data where the TC center was greater than 100 km from the nearest coastline. Their study supported the conclusion of DeMaria et al. (2012), in which intensifying TCs had substantially lower inner-core flash density compared to steady-state and weakening TCs, with the magnitude change in flash density typically occurring 6-12 hours prior to weakening. Furthermore, of the intensifying systems, TCs that underwent RI had significantly smaller flash density (approximate factor of 2) than the non-RI intensifying storms. The inner-core flash density decrease for these TCs occurred 12-18 hours prior to the onset of RI.

Stevenson et al. (2016) focused on ENP and NA TCs observed by WWLLN from 2006-2014. For tropical depressions and tropical storms, the normalized flash density was greater in non-intensifying TCs than for intensifying TCs in both basins, but the differences were only statistically significant in the ENP. Weak hurricanes (Category 1 and 2) also showed larger flash densities in non-intensifying scenarios compared to changing intensity cases, at a statistically significant level in both basins. The relationship was in opposition for major hurricanes, but neither basin had a statistically significant result.

c. Inner-Core Flashes Relative to the RMW

Musgrave et al. (2012) used the geopotential tendency equation to illustrate that vortex intensification is dependent on the location of diabatic heating relative to the small and large Rossby length regions and therefore the RMW. Rossby length, or Rossby radius of deformation (Schubert & McNoldy 2010), refers to “the distance that cold pools of air can spread under the influence of the Coriolis force” (“Rossby radius” 2012). Deep

convection in a region of small Rossby length, which corresponds to locations inside the RMW, is critical to achieve RI. Radar studies support this result, such as the Corbosiero et al. (2005) evaluation of 1985 NA basin Hurricane Elena, which had deep convection become concentrated in the eyewall near the beginning of its RI phase. Rogers et al. (2013) found that intensifying TCs contain a larger number of convective bursts interior to the RMW, whereas steady-state storms generally have bursts exterior to the RMW.

Stevenson et al. (2016) hypothesized that higher flash densities in the inner-core can indicate either intensification or weakening, depending on the location of convection as indicated by lightning. Their theoretical proposal was that the RMW discriminates whether the lightning is occurring interior or exterior to the inertially stable core and therefore implies the sign of intensity change. This suggestion was solidified by the 10-

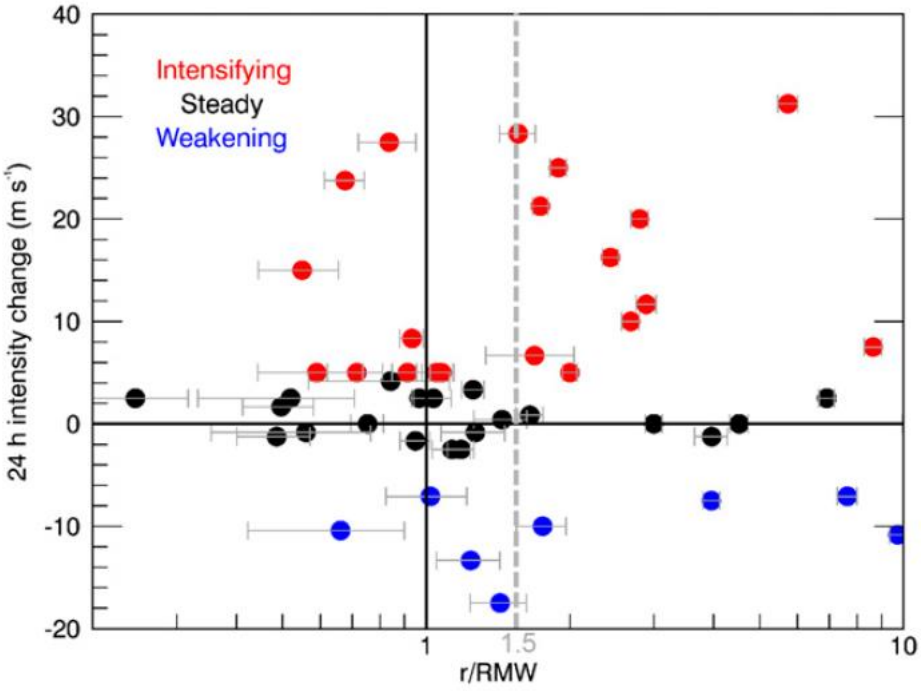

Figure 1.1. Stevenson et al. (2018) IC vs. r/RMW. Reproduced from Stevenson et al. (2018), their Figure 8. NA ICLBs are plotted as a function of their 24-hr forward intensity change and relative position with respect to the RMW. Note the apparent gap in intensifying TCs with an ICLB between 1 and 1.5 RMW.

year WWLLN survey over both the NA and ENP ocean basins conducted by Stevenson et al. (2018). As illustrated in Figure 1.1, their dataset indicated that ICLBs occurring between 1 and 1.5 multiples of the RMW tended to indicate steady-state or weakening TCs in the 24-hour period following the lightning burst, with an average change of -2.6 m s^{-1}, or -5.1 kts. When the ICLB occurred interior to the RMW, or beyond 1.5 RMW, the 24-hour intensity change was primarily intensification, with an average change of +5.3 m s^{-1}, or +10.3 kts. Stevenson et al. (2018) also noted a basin dependence, with the majority of ENP TCs remaining at or near constant intensity 24 hours following the ICLB, while the majority of NA TCs experienced intensification.

d. RMW Observations

The rate of RMW contraction during storm strengthening and relaxation during storm weakening remains an active area of research. Vigh (2010) found that RMW contraction often slowed down markedly around the time of eye formation. Stern and Nolan (2011) suggested that the initial size of the RMW has a greater impact on the time scale of contraction than on the final quasi-steady size. Generally, the rate of contraction decreased with increasing initial size. They also found that the large majority of contraction occurred prior to the large majority of intensification, and this finding was supported for major hurricanes with the idealized numerical simulations run by Stern et al. (2015). Another finding was for RMW contraction and TC intensification that began simultaneously, the RMW contraction ended well before peak intensity was reached (Stern et al. 2015).

Alternative methods to estimate the RMW in the absence of in-situ data have been considered. Kossin et al. (2007) took infrared satellite imagery and estimated the RMW through different methods depending on the definition of the TC eye. Lajoie and Walsh (2008) extended this work by adding microwave satellite imagery. Their technique is dependent on eye radius and distance from the TC center to the top of the most developed cumulonimbus. The effect of vertical wind shear on their RMW accuracy is not quantified, however. Knaff et al. (2015) developed an independent algorithm using operationally available information and produced a best-fit equation for a climatological RMW as a function of storm intensity and latitude. Knaff et al. (in press) suggested that the best source for RMW values would be co- and cross-polarized spaceborne synthetic aperture radars; however, their sporadic availability makes them impractical for most applications. High-frequency radiometers for large RMW cases and scatterometers for systems early in development are additional options (Knaff et al. in press).

e. GLM Instrument

Another new source of data available for observing TC deep convection and measuring lightning is NOAA's (National Oceanic and Atmospheric Administration) Geostationary Lightning Mapper. The GLM resides on two satellites and provides continual monitoring over the Americas and adjacent ocean regions, with overlapping regions of coverage in the central continental United States (Goodman et al. 2013). GOES-16 is located at 75.2° W, which covers the north Atlantic Ocean basin TC development (including the Gulf of Mexico), and GOES-17 is located at 137.2° W,

which covers the eastern north Pacific Ocean basin TC development (Rudlosky & Virts 2021). Latitudinal coverage extends to 54° N/S (Bruning et al. 2019).

The instrument detector is a variable pitch charge-coupled device, with an array of 1372 by 1300 pixels. The variable pitch keeps the ground distance sampled by each GLM pixel largely uniform across the field of view, growing from 8 km at nadir to approximately 14 km at the limb (GOES-R Series Program Office 2017, Rudlosky et al. 2019). Observations are made in a narrow (approximately 1 nm) spectral band in the near infrared, centered at the oxygen triplet at wavelength $\lambda = 777.4$ nm (Bruning et al. 2019). While the instrument does not distinguish between classifications, GLM observes both intracloud (IC) and cloud-to-ground (CG) flashes.

GLM data is reported as pixel-level triggers on a frame-by-frame basis (2 ms duration), where the instrument electronics detect the background brightness level and determine a threshold that pixels must surpass. Filters are also applied to remove false triggers caused by shot noise, ocean glint, blooming, and other artifacts (GOES-R Series Program Office 2019, Goodman et al. 2010, Rudlosky et al. 2019). A three-tier hierarchy is used to reconstruct flashes from these individual triggered pixels, which are called events. The second-tier classification are known as groups, which are the triggered pixels within a single frame immediately adjacent to each other. The third-tier arrives at a GLM flash, in which groups within 16.5 km and 330 ms (Goodman et al. 2010) in weighted Euclidean distance (Mach et al. 2007) are clustered together. For every event, group, and flash in this hierarchy, the dataset includes the location in latitude, longitude, and time information (start and end time for flashes, single time for events and groups). Identification numbers are assigned to each level of the hierarchy in order to move

between the three tiers. Reported physical parameters include optical energy, group area, and flash area (Bruning et al. 2019).

Quantifying detection efficiency (DE) for GLM across the field of view by factors such as geographic location, time of observation, and meteorological condition is important for data comparisons between detection networks. Zhang and Cummins (2020) checked a year of GLM data in a spatial domain over central Florida in order to study its detections relative to the Lightning Mapping Array (LMA) at Kennedy Space Center, which has well-characterized location uncertainty (Rison et al. 1999; Thomas et al. 2004). GLM recorded a daily mean flash DE of 73.8% relative to the LMA, with daily ranges from 51% to 98%. The average nighttime DE was 87.8%. Unexpectedly, GLM produced a higher DE for cloud-to-ground flashes (CGs) than for intracloud flashes (ICs). This could be attributed to optical signals from CGs typically having brighter and/or larger groups than ICs, since GLM DE increases with increasing flash duration and increasing flash area. Considering other geographic domains outside of Florida, flash DE can decrease substantially near the edges of the field of view. For instance, flash DE by GOES-16 in the northwest continental United States decreased substantially from flash DE in the eastern United States, Caribbean, and Atlantic Ocean (Cummins 2019). The same concept is applicable to GOES-17, which demonstrated lowered flash DE in the American Midwest and further eastward. Moving from the edge of the field of view closer to nadir, absolute flash DE stabilizes near 0.8 or greater for the Gulf of Mexico, Caribbean, and Atlantic Ocean basins in GOES-16 and near 0.7 for the ENP in GOES-17 (Cummins 2019).

f. Synopsis

In summary, the TC literature contains several established lightning trends that have been observed by multiple detection networks, covering both Atlantic and Pacific Ocean basins and storms of all intensity regimes. However, significant uncertainties remain in what inner-core flashes suggest about upcoming TC strengthening or weakening, as evidenced by the diverging intensity changes presented in Chapter 2.a. and 2.b. The hypothesis that ICLB position relative to the RMW as explored by Stevenson et al. (2018) suggests a solution to this conflict in the literature. GLM provides a new, continuous dataset that enables the study of over-water TCs to an unprecedented degree and can be used to evaluate this RMW relationship. However, practical challenges in obtaining high accuracy RMW measurements may constrict the clarity of such a result. Furthermore, different physical environments (e.g., sea surface temperature gradients) in the different ocean basins implies that a single relationship between lightning activity and storm intensity change is unlikely to be sufficient for all locations.

CHAPTER 3

METHODOLOGY

The open-source Python package *glmtools()* (Bruning 2019) is used to read and manipulate the raw GLM data (Bruning et al. 2019). This package constructs the GLM Level 2 (L2) data files (GOES-R Series Program Office 2017) into an event, group, and flash hierarchy and then provides the framework for coordinate transformations to turn the point locations into imagery. In this work, the data were gridded onto 2-kilometer pixels. Parallax was taken into account by assuming a cloud-top height and creating a lightning ellipsoid slightly larger than the ellipsoid representing Earth's mean sea level. See Bruning et al. (2019), Figure 5 for an illustration.

Important GLM flash parameters include Flash Extent Density (FED), which is a count of all flashes that passed through a particular geographic location (i.e., grid box) during some period of time (1 minute, 5 minutes, etc.) as first defined by Lojou and Cummins (2004). Average Flash Area (AFA) was introduced by Bruning and MacGorman (2013) and differentiates between less spatially extensive flashes, perhaps in a TC storm core, and more spatially extensive flashes, perhaps in TC rainband thunderstorms. This quantity will be reported in km^2. Total Optical Energy (TOE) is the illumination or total energy as observed at the GLM charge-coupled device (CCD) array, so the appropriate unit for most TC cases is pJ.

Instrument detection efficiency is an important factor to consider when analyzing the validity of observed changes in FED, AFA, TOE, and other flash characteristics across different geographic locations and observation times. Figures 3.1 – 3.3 plot both the average and minimum detected energy for 1-hour periods in different TCs. Two 2019

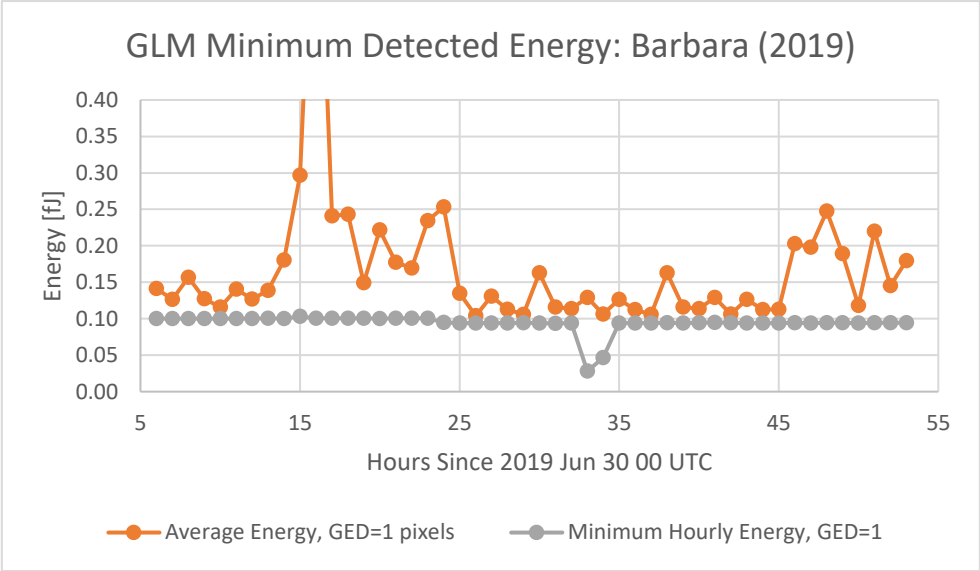

Figure 3.1. Minimum Detected Energy: Barbara (2019). Minimum detected energy and average detected energy from Hurricane Barbara (2019 ENP) in 1 hr time bins for 2 km GLM pixels with group extent density of 1.

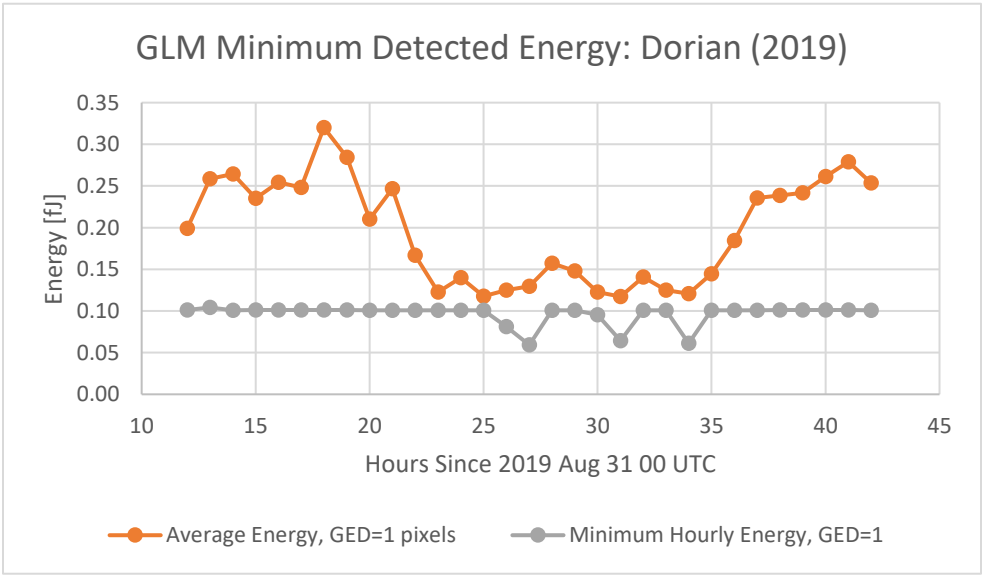

Figure 3.2. Minimum Detected Energy: Dorian (2019). Minimum detected energy and average detected energy from Hurricane Dorian (2019 NA) in 1 hr time bins for 2 km GLM pixels with group extent density of 1.

storms (Barbara [ENP] and Dorian [NA]) and one 2020 storm (Isaias [NA]) were checked to cover both ocean basins and multiple years. Only the 2 km GLM pixels with a group extent density of 1 were retained, allowing for comparison of single groups and

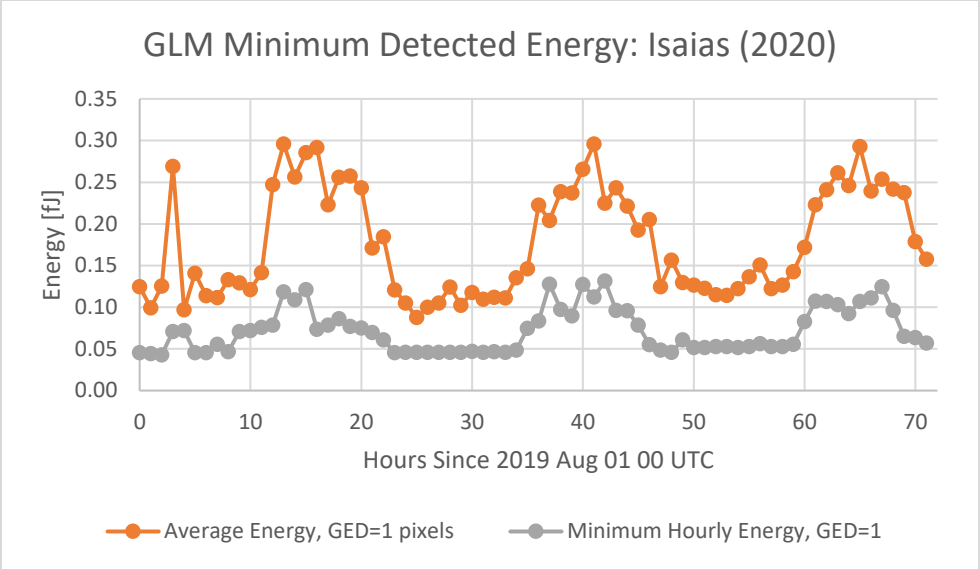

Figure 3.3. Minimum Detected Energy: Isaias (2020). Minimum detected energy and average detected energy from Hurricane Isaias (2020 NA) in 1 hr time bins for 2 km GLM pixels with group extent density of 1.

their weakest observed outer pixels over multi-day periods. In each case, the change in minimum observed energy is only a few hundredths of a femtojoule, which is several factors smaller than the changes seen in particular TC cases. This analysis supports that the observed changes in flash parameters are the result of actual changes in the storm dynamics and not just an instrument artifact due to time of observation or another instrument variable. Figure 3.3 checks the 2020 NA basin case of Isaias and does show evidence of a diurnal cycle response. This is attributed to a change in the precision in the reporting of the satellite data, which allows GLM to resolve this day-to-night variability that was previously unseen. While this reporting change took place after the storms considered in this work, this variation could be neglected in most cases as it is small in magnitude relative to the changes seen in most TCs.

This work selected 14 GLM-observed TCs for analyses. This subset was chosen from the NA storms in 2018 and 2019 and ENP storms in 2019, and intentionally

includes TCs with a range of lightning activity, overall storm intensity, and geographic locations. Landfalling conditions were excluded. These TCs were checked for remaining artifacts not removed in the instrument data filtering. For example, one TC not included in the final analysis, Florence (2018 NA), showed significant Bahama bar (Rudlosky & Virts 2021) effects in several consecutive days of observation (e.g., 9 and 10 September, see Figure 3.4).

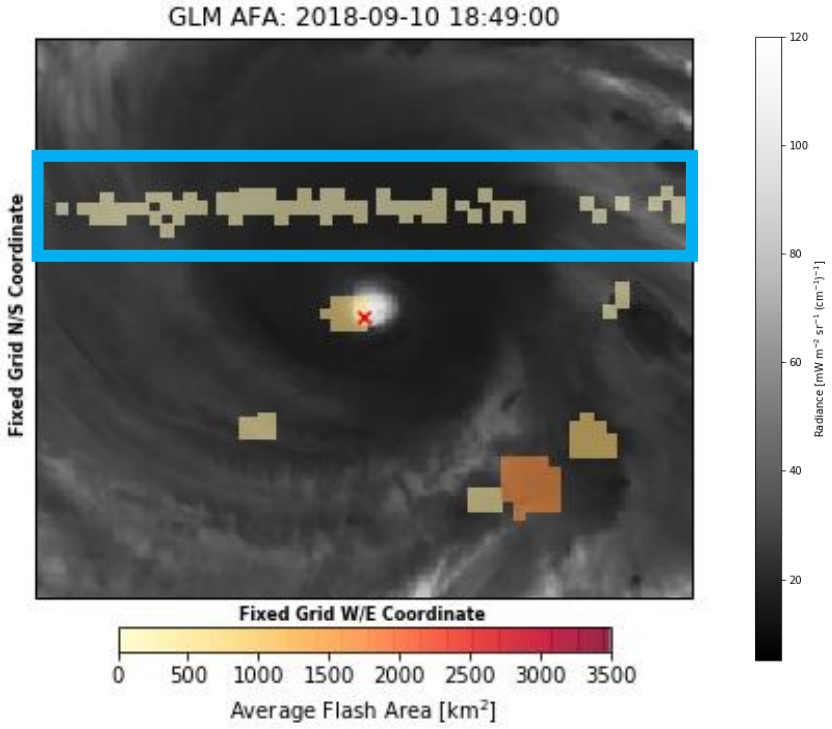

Figure 3.4. Bahama Bar: Florence (2020). Hurricane Florence (2018 NA) on 10 September with 1 minute of GLM flashes colored by AFA, overlayed on GOES-16 Advanced Baseline Imager Channel 14 satellite imagery. The feature highlighted by the light blue box is an observational artifact called the Bahama bar.

All TC location tracks and intensities are obtained from the National Hurricane Center (NHC) Best Track dataset, unless otherwise stated. The best tracks are constructed by a TC expert with all available information after the storm has completed its life cycle progression (Jarvinen et al. 1984, Landsea & Franklin 2013). Tracks have coordinates of

latitude and longitude provided to the nearest tenth of one degree every six hours. Intensities are reported as minimum central pressure to the nearest millibar and maximum sustained 1-minute, 10-meter wind speed in intervals of 5 kts.

RMW values were obtained with NOAA 42 reconnaissance flight data, when available. The flight data includes the departure value, or D-value, which describes the altitude of a point on a constant-pressure surface by its departure from standard altitude ("D-value" 2012). This parameter enables a very precise determination of storm center location (see Figure 3.5), which is of great importance for TCs with a highly contracted RMW (<20 km). This process does make the assumption that the reconnaissance aircraft passed through the TC center. Once the TC center is identified, wind speed vs. radial distance plots were produced and the x-value at the peak of each curve (two legs per storm center pass) was selected as the RMW. Since flight-level data is reported once every second and contains observational noise, the locations of the 10 highest wind speeds collected were averaged to compute the RMW. Several TCs display an asymmetry

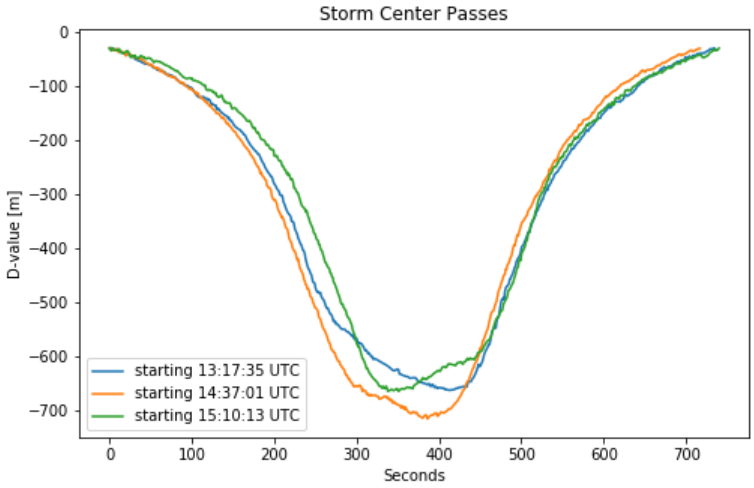

Figure 3.5. Dorian D-Values. Example from Hurricane Dorian (2019 NA) on 1 September of clear local minimums in D-value, recorded by a NOAA 42 reconnaissance flight, that can be used to identify a very precise location of the minimum central pressure of the TC on each flight pass.

in this feature, such as was seen in a particular flight pass of Dorian (2019 NA), shown in Figure 3.6. For the asymmetric cases in this study, a storm-average RMW is computed and utilized in the analysis. Some other TC work utilizes a one-sided RMW (Stephanie Stevenson, personal communication, 25 November 2019), which for highly asymmetric systems, can create big differences in the reported r/RMW ratio for a given ICLB.

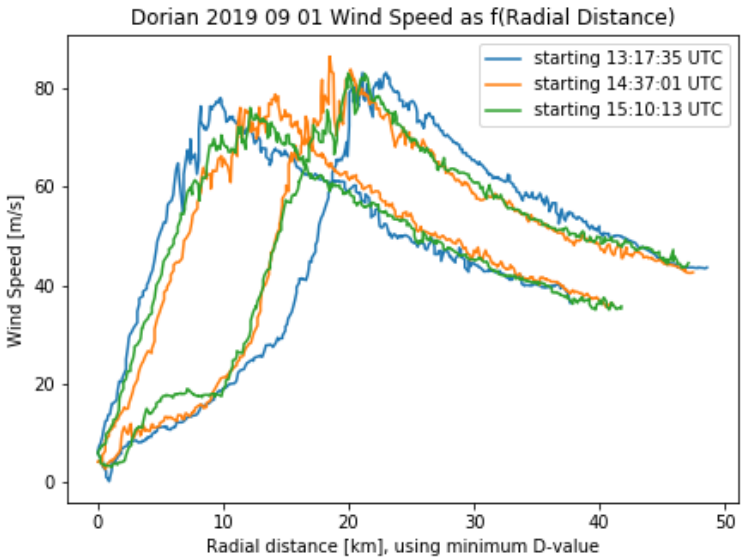

Figure 3.6. Dorian Wind Speed using D-Value as TC Center. Sustained wind speeds [m s^{-1}] in Hurricane Dorian (2019 NA) on 1 September, observed by a NOAA 42 reconnaissance flight. RMW values were calculated from these curves by finding the 10 max wind speeds for each leg of a storm center pass and averaging their locations.

For time periods in which reconnaissance flight data is not available, RMW values are obtained from the Automated Tropical Cyclone Forecast (ATCF) System b-decks (Sampson & Schrader 2000). These files contain best estimates of storm parameters based on operational data during the hurricane season, and then once the TC season has completed, they are reviewed by the National Hurricane Center and updated with more accurate values where needed (Vigh 2021). However, the ATCF b-decks do not include an uncertainty with the RMW values they provide. NOAA 42 flight data has

the benefit of providing a direct probe of the RMW with in-situ measurement but is only available at select times, often only during intensification and rarely during weakening. Therefore, a combination of both RMW sources is utilized for the estimations in this study.

TC center coordinates were interpolated from the 6-hour interval best track to 5-minute increments using SciPy's interpolate.splprep() and interpolate.splev(). interpolate.splprep() was used to find the B-spline representation for the best track locations in latitude and longitude, and interpolate.splev() evaluates the spline and selects the locations with 5-minute precision. GLM flash data is subset from a circular region centered at the TC location and extended into the outer rainbands, with the radial distance typically considered to 150 km, but extended to 300 km from the center for very weak storm intensities and highly disorganized systems. Each flash retains reference to its range. The domain under consideration was updated with the interpolated TC center coordinate every five minutes.

For each TC in this dataset, a time history of GLM-observed flash activity was plotted as a function of radial distance from the TC center and colored by GLM parameters FED, AFA, and TOE. Joint histograms of AFA vs. FED and AFA vs. TOE were produced, both interior and exterior to the RMW, and divided in time based on intensity change (slow strengthening, RI, RW, etc.). The aim was to determine if regular patterns emerged in the typical flash activity of an intensifying or weakening TC.

CHAPTER 4

RESULTS

GLM data from 14 TCs were gridded and analyzed to inform what lightning flash activity, when present, indicates about upcoming storm intensity change. This subset of GLM-observed TCs was chosen from the NA and ENP storms in 2018 and 2019, and intentionally includes TCs with a range of lightning activity, overall storm intensity, and geographic locations. Eight of the 14 TCs experienced at least one period of RI: Barbara, Erick, Juliette, and Kiko from the 2019 ENP; Chris and Michael from the 2018 NA; Dorian and Jerry from the 2019 NA. Seven of the 14 TCs experienced RW: Alvin (2019 ENP), Barbara, Erick, Kiko, Dorian, Humberto (2019 NA), and Jerry.

a. Alvin (2019 ENP)

The first named storm in the 2019 ENP basin, Alvin, developed southwest of Mexico. The system was first identified as a tropical depression at 1200 UTC 25 June. After an early struggle to develop with limited convective banding, Alvin entered a favorable environment of warm sea-surface temperatures (SSTs) and light shear (Latto 2019 a). Convective organization increased, and the TC strengthened into a tropical storm (TS) by 1200 UTC 26 June and a Category 1 hurricane by 0000 UTC 28 June. Further travel to the northwest placed the storm over cooler SSTs and increasing southwesterly shear weakened the storm back to TS status by 0600 UTC 28 June (Latto 2019 a). While the storm did not achieve the RI criterion during its strengthening, Alvin did undergo rapid weakening (30 kt or greater decrease in a 24-hour period) from 0600 UTC 28 June to 1200 UTC 29 June as it deteriorated to a remnant low.

In the 48 hours of strengthening leading up to its peak intensity (992 mb minimum central pressure, 65 kt sustained wind speed), Alvin produced 66 lightning flashes within 150 km of its center. One time cluster of ~15 flashes occurred early in this period of strengthening at 20-80 km distance from the TC center, which all fell interior to the RMW reported in the ATCF b-decks. Another ~15 flashes occurred exterior to the RMW just prior to 0000 UTC 27 June. The RMW was reported to have contracted from 93 km to 19 km during this time interval, and it remained at 19 km until after 0000 UTC 29 June, deep into the rapid weakening phase. The storm was devoid of any RMW interior flashes during weakening, with the nearest burst occurring at ~7 RMW, exterior to the inner-core, and containing more energetic flashes than seen at any point during the period of strengthening.

b. Barbara (2019 ENP)

The second named storm in the 2019 ENP basin, Barbara, rapidly intensified to a strong Category 4 hurricane on the SSHWS. A well-defined center was apparent by 0600 UTC 30 June when the storm was first classified as a TS. Barbara had two main phases of intensification. Early on, the intensification was a steady 5 kt wind speed gain per 6-hour period, as the system encountered moderate shear and nearby dry air (Cangialosi 2019). On 1 July, the shear decreased, the TC became more symmetric, and over warm SSTs, Barbara underwent RI in favorable conditions (1800 UTC 30 June – 0000 UTC 3 July; 54 hours in duration). At peak intensity (930 mb, 135 kt), Barbara had a well-defined, 15 n mi diameter eye (Cangialosi 2019). This RI was nearly immediately followed by RW, which occurred from 0600 UTC 3 July – 0000 UTC 6 July (66 hours) due to ever-

increasing wind shear, cooler SSTs, and encountering a more stable air mass (Cangialosi 2019).

Within 150 km of the storm center, Barbara's greatest flash density occurred early in its lifespan during the phase of slower intensification (820 flashes from 0600 UTC 30 June – 1200 UTC 1 July). There were three noteworthy RMW-interior lightning bursts during this interval: a cluster of ~25 flashes with small AFA and small TOE at 1000 UTC 30 June; a cluster with higher flash count and increasing FED cluster at 2000 UTC 30 June; and a cluster with the largest FED in this group at 0300 UTC 1 July that had small AFA and moderate TOE. The RMW was still moderately large at this stage, contracting from 93 km to 56 km. Still early in the RI phase, another RMW-interior burst occurred just past 1200 UTC 1 July, though this one exhibited significantly larger FED, AFA, and TOE characteristics than any of the other inner-core bursts in this TC. Shortly thereafter, the RMW had decreased to 28 km, and it would reach 19 km by the time of peak intensity. After a few more sporadic flashes until 0000 UTC 2 July, the lightning completely ceased in Barbara's inner-core until RW was underway. A loose cluster of ~15 flashes centered approximately 1.7 RMW from the storm center was the most significant group through 0000 UTC 5 July. There were no flashes interior to the RMW during this portion of the weakening phase.

c. Erick (2019 ENP)

TC Erick developed slowly initially, likely due to its elongated circulation and the presence of mid-level dry air (Blake & Wroe 2021). Unusually, the ATCF b-decks for Erick show a highly contracted RMW from very early on in the storm's lifespan. At 0000 UTC 28 July, Erick was a weak tropical storm (1005 mb, 35 kt) and was shown to have a

37 km RMW, significantly less than other ENP basin storms in this sample. The storm's intensification resumed and quickened once its low-level center reformed and reached lighter shear with warm SSTs (Blake & Wroe 2021). Erick underwent RI from 1200 UTC 29 July – 1800 UTC 30 July, when it achieved its peak intensity as a Category 4 hurricane on the SSHWS (952 mb, 115 kt). Weakening began slowly, before accelerating within an environment of increasingly strong vertical wind shear (Blake & Wroe 2021). Erick met the RW criterion for a 60-hour period (0600 UTC 31 July – 1800 UTC 2 August).

For an ENP system, Erick produced a large amount of lightning. GLM observed more than 800 flashes in its inner 150 km in a 20-hour period beginning at 1200 UTC 28 July. Several notable bursts occurred, including two clusters at 40 km from the TC center, both of which contained many high TOE flashes. Another cluster occurred at 2100 UTC 28 July centered around 10 km from the center, though despite relatively large FED values, the cluster contained all small AFA and small TOE flashes. Flash activity stopped entirely in the inner-core from 0800 UTC 29 July – 1200 UTC 30 July. Lightning began occurring regularly again around 1500 UTC 30 July, and the flash activity was virtually continuous for more than 24 hours, all of which occurred very near to the RMW. These flashes primarily exhibited large FED and large AFA and were located slightly further from the TC center as weakening commenced.

d. Juliette (2019 ENP)

An example of a low flash count storm was Juliette, also from the 2019 ENP basin. This TC experienced low shear, deep moisture, and warm SSTs (Latto 2019 b), causing it to undergo RI from 0000 UTC 2 September to 1200 UTC 3 September, when it

reached its peak intensity as a strong Category 3 on the SSHWS (953 mb, 110 kt). The storm inner-core passed over Clarion Island around this time. Juliette's weakening did not meet the RW criterion, though the storm did lose 20 kt over 12 hours from 0000 UTC to 1200 UTC 4 September with its eyewall collapse. Weakening continued over cooler SSTs and an increasing southwesterly shear environment (Latto 2019 b).

There were a total of 147 flashes in the inner 150 km of Juliette over the 60 hours it strengthened from 35 kt to 110 kt sustained wind speed. A cluster of ~20 of those flashes occurred at 25 km from the TC center (0.31 RMW), which was rapidly followed by a contraction in the RMW, according to the ATCF b-decks. However, the validity of this RMW value is questionable given the storm's continued intensification and the unusual re-expansion of the RMW prior to further contraction shown in the b-decks. Very few flashes occurred within the inner-core from 1400 UTC 1 September to 0000 UTC 3 September. Near the end of intensification, moderately energetic flashes appeared at 1.08 RMW and 1.14 RMW, and as the transition to weakening began, the flashes grew more distant from the storm center (1.89 RMW), though according to the b-decks, the RMW did not relax more than one 5 kt increment total through 1800 UTC 6 September. Nearly all flashes during early weakening were found exterior to the RMW.

e. Kiko (2019 ENP)

The 2019 ENP basin storm Kiko underwent RI and RW early in its lifespan and then persisted as a tropical storm for more than seven days. Following a 24-hour period where the storm was disorganized and remained at constant intensity (1004 mb, 35 kt), a compact inner-core developed and promoted the beginning of RI (Zelinsky 2020). Kiko gained 55 kt in sustained wind speed over 24 hours, far surpassing the RI criterion. It

achieved maximum intensity at 1200 UTC 15 September as a Category 4 hurricane on the SSHWS (950 mb, 115 kt). The RW criterion was then met for a period of 54 hours, 1800 UTC 15 September – 0000 UTC 18 September, as Kiko wrapped dry mid-level air into its circulation and faced moderate northeasterly wind shear (Zelinsky 2020).

Flash counts in Kiko were low during its very swift intensification. From 0000 UTC 14 September – 1200 UTC 15 September, GLM detected 81 flashes in its inner 150 km, with two main clusters in time. Just past 0600 UTC 14 September, several flashes appeared interior to the RMW, dispersed from 5 km to 60 km from the center. FED, AFA, and TOE all increased for the flashes in this loose cluster with increasing storm center distance. Flash activity entirely ceased for about 14 hours, ~ 0800 UTC – 2200 UTC. The next noteworthy burst occurred near 0300 UTC 15 September, with ~10 low TOE flashes at 1.89 RMW, which by this point had contracted to its minimum storm value of 19 km. In the first 30 hours of constant intensity and early weakening, 280 flashes appeared in the inner 150 km, nearly all between 2100 UTC 15 September – 0200 UTC 16 September. FED increased later in this time interval, with the largest energy flashes occurring furthest from the TC center. While AFA remained primarily small in this cluster, the largest relative flashes occurred further inward, near to the RMW. Following this burst, the lightning ceased again until 17 September, when a ~1000 flash cluster appeared around 0200 UTC, stretching from 5 km – 55 km distant from the center. This cluster contained the largest FED, AFA, and TOE flashes in Kiko for the time periods evaluated in this study.

f. Lorena (2019 ENP)

Lorena, a 2019 ENP basin TC, experienced two separate periods of strengthening due to its land interaction with the west Mexico states of Jalisco and Baja California Sur (Avila 2019). The system first achieved tropical storm status at 0600 UTC 17 September. It strengthened into a Category 1 hurricane on the SSHWS, with a maximum 24-hour intensity increase of 25 kt, so it did not meet the RI criterion. Lorena weakened back to a tropical storm as it moved along the coastline near Manzanillo and Cabo Corrientes. The TC then moved over the Gulf of California, where warm SSTs promoted restrengthening (Avila 2019). Its peak intensity was achieved at 1800 UTC 20 September (986 mb, 75 kt), during which an eye was observed with satellite imagery. Lorena made its second landfall shortly thereafter. The high terrain of Baja California Sur promoted the initial gradual weakening.

This TC exhibited huge flash counts during its two weakening phases in comparison to its two strengthening phases, which was a consequence of its land interaction and outside the scope of this study. During the initial storm strengthening, GLM observed several bursts interior to the 37 km ATCF b-deck reported RMW, the majority of which exhibit small AFA and large TOE. Just prior to the next RMW contraction around 1100 UTC 18 September, there was an ICLB at 0.81 RMW with large AFA and small TOE, which was followed about 2 hours later by a cluster of flashes with similar FED but larger TOE. The inner-core lightning largely ceased for approximately 8 hours before a single moderate FED, low AFA, low TOE burst at 0.36 RMW around the time of peak intensity. After straddling the west coast of Mexico and re-emerging over water, Lorena had a single cluster of low AFA flashes interior to the RMW during the

entirety of the second intensification phase. Most of the flashes within 150 km of the TC center during this time period (257 total in 18 hours) were scattered in their radial distribution, but generally dispersed further from the storm center as time progressed.

g. Raymond (2019 ENP)

Raymond was a late-season 2019 ENP basin TC that achieved tropical storm status but did not intensify beyond 45 kt maximum sustained wind speed. An environment of moderate northwesterly shear dampened early strengthening, though an increase in deep convection was seen in the eastern portion of the storm as it reached tropical storm status (Brown 2020). It maintained its 1001 mb peak intensity for 18 hours before encountering increasing southwesterly vertical wind shear from a mid- to upper-level trough that led to gradual weakening and eventual dissipation (Brown 2020).

This TC had three notable ICLBs in the 24-hour period preceding its maximum intensity. At 0300 UTC 15 November, a cluster of ~10 moderate AFA, low TOE flashes appeared about 80 km from the TC center, which were followed just before 0600 UTC with a burst containing greater FED and significantly larger TOE centered 60 km from the TC center. At 1400 UTC, a burst appeared at 85 km from the TC center and contained primarily low AFA, large TOE flashes. Highly unusually, the b-deck RMW values reported for this storm expanded considerably during TC intensification (increasing from 93 km to 148 km), which is in opposition to the established trend from other TCs. Confidence in the validity of these values would be improved with additional verification via satellite imagery or another appropriate method. During the onset of weakening in the 36-hour period from 0000 UTC 16 November to 1200 UTC 17 November, GLM

observed 702 flashes in the inner 150 km of Raymond, which were all interior to the RMW, according to the ATCF b-decks.

h. Alberto (2018 NA)

The first named storm in the 2018 NA basin, Alberto, reached its peak intensity (990 mb, 55 kt) in the Gulf of Mexico before making landfall in the Florida panhandle. This system strengthened from a subtropical depression into a tropical storm, with notable deep convection moving closer to the TC center on 27 May and a 50 nautical mile (93 km) decrease in the RMW (Berg 2018). Landfall occurred around 2100 UTC 28 May, but Alberto was already weakening for a 15-hour period preceding this, evidenced both by a decline in deep convection and maximum sustained wind speed decrease (Berg 2018).

Alberto produced 1330 GLM flashes over the 24 hours of 27 May that immediately preceded peak intensity. Several clusters of flashes presented in the first 9 hours of 27 May, all with greater FED, AFA, and TOE characteristics than the remaining clusters that appeared later in the day. Virtually all of the flash activity in the inner 150 km for 27 May occurs interior to the ATCF b-deck reported RMW. Lightning then ceased entirely, less 3 flashes near 1000 UTC 28 May, around 2300 UTC 27 May until just prior to landfall, an approximately 20-hour period of dormancy.

i. Chris (2018 NA)

This NA basin TC was slow to strengthen early in its development, not reaching tropical storm status until 42 hours after it was first classified as a tropical depression. It drifted southeastward due to an approaching cold front, and over warm water began intensifying more quickly on 9 July, when a more well-defined inner-core was evident in

satellite imagery (Blake 2018). Low shear and previously undisturbed warm SSTs (Blake 2018) enabled a period that exactly achieved the RI criterion, ending at the point of TC peak intensity (969 mb, 90 kt), reaching Category 2 on the SSHWS. Encountering cooler SSTs and interaction with a mid-latitude trough caused it to grow in size, which weakened Chris, moving the system into its extratropical transition (Blake 2018). Its largest 24-hr wind speed decrease while still classified as a hurricane or tropical storm was 25 kts. A 30 kt decline took place from 0000 UTC 12 July to 0000 UTC 13 July, however, the storm was already considered extratropical by 1800 UTC 12 July.

In the 72 hours preceding peak intensity, GLM observed 788 flashes in the inner 150 km of Chris, of which fewer than 100 occurred during the 24-hour period of RI. In addition to the ATCF b-decks, RMW values for this TC were obtained at several times during strengthening with NOAA 42 flight mission data. Many episodic lightning clusters appeared between 1100 UTC 8 July and 0500 UTC 9 July. The three largest inside of 100 km from the TC center all presented different properties, despite occurring at similar physical distances (65, 60, and 65 km) from the storm center . The first of these at approximately 1200 UTC 8 July occurred at 0.81 RMW and exhibited the greatest TOE but small AFA, relative to the other clusters in this sample. At 2200 UTC, the RMW was contracting and an ICLB occurred at approximately 0.97 RMW with slightly larger AFA but significantly lower relative TOE. Then at 0300 UTC 9 July, this ICLB occurred at 1.25 RMW with the largest AFA of these three clusters, though it is comparable in TOE to the burst that preceded it by 5 hr. There was another noteworthy cluster of flashes very near to the start of the period of RI, around 0000 UTC 10 July at 2.16 RMW, before lightning activity diminished to near zero for about 15 hours. Two small-count clusters

appeared at 2100 UTC and 2300 UTC 10 July, just prior to the storm achieving peak intensity. Within 100 km, the onset of weakening contained only one significant ICLB, centered around 85 km from the TC center at 3.1 RMW.

j. Michael (2018 NA)

This NA basin TC reached strong Category 4 status on the SSHWS (920 mb, 135 kt) according to the NHC Best Track, but post-analysis estimates place its estimated maximum sustained wind speed at the time of landfall at 140 kt (Beven II et al. 2019), which would equate to a Category 5 storm. Initial strengthening quickly transitioned into a period of RI (0600 UTC 7 October – 0000 UTC 9 October; 42 hours in duration) despite occurring in an environment with moderate-to-strong southwesterly wind shear. Strengthening slowed briefly early on 9 October alongside the decay of eyewall convective structure (Beven II et al. 2019). However, RI then resumed (0600 UTC 9 October – 1800 UTC 10 October; 36 hours in duration) until Michael made landfall in the Florida panhandle near Mexico Beach and Tyndall Air Force Base, where it caused significant damage and 16 fatalities (Beven II et al. 2019).

Both ATCF b-deck and NOAA 42 flight mission data were used to determine RMW values for this TC. Michael produced considerable flash activity, including 1855 flashes in the 30 hours preceding its landfall in its inner 150 km. Many flashes during the first period of RI in Michael demonstrated relatively low AFA and TOE, in comparison to the ICLB that occurred at 0500 UTC 9 October, or just prior to the start of the second phase of RI. This burst included flash activity from the TC center out to 50 km, with its center well interior to the RMW at 0.53 RMW. AFA for this burst was larger nearer to the TC center, whereas the inverse relationship presented in the TOE, as it increased

alongside FED with increasing distance from the storm center. There was a period of comparatively low flash activity following this ICLB until about 1800 UTC 9 October, when inner-core flash activity ramped up significantly until the TC made landfall. From 2300 UTC until landfall, flash activity was nearly continuous, similar to several other TCs (Barry, 2019 NA; Dorian, 2019 NA; Erick, 2019 ENP). This TC provides another candidate case for the flash locations being approximately representative of the RMW.

k. Barry (2019 NA)

The second named storm in the 2018 NA basin, Barry, formed in the Gulf of Mexico and moved west-northwestward on its path to making landfall in Louisiana. This TC briefly achieved hurricane status as a Category 1 on the SSHWS, though it never intensified at a rate greater than 5 kt in any 6-hour period. Northerly shear and dry mid-levels kept nearly all of the convection, which increased in intensity and coverage as the storm strengthened, confined south of the TC center (Cangialosi et al. 2019). Barry remained highly asymmetric throughout its lifespan, never presenting the appearance of a classical hurricane in satellite imagery (Cangialosi et al. 2019). This storm underlined the potential issues that stem from choosing a rigid 100 km inner-core definition and assigning RMW values to highly asymmetric systems. The minimum central pressure of the storm, 993 mb, was first reported at 1800 UTC 12 July and remained constant according to the NHC Best Track until landfall at 1500 UTC 13 July. Peak sustained wind speeds of 65 kt first occurred at 1200 UTC 13 July. Weakening occurred following landfall.

Barry produced many flashes observed by GLM during strengthening, with 4078 flashes occurring in the 42-hour period beginning at 1800 UTC 11 July in the inner 150

km of the storm. Flashes were nearly continuous beginning around 0600 UTC 12 July and remained at that rate for 24 hours. Supporting the prior description that convection was distributed unusually in this storm, Barry was devoid of flashes within 60 km of the storm center for that full period. The long duration activity period was seen in other TCs (Dorian, 2019 NA; Erick, 2019 ENP); however, Barry was a tropical storm for the entirety of this period with an RMW larger than 100 km, according to the ATCF b-decks. Among the TCs investigated in this study, other systems with similar virtually continuous flash features were more organized, symmetric, and contained a contracted RMW of no more than 30 km. Two specific times with noteworthy flash activity occurred during strengthening: 0200 UTC and 0900 UTC 13 July. The first of these occurred within the 24-hour burst but was nearest the center of that long time cluster at around 70-80 km distant. These flashes displayed enormous AFA (several flashes larger than 4000 km^2), dwarfing other flashes in this sequence. Several of these flashes presented with large TOE; however, other time clusters earlier in Barry's history also showed similarly large TOE. At 0900 UTC, flash activity was present interior to 60 km for the first time, centered approximately 30 km from the TC center. This time cluster demonstrates larger AFA nearest to the TC center but larger TOE with increased distance from the TC center.

l. Dorian (2019 NA)

One of the strongest NA basin TCs on record, Dorian produced remarkable long duration (>15 hours), continuous inner-core lightning both during RI and in the beginning hours of weakening. This TC remained a tropical storm for several days early in its lifespan due to frequent intrusions of dry air (Avila et al. 2020). After the system passed over the mountainous island of Saint Lucia, Dorian achieved hurricane status (at 1530

UTC 28 August) and developed an eye visible in satellite imagery, but it did not intensify beyond Category 1 on the SSHWS until 30 August. By this point, the TC had reached a region of low vertical wind shear, very warm SSTs, and large amounts of atmospheric moisture, which promoted an extended period of strengthening from 0000 UTC 30 August to 1640 UTC 1 September, including two overlapping periods of RI and the development of a 12 n mi diameter eye surrounded by deep convection (Avila et al. 2020). At peak intensity, Dorian reached 910 mb minimum central pressure and 160 kt sustained wind speed, a Category 5 on the SSHWS, while its forward motion reduced to near zero. A combination of island land interaction and ocean cooling beneath the TC contributed to early weakening (Avila et al. 2020), before higher shear and additional cooler SSTs induced RW.

Prior to the aforementioned long, continuous bursts, Dorian produced several inner-core bursts isolated in time. Both at 1900 UTC 29 August and 0200 UTC 30 August, ICLBs occurred exterior to the RMW and exhibited particularly large AFA further from the TC center (average positions 30 km and 35 km distant). A local peak in flash activity from 1600 to 2200 UTC 30 August largely occurred immediately interior to the RMW, which is estimated at 20 km considering both NOAA 42 data and ATCF b-deck values. Inner-core lightning largely stopped for about 6 hours, before resuming around 0600 UTC 31 August and continuing for 27 consecutive hours (ending 0900 UTC 1 September). This period aligns in time with the phase of strengthening that fell beneath the RI criterion (20 kt increase 24 hours following 0000 UTC 31 August; 25 kt increase 24 hours following 0600 UTC 31 August). Slight variations in the radial distance from the TC center occurred but the flashes were very near to the RMW for the duration of this

burst. Inner-core flashes halted for less than 4 hours before resuming again around 1300 UTC 1 September and continuing for 16 hours (ending near 0500 UTC 2 September). These flashes occurred exterior to the one-sided RMW values that appear to be reported in the ATCF b-decks but centered on the two-sided storm average RMW estimate calculated with NOAA 42 flight data. Later in the RW phase, flashes that exhibited low AFA and low TOE continued sporadically in the inner-core exterior to the RMW.

Comparing the two long-duration, continuous burst features with joint histograms of AFA vs. FED and AFA vs. TOE reveals a clear flash characteristic difference between the two bursts. The earlier burst that occurred entirely during storm strengthening exhibited smaller FED, larger AFA, and larger TOE than in the burst that continued into the onset of weakening. The physical explanation for this flash characteristic shift was evaluated in Duran et al. (2021) and found to be a consequence of vertical wind shear, barotropic mixing, and secondary eyewall formation.

Date	NHC Best Track Latitude [°N]	NHC Best Track Longitude [°W]	Modified Track Latitude [°N]	Modified Track Longitude [°W]
2019 Aug 31 00 UTC	25.3	71.1	25.42	71.04
2019 Aug 31 06 UTC	25.6	72.1	25.68	72.07
2019 Aug 31 12 UTC	25.9	73.0	25.90	72.91
2019 Aug 31 18 UTC	26.1	74.0	26.13	73.92
2019 Sep 01 00 UTC	26.3	74.7	26.30	74.70
2019 Sep 01 06 UTC	26.4	75.6	26.40	75.65
2019 Sep 01 12 UTC	26.5	76.5	26.52	76.40
2019 Sep 01 18 UTC	26.5	77.0	26.62	77.10
2019 Sep 02 00 UTC	26.6	77.7	26.68	77.65
2019 Sep 02 06 UTC	26.6	78.0	26.65	78.10
2019 Sep 02 12 UTC	26.7	78.3	26.76	78.30
2019 Sep 02 18 UTC	26.8	78.4	26.88	78.40
2019 Sep 03 00 UTC	26.9	78.5	26.90	78.46

Table 4.1. Dorian Higher Precision Coordinates. Two center coordinates for Dorian (2019 NA): the NHC best track and a set of modified, higher precision coordinates intended to better capture the flashes interior to the RMW.

With Dorian's highly contracted RMW, the NHC Best Track resolution for latitude and longitude (nearest tenth of one degree every six hours) appeared to lack the precision needed to accurately capture interior RMW flashes at certain times around peak intensity. The center coordinates from this TC were modified slightly from the best track by overplotting them on GOES-16 Advanced Baseline Imager Channel 14 satellite imagery and manually adjusting the center coordinates at each 6-hour increment. Updated values are recorded in Table 4.1. Plots in the Appendix for Dorian are provided using both the NHC Best Track and using the higher precision coordinates. The joint histograms for flashes interior to the RMW demonstrate the significant shift in flash parameters that can be apparent from even small differences in center coordinate for storms with highly contracted RMWs.

m. Humberto (2019 NA)

Another 2019 NA basin storm, Humberto, achieved major hurricane status but produced relatively few GLM-observed flashes, especially relative to other NA basin systems. It did not experience any period of RI and never intensified at a rate greater than 5 kt in any 6-hour period according to the NHC Best Track. Early strengthening of Humberto took place in an environment of moderate southwesterly to westerly vertical wind shear (Stewart 2020). It reached hurricane status at 0000 UTC 16 September and peak intensity (950 mb, 110 kt) at 1800 UTC 18 September, which lasted for nine hours, categorized as a strong Category 3 on the SSHWS. Humberto passed within 55 n mi of the island of Bermuda before it underwent an acceleration in forward motion northeastward. This TC underwent RW in a strong south-southwesterly vertical wind shear environment and entrained very dry mid-level air (Stewart 2020).

NOAA 42 flight mission data provided RMW values for Humberto during TC strengthening, and ATCF b-deck RMW values were used around the time of peak intensity and during weakening. Three small-count clusters of flashes occurred within 24 hours during early strengthening (0500 UTC 14 September, 1800 UTC, 0200 UTC 15 September), all of which occurred outside the traditional 100 km inner-core definition but were between 1 and 1.5 multiples of the RMW. The only significant flashes interior to the RMW occurred at 0400 UTC and 0500 UTC 16 September, all of which demonstrate low AFA and low TOE. Flash activity in the inner 100 km was minimal from 0800 UTC 16 September until 1400 UTC 18 September. As Humberto reached its peak intensity, time clusters of low count flashes appeared at 1.89 RMW, 1.76 RMW, and 1.35 RMW. With the onset of weakening, a few distinct flash clusters appeared in an otherwise period of primarily inactivity. The burst around 0400 UTC 19 September (1.53 RMW) contains large AFA, low TOE flashes, whereas the more radially expansive cluster near 0700 UTC (1.87 RMW) exhibited the inverse properties: smaller AFA and larger TOE.

n. Jerry (2019 NA)

This 2019 NA basin TC did experience RI but did not achieve major hurricane status. Its early strengthening occurred slowly, as an environment of moderate northeasterly vertical wind shear pushed its center towards the edge of deep convection. The rate of intensification increased once over warm SSTs and the vertical wind shear dropped substantially (Brown 2019). Jerry underwent RI for 30 hours beginning at 1800 UTC 18 September and peaked in intensity at 0000 UTC 20 September (976 mb, 90 kt) as a Category 2 on the SSHWS. during which a low-level eye was observed in microwave imagery (Brown 2019). This TC transitioned immediately from the end of RI

to the beginning of RW, returning to tropical storm status by 0000 UTC 21 September. This quick decrease in intensity was attributed to strong northwesterly upper-level winds (250 mb) and dry mid-level air (Brown 2019). The system remained a tropical storm for several days before eventually transitioning to a remnant low around 1800 UTC 24 September.

During the first phase of strengthening, GLM detected lightning at several radial ranges in Jerry. Around 0800 UTC 18 September, a cluster of flashes with moderate AFA and large TOE occurred within 20 km of the TC center (0.36 RMW). This was promptly followed with a burst 75 km from the center (1.35 RMW) with comparable, moderate AFA but substantially smaller TOE. The next 5 hours included several clusters of flashes between 100 and 150 km distant and minimal activity inside of 80 km. Three bursts interior to the RMW, all with small AFA and small TOE, occurred near the beginning of RI at 1800 UTC 18 September, 2200 UTC, and 0000 UTC 19 September. These preceded 15 hours of lightning inactivity in the inner 80 km. As RI ended and RW began (2100 UTC 19 September to 0800 UTC 20 September), several bursts appeared exterior to the RMW, according to the ATCF b-decks, which do not reflect a relaxation in the RMW until 1200 UTC 21 September.

o. Multi-Storm Analysis

Two types of episodicity emerged from the TCs under consideration in this dataset. The majority of systems (11 of 14, 78.6%) produced distinct clusters of flashes in time, in which the lightning would cease for a variable amount of time (frequently >1 hr) before beginning the next period of flash activity. However, three TCs (Barry, 2019 NA; Dorian, 2019 NA; Erick, 2019 ENP) exhibited nearly or completely continuous periods

of flash activity that continued for 15 hours or more and produced several thousand GLM flashes each during those times. Michael (2018 NA) likewise had a nearly continuous burst in the approximate 18 hours preceding its landfall but will not be considered here due to the influence of land.

Notably, Dorian (two bursts of 27 hr and 16 hr) and Erick (one burst of 30 hr) both had tightly contracted RMWs (<25 km) during these extended, continuous bursts, but Barry had an RMW of approximately 115 km for its 24-hour burst. In all three cases, the flash activity occurred very near to the estimated RMW, suggesting that in future continuous long burst cases, the relative radial lightning position could potentially be used as another measure to estimate the RMW. The presence of nearly continuous flashes suggests these three storms have a different set of physical dynamics than the more episodic flashes of other TCs. This topic will be revisited in the Conclusions.

Since Barry, Dorian, and Erick had these long duration lightning events, classifying each of these approximately day-long bursts as a single ICLB would significantly underrepresent the amount of flash activity in these storms and considerably undersample the 24-hr intensity change and location information available for these cases. Thus for the following scatter plot analysis, each graph will contain datapoints that correspond to two-hour ICLB activity periods. This time restriction enables more frequently updated values of average ICLB position, RMW, and 24-hr intensity change data that would be lost if the entire ICLB was considered at once.

Another classification consideration is that, as suggested in Stevenson et al. (2016), the traditional 100 km inner-core definition may not be sufficient to capture the inner-core processes for storms with large RMW. In this work, lightning detections

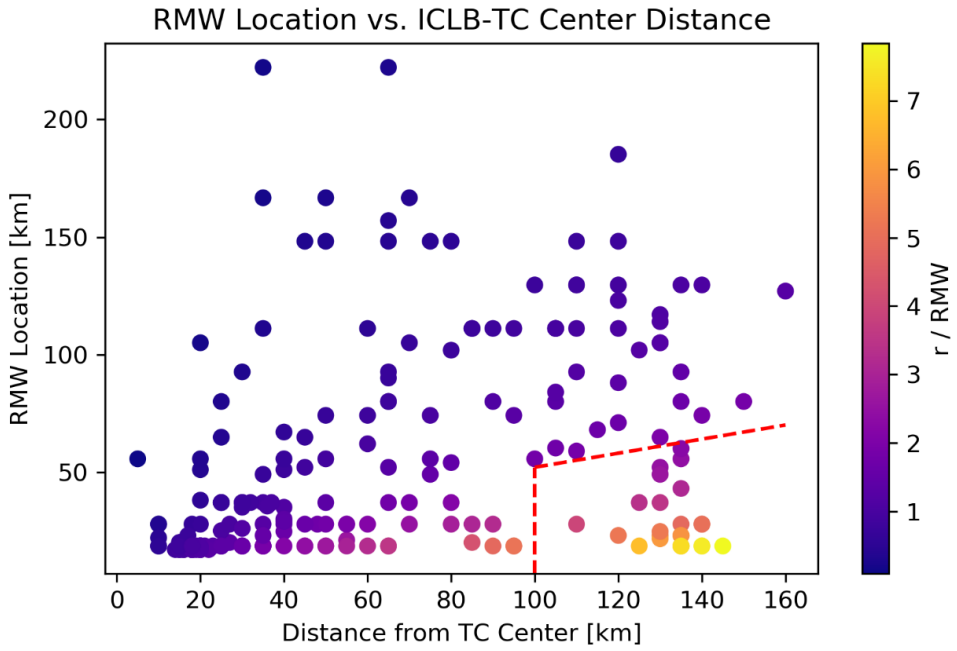

Figure 4.1. RMW Location vs. ICLB-TC Center Distance, All Periods. 220 two-hour lightning activity periods (excluding bursts shortly before major landfalls), where the color fill identifies RMW multiple, the y-axis is the RMW in km, and the x-axis is lightning activity distance from TC center. The region enclosed to the right of the dashed red lines are the clear rainband flashes excluded from the sample hereafter.

interior of 150 km distant from the TC centers are plotted in Figure 4.1. When the RMW is 50 km or smaller, the TC is adequately compact to use the traditional interior 100 km inner-core definition, meaning the flashes to the right of vertical dashed red line are clearly rainband flashes and will be removed from the sample under consideration. However, for RMW values larger than 50 km and lightning bursts occurring at r/RMW < 2.5, it is not immediately clear if bursts in these locations are most similar to traditional inner-core flash activity or rainband flash activity. Satellite imagery and GLM flash parameters can be evaluated for each burst to check, but for the purposes of this RMW analysis, flashes in the 100 km < r < 150 km range are kept if the RMW > 50 km and r/RMW < 2.5.

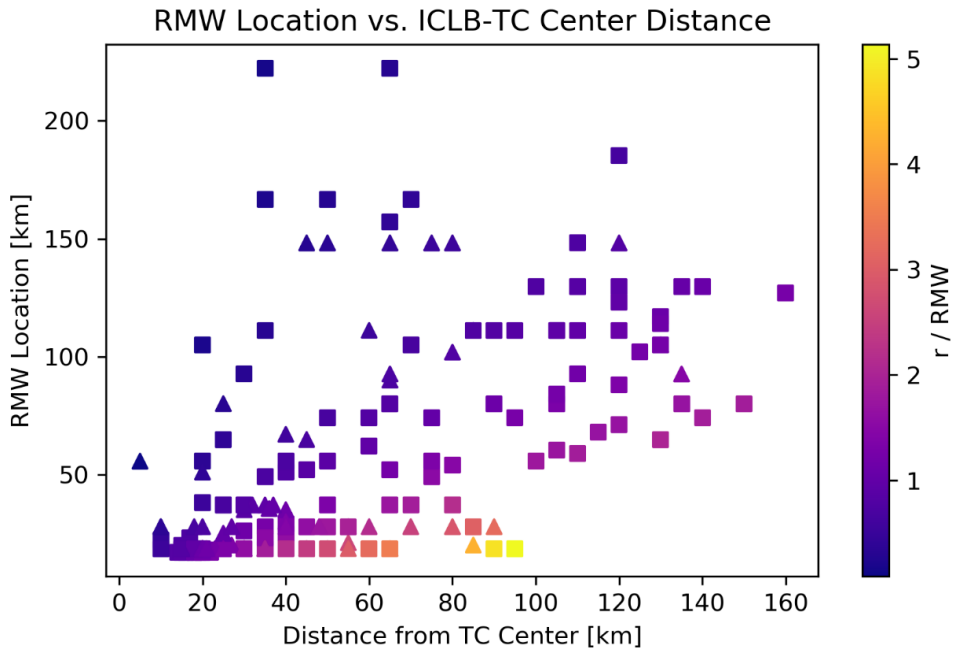

Figure 4.2. RMW Location vs. ICLB-TC Center Distance, Modified Inner-Core. 194 two-hour lightning activity periods, where the color fill identifies RMW multiple, the y-axis is the RMW in km, and the x-axis is lightning activity distance from TC center. Squares denote NA TCs; triangles denote ENP TCs. The data points that occupied the white space region in the lower right (Figure 4.1) have been removed from the sample.

For the time periods considered for the 14 TCs described previously, there are 231 two-hour lightning burst periods within 150 km of the storm center. Removing remaining bursts preceding landfalls along extensive coastlines and removing only the clear rainband bursts as described by the modified inner-core definition above, the dataset contains 194 two-hour ICLB activity periods, plotted in Figure 4.2. Of these, 51 periods correspond to the nearly continuous flash cases, and 143 periods fall in the non-continuous regime. 125 periods occur in the NA ocean basin (squares in Figure 4.2), with 69 periods in the ENP (triangles).

Figure 4.3 contains four histograms that show the general distribution of the 194 two-hour ICLB activity periods in various parameter spaces, and which generally support several previous conclusions in the TC literature. For example, DeMaria et al. (2012)

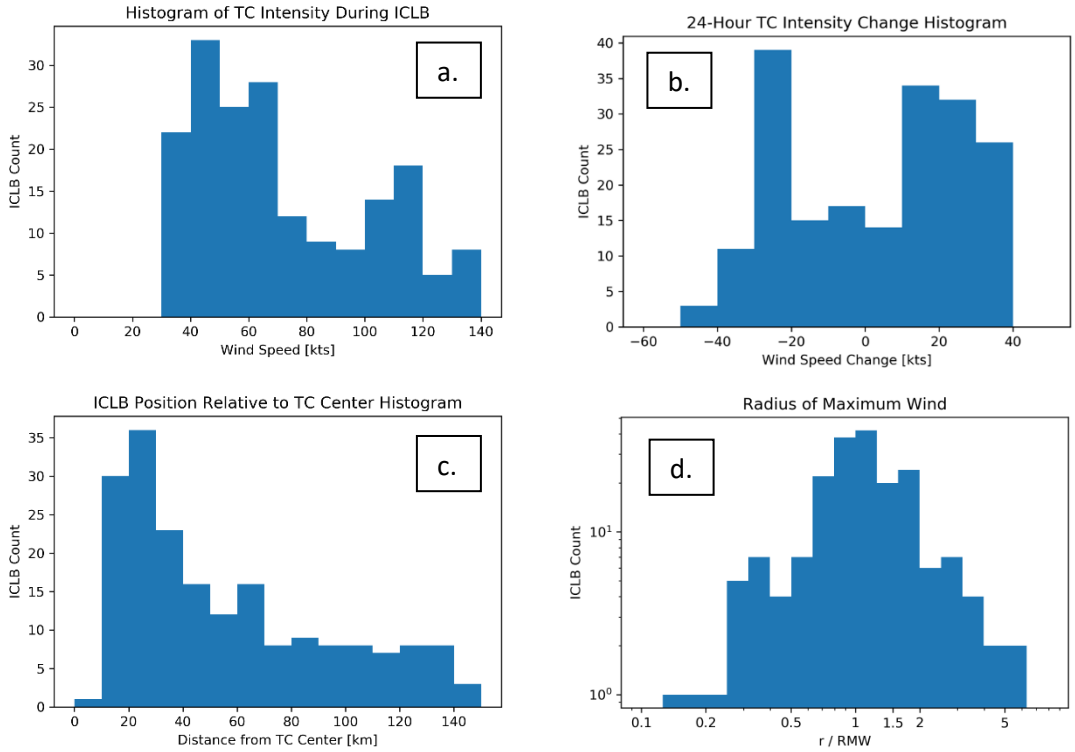

Figure 4.3. ICLB Distribution Histograms. Histograms showing the (a.) TC intensity at the time of the ICLB measured in sustained wind speed in kt, (b.) the distribution of 24-hour post-ICLB TC wind speed intensity change in kt, (c.) the distance the ICLBs occurred from the TC center in km, and (d.) the ICLB position relative to multiple of the RMW, plotted on a logarithmic x-axis.

found weaker TCs tend to have more lightning than stronger TCs. Figure 4.3.a plots TC intensity at the time the flash activity occurred and shows a positive- or right-skewed distribution, meaning a greater number of the two-hour periods occurred while the TCs were still tropical storms or Category 1 hurricanes as opposed to major hurricanes. It is notable that there is a secondary peak in ICLBs for major hurricanes, which may support Vagasky (2017), who identified lightning features that enveloped the eyewall for several

hours in intense TCs. Figure 4.3.b exhibits a bimodal distribution of 24-hr intensity change following the ICLBs, from which it is clear that the mere presence of an ICLB is not sufficient to inform intensity change forecasts. Figure 4.3.c plots the radial ICLB position, and its right-skewed distribution indicates a decrease in ICLB frequency with increasing radial distance from the TC center. Perhaps the most insightful plot from these histograms is Figure 4.3.d, which displays ICLBs as a function of their position relative to the RMW, and exhibits an approximately log-normal distribution (-0.40 skewness; +1.4 kurtosis in logarithmic space). The curve peaks in the two bins nearest to 1 RMW, with the majority of the dataset positioned within $0.5 < r < 2$ RMW, where r is the relative position of the ICLB. The extent of the peak near one RMW is partially explained by the method of plotting two-hour lightning activity periods. All three of the aforementioned TCs with near continuous flashes would be contributing towards the center bins of that distribution, so under an ICLB definition with discrete bursts of O(1 hr), the peakedness of the curve would be expected to decrease.

Given the 194 two-hour ICLB activity periods, several 24-hour intensity change means can be computed for various TC groupings. Naively computing the 24-hour intensity change average for all 194 periods together, ignoring position relative to the RMW, returns a very slight preference for intensification at +1.1 kt. Considering only the episodic, non-continuous bursts returns a stronger preference for intensification at +3.1 kt. In contrast, averaging the continuous cases together produces a net preference for weakening in the following 24 hours at -4.3 kt.

Now considering these data in the context of the RMW relationship described in Stevenson et al. (2018), Table 4.2 summarizes the average 24-hour intensity change of the sample divided into three RMW groupings (interior to 1 RMW, between 1 and 1.5 RMW, and exterior to 1.5 RMW) for several TC categorizations, including by burst duration, basin, and inner-core definition.

Categorization	r/RMW <= 1	1< r/RMW <= 1.5	r/RMW > 1.5
All 2-Hr Periods	9.07	-2.84	-9.04
All 2-Hr Count	89	58	47
Non-Continuous Only	13.63	-1.21	-8.59
Non-Continuous Count	64	33	46
Continuous Only	-2.60	-5.00	-30.00
Continuous Count	25	25	1
ENP Only	6.89	-11.97	-11.91
ENP Count	33	19	17
NA Only	10.36	1.60	-7.42
NA Count	56	39	30
Rigid 100 km Cutoff	8.75	-6.08	-11.28
100 km Count	78	44	39

Table 4.2. 24-Hour Intensity Change Averages Following ICLB. Average 24-hour intensity change following a two-hour ICLB activity period from the GLM-observed dataset. Positive values indicating upcoming storm strengthening are highlighted in peach, negative values indicating upcoming storm weakening are highlighted in blue. Number of values included in each average are displayed below each mean.

Figure 4.4 visualizes the complete distribution of counts by RMW and intensity change for all 2-hr periods in Table 4.2 and Figure 4.2. Interior to 1 RMW, there are more ICLBs preceding intensification, and the inverse for ICLBs beyond 1.5 RMW, where there are more ICLBs preceding weakening. Lightning activity periods interior to the RMW preceded an average period of strengthening of +9.1 kt (Table 4.2, first row),

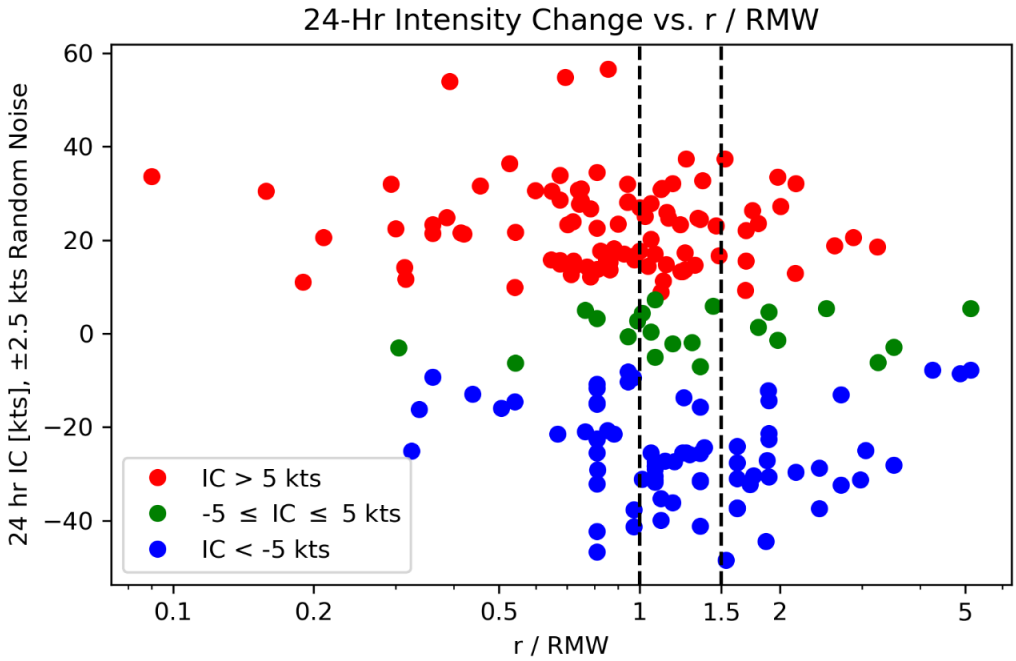

Figure 4.4. 24-Hour Intensity Change vs. r/RMW, Strengthening / Weakening. Semi-logarithmic scatter plot of 24-hr storm intensity change vs. ICLB burst position relative to the RMW. Data points are colored to emphasize increasing intensity (red), near constant intensity (green), and decreasing intensity (blue). ±2.5 kt of random noise have been added to the intensity change values for data visualization purposes. Vertical dashed lines mark 1 and 1.5 RMW.

whereas a nearly equal in magnitude period of weakening occurs for those exterior to 1.5 RMW at -9.0 kt. The 1 < r/RMW <= 1.5 range demonstrates a much more evenly distributed set of points, with the average presenting a small preference for future weakening. Further removing all storms beyond the traditional rigid inner-core cutoff of 100 km produces a stronger preference for weakening between 1 and 1.5 RMW, but otherwise generates comparable means. Notably, the gap in strengthening storms that existed in Stevenson et al. (2018)'s plot between 1 and 1.5 RMW is not present in this GLM dataset.

Isolating the non-continuous ICLBs, the averages become more positive overall, with an especially noteworthy preference for intensification for RMW-interior bursts,

reaching +13.6 kt. This is the strongest magnitude change in any categorization with more than one data point, and especially highlights a likely separation in storm dynamics between continuous and non-continuous ICLBs. For the continuous bursts, all three radial RMW ranges averaged to values of future weakening.

Across the two ocean basins, the results are consistent for the two extreme RMW ranges but diverge for the intermediate range between 1 and 1.5 RMW. In this 1 to 1.5 RMW range in the NA, an average of 39 two-hour periods results in a slight preference for intensification at +1.60 kt, the only classification that returns a net positive mean for this radial RMW range. ENP storms reflected a much stronger preference for future weakening at -11.97 kt.

Fitting trendlines to the data in Figure 4.4 is another way to confirm the overall decrease in 24-hour intensity change with increasing ICLB position expressed as an RMW multiple. A linear function will appear curved in the semi-log plot, whereas a logarithmic best-fit appears as a line. The best fit curves obtained were IC [kt] = -6.95 * (r/RMW) + 9.78 with an R^2 value of 0.05567, and IC [kt] = -11.8 * ln(r/RMW) + 1.54 with an R^2 value of 0.09004. While the R^2 values are low, the negative slopes confirm a decrease in 24-hour intensity change as RMW increases.

Recall that Stevenson et al. (2018) found a preference for intensification both interior to 1 RMW and exterior to 1.5 RMW, with the steady-state or weakening preference occurring between these two points. Table 4.3 evaluates this GLM sample against their 24-hr intensity change findings, as an independent test of their prediction. 31% of the two-hour periods produce intensity changes that are in opposition to the RMW relationship they established. Notably, the GLM data largely agreed with the

established relationship for future periods of RI. Accounting for RMW uncertainty by including ambiguous periods, up to 93% of the two-hour RI periods in this study could be counted as correctly predicted. In contrast, one-third of the RW periods were incorrectly

Periods	2-Hr ICLB Activity	RI	RW
Count	194	26	36
Agree w/ S18	106	23	14
Agree %	55%	79%	39%
Ambiguous	27	4	10
Ambiguous %	14%	14%	28%
Disagree w/ S18	61	2	12
Disagree %	31%	7%	33%

Table 4.3. RI and RW Comparison to S18. Statistics of GLM-observed two-hour ICLB activity periods that agree or disagree with the RMW-relative location-implied upcoming intensity change hypothesis noted by Stevenson et al. (2018).

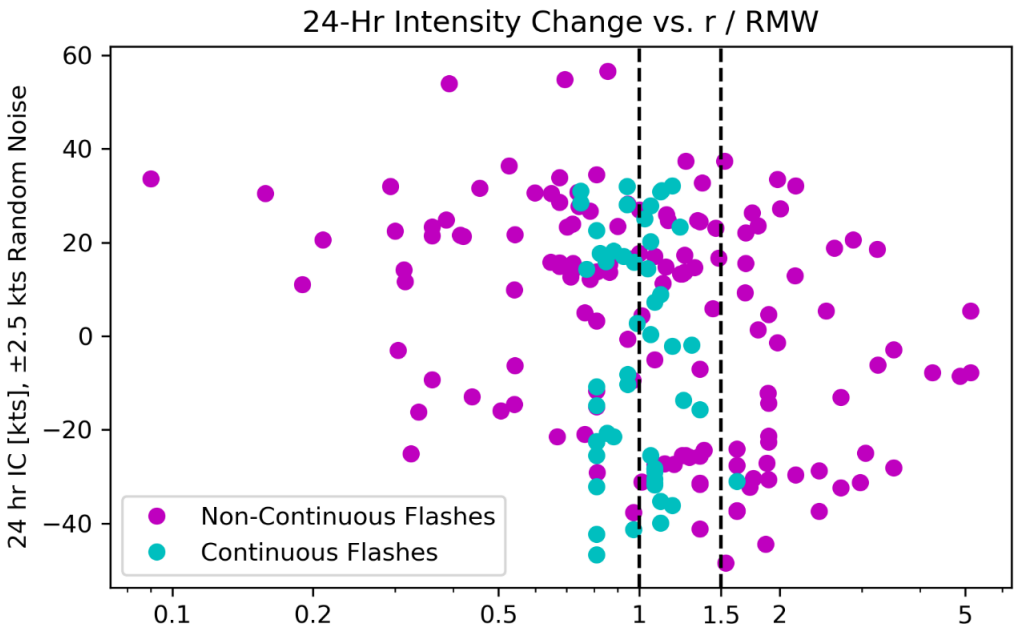

Figure 4.5. 24-Hour Intensity Change vs. r/RMW, Continuous / Non-continuous. Semi-logarithmic scatter plot of 24-hr storm intensity change vs. ICLB burst position relative to the RMW. Data points are colored to separate non-continuous two-hour flash periods (magenta) from the continuous two-hour flash periods (cyan). ±2.5 kt of random noise have been added to the intensity change values for data visualization purposes. Vertical dashed lines mark 1 and 1.5 RMW.

predicted. An additional 28% of the periods were ambiguous based on the RMW imprecision, giving a 67% maximum success rate for RW cases.

Recoloring Figure 4.4 based on alternate classifications offers further insights in some cases. Separating the nearly continuous flash periods from the non-continuous cases in Figure 4.5 reveals a much wider radial distribution in the non-continuous regime. Nearly all of the continuous flash events are centered around 1 RMW, rarely deviating more than about two tenths of an RMW multiple away. That fact provides further evidence that these continuous flashes seem to approximately track the RMW, and in the absence of aircraft reconnaissance data, may provide an additional RMW estimate independent of satellite imagery.

Figure 4.6 recolors the same data again based on ocean basin. Each quadrant of the plot contains storms in both the NA and the ENP. Stevenson et al. (2018) had seen evidence for a basin dependence, with NA TCs experiencing a greater preference for intensification than ENP TCs. While the means from Table 4.2 do weakly agree with those findings, the strongest intensification rate of any storms in the sample were in Barbara and Kiko (+55 kt in 24 hr), both ENP basin storms. This GLM data set does not support a significant basin dependence, especially interior of 1 RMW and exterior of 1.5 RMW. Between these two limits, there is a net 13.57 kt difference in 24-hr intensity change between the two basins (Table 4.2), though only 19 two-hour periods for the ENP occurred in this dataset, so this may be a function of small number statistics more so than a truly different physical response between basins.

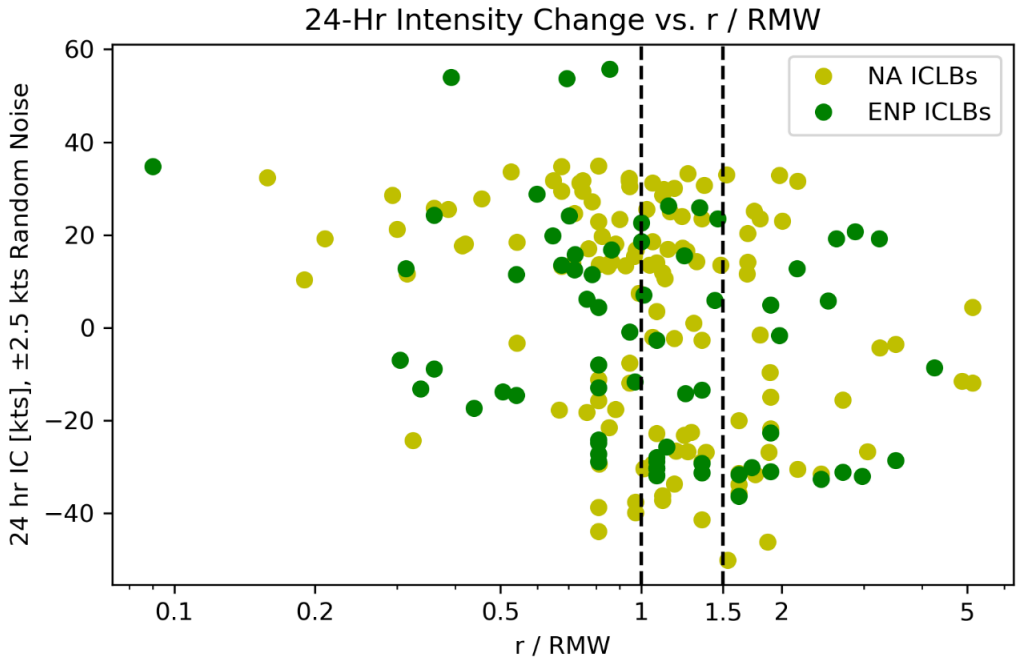

Figure 4.6. 24-Hour Intensity Change vs. r/RMW, NA / ENP. Semi-logarithmic scatter plot of 24-hr storm intensity change vs. ICLB burst position relative to the RMW. Data points are colored to separate NA basin two-hour flash periods (gold) from ENP basin two-hour flash periods (green). ±2.5 kt of random noise have been added to the intensity change values for data visualization purposes. Vertical dashed lines mark 1 and 1.5 RMW.

The next recoloring is shown in Figure 4.7 and displays actual physical distance the ICLB period occurred from the TC center. This plot does not appear to have significant structure but is included for completeness. ICLBs with an average TC center distance of 20 km precede both periods of +30 kt RI and -30 kt RW. Likewise, TC center distances near 100 km fill the parameter space, covering both intensification and weakening cases.

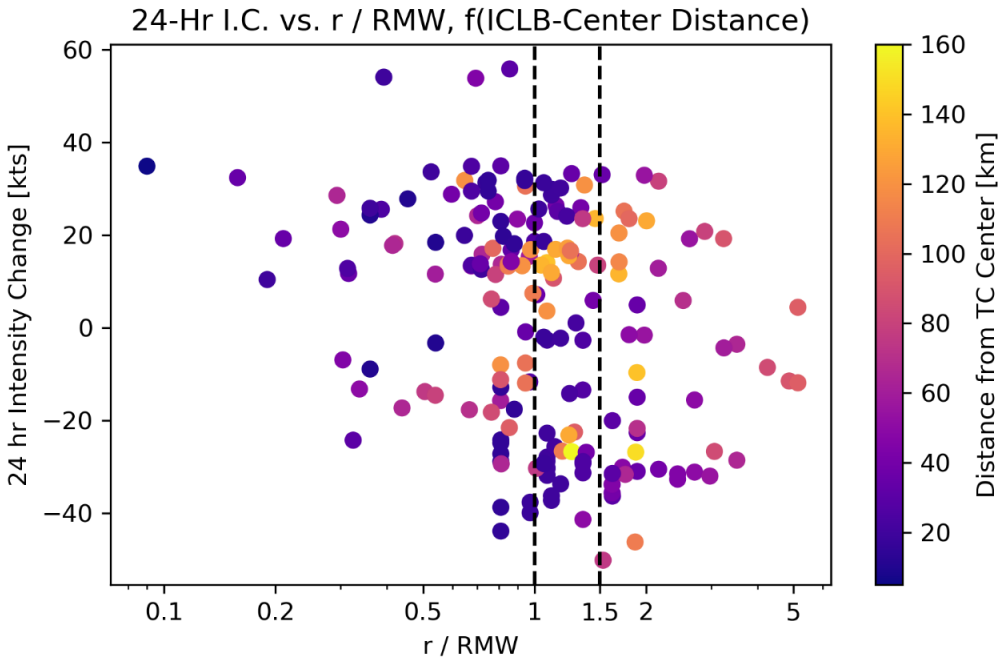

Figure 4.7. 24-Hour Intensity Change vs. r/RMW, Distance from TC Center. Semi-logarithmic scatter plot of 24-hr storm intensity change vs. ICLB burst position relative to the RMW. The color fill corresponds to the physical distance each two-hour ICLB period occurs from the TC center [km]. ±2.5 kt of random noise have been added to the intensity change values for data visualization purposes. Vertical dashed lines mark 1 and 1.5 RMW.

The symbol color in Figure 4.8 shows the maximum sustained wind speed of the TC at the time GLM observed the ICLB. This plot reveals that the stronger the intensity of the storm, the greater the preference for the lightning to be located near 1 RMW. The large majority of ICLBs at either RMW extreme are Category 1 or weaker on the SSHWS. Notably, there appears to be little difference in the 24-hr intensity change preference as a function of maximum sustained wind speed, other than SSHWS Category 5 storms (≥137 kt wind speeds) typically preceding weakening. However, several Category 3 and 4 TC bursts precede a 24-hr period of intensification of at least 17.5 kt, so both directions of intensity change are observed in major hurricanes.

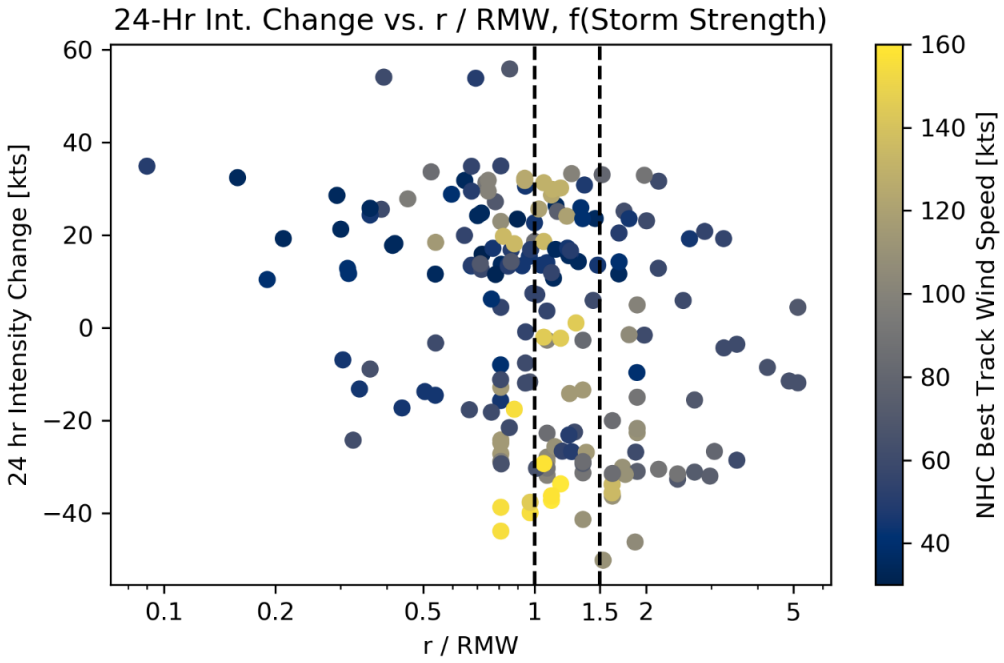

Figure 4.8. 24-Hour Intensity Change vs. r/RMW, Wind Speed. Semi-logarithmic scatter plot of 24-hr storm intensity change vs. ICLB burst position relative to the RMW. The color fill corresponds to the maximum sustained wind speed [kt] at the time of the ICLB, as reported by the NHC Best Track. ±2.5 kt of random noise have been added to the intensity change values for data visualization purposes. Vertical dashed lines mark 1 and 1.5 RMW.

p. GLM Flash Characteristic Trends

Plotted on axes of radial distance from TC center vs. time, most TC flash activity clusters evaluated appear as vertical signals, meaning at a given time interval, the flashes in the burst occurred at a range of radial distances. However, some signals have distinct non-vertical components to their slopes, suggesting lightning that is associated with a particular TC convective cell or propagating wave and that the detections are tracking the local storm cell motion towards or away from the TC center. For example, a positive-slope signal (indicating outward movement) appeared in Barbara (2019 ENP) during early strengthening (pre-RI) around 0600 UTC 1 July exterior to the RMW and in

Raymond (2019 ENP) during weakening around 1100 UTC 16 November interior to the RMW. Negative-slope signals (indicating movement towards the TC center) were seen in Jerry (2019 NA), Kiko (2019 ENP), and Lorena (2019 ENP), all during weakening phases (though Lorena's was influenced by land interaction).

Of the 8 TCs which underwent RI, two primary lightning locations emerged associated with this rapid strengthening. In Barbara, Kiko, Michael (2018 NA), and Jerry, an ICLB occurred interior to the RMW very near the beginning of RI. Then as the RI phase was reaching its conclusion, ICLBs occurred exterior to the RMW in Juliette (2019 ENP), Kiko, Chris (2018 NA), Dorian (2019 NA), and Jerry. Erick (2019 ENP) and Dorian both contained the long-duration, approximately RMW-tracking nearly continuous bursts. Erick's began at the end of RI and continued through early, slow, initial weakening, which is very similar in time relative to the storm cycle as the second sequence of continuous bursts in Dorian. The first two-thirds of Dorian's first long-duration ICLB occurred during a phase of strengthening that did not meet the RI criterion, though the final-third did align with the beginning of Dorian's second RI phase.

Of the 7 RW TC cases, fewer patterns emerged in flash radial location. Alvin (2019 ENP) and Barbara contained minimal flash activity within 100 km of the TC centers. Dorian and Erick's continuous bursts continued into the early portions of RW before a decline in flash rate and a return to more discrete time clusters of flash activity. Humberto (2019 NA) had a quicker outward propagating burst during early RW, though this was primarily at 75 km and larger from the TC center. Kiko and Jerry both had bursts that covered wide radial distance ranges later in their weakening phases. Both appear to

be inward-propagating features, though the signal is more pronounced and from a greater radial distance in Jerry than in Kiko.

Around the onset of weakening, Alberto (2018 NA), Alvin, Barbara, Chris, Humberto, Jerry, and Juliette (2019 ENP) all had a distinct lack of flashes interior to the RMW, with varying degrees of flash activity exterior to the RMW. Kiko produced a few flashes interior to the RMW, but most detections in that loose time cluster occurred exterior to the RMW. Barry (2019 NA), Dorian, and Erick, the three TCs with the nearly continuous bursts, had ICLBs that approximately tracked the RMW during this transition to weakening. Michael and Lorena's weakening periods were influenced by land interaction so are neglected here. This leaves Raymond as the only weakening TC in this study with significant flash activity interior to the RMW. While the validity of the ATCF b-deck reported RMW values for this system are questionable due to their atypical expansion with storm intensification, flashes were present interior to 0.5 RMW. It is notable that Raymond was the weakest TC in this study at peak intensity in terms of both sustained wind speed and minimum central pressure. In future work, checking other weak TCs for this interior RMW signal may diagnose a difference in expected flash signals between similar storms with weakly defined inner-cores and more organized TCs.

Dorian was the only TC in the sample that exhibited the FED increase, AFA decrease, and TOE decrease as it transitioned to weakening to the extent that it did, which was placed in physical context in Duran et al. (2021). Michael produced large AFA throughout its period of strengthening and underwent a flash rate increase alongside RI, but TOE decreased interior to the RMW while the storm was still strengthening. Barbara did not have flashes interior to the RMW during weakening, but those exterior to it were

smaller in AFA and smaller in TOE. However, FED had declined significantly as well. Alberto presented a similar signal, with FED, AFA, and TOE all declining from early strengthening as the storm approached peak intensity. AFA in Erick increased as the storm progressed from initial strengthening to RI to weakening, and TOE remained large. Kiko had its largest TOE flashes deep into its weakening process. Although a general pattern connecting changes in these parameters relative to storm intensity change has not emerged, future work should revisit these trends as GLM accumulates data on more TCs.

Within a particular ICLB, differences based on radial distance from the TC center emerged in certain storms. Checking ICLBs interior to the RMW during strengthening, Alvin and Barbara had bursts with AFA largest further from the TC center but TOE largest nearest the TC center. Kiko's had larger AFA with greater radial distance, but FED and TOE were larger with distance as well. Exterior to the RMW nearing the end of strengthening, Humberto had an ICLB similar to Kiko in that AFA and TOE were larger further from the TC center, though this was not reflected in FED. Interior to the RMW, Michael and Raymond had bursts with largest AFA nearest to the TC center and TOE was greater with increased TC center distance. Though these trends described above are noted in select subsets of the 14 TCs studied, no clear pattern was identified across the set of ICLBs in this dataset.

CHAPTER 5

CONCLUSIONS

Continuous monitoring of both the ENP and NA ocean basins by GLM has provided a new dataset with which to probe lightning in TC environments and determine if its location or physical parameters can be used to diagnose 24-hour TC intensity change. Checks of detection efficiency with minimum detected energy in single groups were carried out over both ocean basins, and minimal variability appeared in either region, providing confidence that shifts in GLM flash parameter statistics recorded were actual physical storm responses and not observation artifacts. 14 TCs have been analyzed, including eight that underwent RI and seven that underwent RW. In total, these TCs produced ICLB activity in 194 two-hour periods in non-landfalling conditions. 11 TCs had distinct, episodic bursts of flash activity only, but three TCs (Barry, Dorian, and Erick) produced four periods of long-duration, nearly continuous flashes for 15-hour periods or longer. Each of these bursts occurred very near to the estimated RMW and is suggestive of a different set of physical dynamics than in the episodic-flash TCs. Raymond was the only TC in this study with significant flash activity appreciably interior to the RMW during the onset of weakening.

Inner-core flash activity as observed by GLM generally supports many previous conclusions about TC lightning obtained with NLDN, WWLLN, and other detection networks. NA TCs tend to have greater flash density than ENP TCs, weaker TCs tend to have more lightning than stronger TCs, the existence of an ICLB alone is not sufficient to predict upcoming intensity change, and lightning in any given TC is episodic. This

episodic nature of lightning in TCs means the absence of inner-core flashes does not necessarily preclude TC strengthening.

ICLBs interior to the RMW preceded an average 24-hour intensity change of +9.07 kt, which is in agreement with the RMW relationship established in Stevenson et al. (2018). Non-continuous burst cases produced an even stronger preference for intensification (+13.63 kt), though the nearly continuous flash cases preceded an average intensity decline of -2.60 kt. Both ENP and NA storms with bursts interior to the RMW had 24-hour preferences for intensification. A marked difference, however, is found from the previously established relationship exterior to the RMW. The gap in intensifying storms between 1 and 1.5 RMW found in Stevenson et al. (2018) has been populated with many cases, bringing the average 24-hour intensity change for TCs with an ICLB here to -2.84 kt. Bursts observed by GLM beyond 1.5 RMW from the TC center averaged a 24-hour intensity change decrease of -9.04 kt, which is in opposition to the findings of Stevenson et al. (2018), who found a preference for intensification. Both ENP and NA basin systems experienced these 24-hour intensity declines, and using the rigid 100 km inner-core definition, the average 24-hour intensity decrease is even larger in magnitude at -11.28 kt. The basin dependence noted in Stevenson et al. (2018) is also not very well supported by the GLM data, particularly interior of 1 RMW and exterior of 1.5 RMW. NA TCs did have about +4 kt more positive average intensity changes than ENP TCs, but both preferred weakening exterior to 1.5 RMW and strengthening interior to 1 RMW. Between 1 and 1.5 RMW, there is a sizeable difference in average intensity change, however, this may be in part a function of having only 19 activity periods in the ENP basin at this range.

Rapidly intensifying storms tended to produce more predictable lightning signals than rapidly weakening TCs. Four of the eight TCs which underwent RI had an ICLB interior to the RMW near the beginning of the rapid strengthening, and five of the eight had an ICLB exterior to the RMW as RI was concluding. Lightning signals associated with RW were more divergent in structure, and nearly one-third of the RW periods recorded were ambiguous in terms of supporting or contradicting the established intensity change expectation due to uncertainty in the RMW.

RMW uncertainty is undoubtedly the largest source of error in this study and will continue to make implementing expectations about future TC development using lightning in operational forecasting a challenge. While work continues in the TC community on algorithms to determine best estimates of the RMW through satellite imagery, presently aircraft reconnaissance remains the ideal method for obtaining this data, but time coverage limitations mean that it often cannot be used as the sole measure for the full TC time history. Use of the ATCF b-deck RMW values allowed for inclusion of several storms without available aircraft data in this analysis, though the lack of uncertainty value is a noted limitation. One wish for future ATCF outputs would be to include an indication of uncertainty on each data point to better understand the confidence in each reported value. In Stevenson et al. (2018), they retained only data points for which there was aircraft reconnaissance available within 1 hour of the observed ICLB. As GLM accumulates more observed TCs, the analysis in this work can be repeated with stricter criteria for inclusion based on availability of aircraft reconnaissance. Additionally, future work might investigate the hypothesis that the dynamics of long-duration, continuous burst cases are explicitly a result of dynamics that

occur at the RMW. That understanding would, in turn, allow the relative radial lightning position to be used as a marker of the RMW in continuous lightning cases, which has significant practical value when relying on satellite observations rather than in-situ data.

REFERENCES

Abarca, S. F., Corbosiero, K. L., & Galarneau Jr., T. J. (2010). An evaluation of the Worldwide Lightning Location Network (WWLLN) using the National Lightning Detection Network (NLDN) as ground truth. J. Geophys. Res., 115, D18206. doi:10.1029/2009JD013411.

Abarca, S. F., Corbosiero, K. L., & Vollaro, D. (2011). The World Wide Lightning Location Network and convective activity in tropical cyclones. Mon. Wea. Rev., 139, 175-191. https://doi.org/10.1175/2010MWR3383.1.

Ahrens, C. Donald. (2013). *Meteorology today: An introduction to weather, climate, and the environment.* Brooks/Cole, Cengage Learning.

Avila, L. A. (2019). Hurricane Lorena (EP152019). Tropical Cyclone Report, National Hurricane Center. 20 pp.

Avila, L. A., Stewart, S. R., Berg, R., & Hagen, A. B. (2020). Hurricane Dorian (AL052019). Tropical Cyclone Report, National Hurricane Center. 74 pp.

Beven II, J. L., Berg, R., & Hagen, A. B. (2019). Hurricane Michael (AL142018). Tropical Cyclone Report, National Hurricane Center. 86 pp.

Berg, R. (2018). Tropical Storm Alberto (AL012018). Tropical Cyclone Report, National Hurricane Center. 44 pp.

Blake, E. S. (2018). Hurricane Chris (AL032018). Tropical Cyclone Report, National Hurricane Center. 12 pp.

Blake, E. S., & Wroe, D. (2021). Hurricane Erick (EP062019). Tropical Cyclone Report, National Hurricane Center & Central Pacific Hurricane Center. 19 pp.

Brown, D. P. (2019). Hurricane Jerry (AL102019). Tropical Cyclone Report, National Hurricane Center. 17 pp.

Brown, D. P. (2020). Tropical Storm Raymond (EP202019). Tropical Cyclone Report, National Hurricane Center. 15 pp.

Bruning, E. C. & MacGorman, D. R. (2013). Theory and observations of controls on lightning flash size spectra. J. Atmos. Sci., 70(12), 4012-4029. https://doi.org/10.1175/JAS-D-12-0289.1.

Bruning, E. C. (2019). glmtools. https://github.com/deeplycloudy/glmtools/.

Bruning, E. C., et al. (2019). Meteorological imagery for the Geostationary Lightning Mapper. J. Geophys. Res. Atmos., 124, 14258-14309. https://doi.org/10.1029/2019JD030874.

Cangialosi, J. P. (2019). Hurricane Barbara (EP022019). Tropical Cyclone Report, National Hurricane Center. 14 pp.

Cangialosi, J. P., Hagen, A. B., & Berg, R. (2019). Hurricane Barry (AL022019). Tropical Cyclone Report, National Hurricane Center. 31 pp.

Corbosiero, K. L., Molinari, J., & Black, M. L. (2005). The structure and evolution of Hurricane Elena (1985). Part I: Symmetric intensification. Mon. Wea. Rev., 133, 2905-2921. https://doi.org/10.1175/MWR3010.1.

Cummins, K. L. (2019). Full domain validation using GLD360. Paper presented at 2019 GLM Annual Science Team Meeting, Huntsville, Alabama. https://goes-r.nsstc.nasa.gov/home/sites/default/files/2019-09/Cummins2019_GLM_GLD360_Sep10.pptx.

DeMaria, M., DeMaria, R. T., Knaff, J. A., & Molenar, D. (2012). Tropical cyclone lightning and rapid intensity change. Mon. Wea. Rev., 140, 1828-1842. https://doi.org/10.1175/MWR-D-11-00236.1.

DeMaria, M., Sampson, C. R., Knaff, J. A., & Musgrave, K. D. (2014). Is tropical cyclone intensity guidance improving? Bulletin of the American Meteorological Society, 95(3), 387-398. https://doi.org/10.1175/BAMS-D-12-00240.1.

Duran, P., et al. (2021). The evolution of lightning flash density, flash size, and flash energy during Hurricane Dorian's (2019) intensification and weakening. Geophys. Res. Lett., 48, e2020GL092067. https://doi.org/10.1029/2020GL092067.

“D-value” (2012). Glossary of Meteorology, American Meteorological Society. https://glossary.ametsoc.org/wiki/D-value.

Fierro, A. O., Stevenson, S. N., & Rabin, R. M. (2018). Evolution of GLM-observed total lightning in Hurricane Maria (2017) during the period of maximum intensity. Mon. Wea. Rev., 146, 1641-1666. https://doi.org/10.1175/MWR-D-18-0066.1.

GOES-R Series Program Office (2017). Product definition and user's guide. Volume 3: Level 1b products. DCN 7035538, Revision F.1, available at https://www.goes-r.gov/users/docs/PUG-L1b-vol3.pdf.

GOES-R Series Program Office (2019). GOES-R series data book. CDRL PM-14 Rev. A., May 2019, available at https://www.goes-r.gov/downloads/resources/documents/GOES-RSeriesDataBook.pdf.

Goodman, S. J., Mach, D. M., Koshak, W. J., & Blakeslee, R. J. (2010). Algorithm Theoretical Basis Document (ATBD) for the GLM lightning cluster-filter algorithm. NOAA/NESDIS Center for Satellite Applications and Research v2.0.

Goodman, S. J., et al. (2013). The GOES-R Geostationary Lightning Mapper (GLM). Atmospheric Research, 125-126, 34-49. https://doi.org/10.1016/j.atmosres.2013.01.006.

Griffin, S. (2017). Climatology of tropical overshooting tops in North Atlantic tropical cyclones, J. Appl. Meteorol. Climatol., 56, 6, 1783-1796. doi:10.1175/JAMCD-16-0413.1.

Jacobson, A. R., Holzworth, R., Harlin, J., Dowden, R., & Lay, E. (2006). Performance assessment of the World Wide Lightning Location Network (WWLLN), using the Los Alamos Sferic Array (LASA) array as ground truth. J. Atmos. Oceanic Technol., 23, 1082-1092. https://doi.org/10.1175/JTECH1902.1.

Jarvinen, B. R., Neumann, C. J., & Davis, M. A. S. (1984). A tropical cyclone data tape for the north Atlantic basin, 1886-1983: Contents, limitations and uses. NOAA Tech. Memo. NWS NHC 22, 21 pp.

Jiang, H. & Ramirez, E. M. (2013). Necessary conditions for tropical cyclone rapid intensification as derived from 11 years of TRMM data. Journal of Climate, 26, 17, 6459-6470. https://doi.org/10.1175/JCLI-D-12-00432.1.

Jorgensen, D. F. (1984). Mesoscale and convective scale characteristics of mature hurricanes. Part I: General observations by research aircraft. J. Atmos. Sci., 41, 1268-1286. https://doi.org/10.1175/1520-0469(1984)041<1268:MACSCO>2.0.CO;2

Jorgensen, D. F., Zipser, E. J., & LeMone, M. A. (1985). Vertical motions in intense hurricanes. J. Atmos. Sci., 42, 839-856. https://doi.org/10.1175/1520-0469(1985)042<0839:VMIIH>2.0.CO;2.

Kaplan, J. & DeMaria, M. (2003). Large-scale characteristics of rapidly intensifying tropical cyclones in the north Atlantic basin. Weather and Forecasting, 18, 6, 1093-1108. https://doi.org/10.1175/1520-0434(2003)018<1093:LCORIT>2.0.CO;2

Knaff, J. A., Longmore, S. P., DeMaria, R. T., & Molenar, D. A. (2015). Improved tropical-cyclone flight-level wind estimates using routine infrared satellite reconnaissance. J. Appl. Meteorol. Climatol., 54, 2, 463-478. https://doi.org/10.1175/JAMC-D-14-0112.1.

Knaff, J. A., et al. (in press). Estimating tropical cyclone surface winds: Current status, emerging technologies, historical evolution, and a look to the future. Tropical Cyclone Research and Review. https://doi.org/10.1016/j.tcrr.2021.09.002.

Kossin, J. P., et al. (2007). Estimating hurricane wind structure in the absence of aircraft reconnaissance. Weather and Forecasting, 22, 1, 89-101. https://doi.org/10.1175/WAF985.1.

Lajoie, F. & Walsh, K. (2008). A technique to determine the radius of maximum wind of a tropical cyclone. Weather and Forecasting, 23, 1007-1015. https://doi.org/10.1175/2008WAF2007077.1.

Landsea, C. W. & Franklin, J. L. (2013). Atlantic hurricane database uncertainty and presentation of a new database format. Mon. Wea. Rev., 141, 3576-3592.

Latto, A. S. (2019 a). Hurricane Alvin (EP012019). Tropical Cyclone Report, National Hurricane Center. 14 pp.

Latto, A. S. (2019 b). Hurricane Juliette (EP112019). Tropical Cyclone Report, National Hurricane Center. 13 pp.

Lay, E. H., Jacobson, A. R., Holzworth, R. H., Rodger, C. J., & Dowden, R. L. (2007). Local time variation in land/ocean lightning flash density as measured by the World Wide Lightning Location Network, J. Geophys. Res., 112, D13111. doi:10.1029/2006JD007944.

"Lightning" (2012). Glossary of Meteorology, American Meteorological Society. https://glossary.ametsoc.org/wiki/Lightning.

Lojou, J.-Y. & Cummins, K. L. (2004). On the representation of two- and three-dimensional total lightning information. In Preprints, Conference on Meteorological Applications of Lightning Data, Paper 2.4, AMS Annual Meeting, San Diego, CA, USA.

Mach, D. M., et al. (2007). Performance assessment of the Optical Transient Detector and Lightning Imaging Sensor. J. Geophys. Res., 112, D09210. https://doi.org/10.1029/2006JD007787.

Molinari, J., Moore, P. K., Idone, V. P., Henderson, R. W., & Saljoughy, A. B. (1994). Cloud-to-ground lightning in Hurricane Andrew. J. Geophys. Res., 99, 16665-16676. https://doi.org/10.1029/94JD00722.

Molinari, J., Moore, P., & Idone, V. (1999). Convective structure of hurricanes as revealed by lightning locations. Mon. Wea. Rev., 127, 520-534. https://doi.org/10.1175/1520- 0493(1999)127<0520: CSOHAR>2.0.CO;2.

Musgrave, K. D., Taft, R. K., Vigh, J. L., McNoldy, B. D., & Schubert, W. H. (2012). Time evolution of the intensity and size of tropical cyclones. J. Adv. Model. Earth Syst., 4, M08001. https://doi.org/10.1029/2011MS000104.

Pan, L., Qie, X., Liu, D., Wang, D., & Yang, J. (2010). The lightning activities in super typhoons over the Northwest Pacific. Sci. China, Ser. D: Earth Sci., 53, 8, 1241-1248. doi:10.1007/s11430-010-3034-z.

Pan, L., Qie, X. & Wang, D. (2014). Lightning activity and its relation to the intensity of typhoons over the Northwest Pacific Ocean. Adv. Atmos. Sci. 31, 581-592. https://doi.org/10.1007/s00376-013-3115-y.

Price, C., Asfur, M., & Yair, Y. (2009). Maximum hurricane intensity preceded by increase in lightning frequency. Nat. Geosci., 2, 329-332. https://doi.org/10.1038/ngeo477.

Rison, W., Thomas, R. J., Krehbiel, P. R., Hamlin, T., & Harlin, J. (1999). A GPS-based three-dimensional lightning mapping system: Initial observations in central New Mexico. Geophys. Res. Lett., 26, 3573-3576.

Rogers, R., Reasor, P., & Lorsolo, S. (2013). Airborne Doppler observations of the inner-core structural differences between intensifying and steady-state tropical cyclones. Mon. Wea. Rev., 141, 2970-2991. https://doi.org/10.1175/MWR-D-12-00357.1.

"Rossby radius of deformation" (2012). Glossary of Meteorology, American Meteorological Society. https://glossary.ametsoc.org/wiki/Rossby_radius_of_deformation.

Rudlosky, S. D., Goodman, S. J., Virts, K. S., & Bruning, E. C. (2019). Initial geostationary lightning mapper observations. Geophysical Research Letters, 46, 1097-1104. https://doi.org/10.1029/2018GL081052.

Rudlosky, S. D. & Virts, K. S. (2021). Dual Geostationary Lightning Mapper observations. Mon. Wea. Rev., 149, 979-998. https://doi.org/10.1175/MWR-D-20-0242.1.

Sampson, C. R. & Schrader, A. J. (2000). The Automated Tropical Cyclone Forecasting System (version 3.2). Bull. Amer. Meteor. Soc., 81, 1231-1240. doi:10.1175/1520-0477(2000)081<1231:TATCFS>2.3.CO;2.

Schubert, W. H. & McNoldy, B. D. (2010). Application of the concepts of Rossby length and Rossby depth to tropical cyclone dynamics. J. Adv. Model. Earth Syst., 2, 7. doi:10.3894/JAMES.2010.2.7.

Shapiro, L. J. & Willoughby, H. E. (1982). The response of balanced hurricanes to local sources of heat and momentum. J. Atmos. Sci., 39, 378-394. https://doi.org/10.1175/1520- 0469(1982)039,0378:TROBHT.2.0.CO;2.

Steranka, J., Rodgers, E. B., & Gentry, R. C. (1986). The relationship between satellite measured convective bursts and tropical cyclone intensification. Mon. Wea. Rev., 114, 1539-1546. https://doi.org/10.1175/1520-0493(1986)114<1539:TRBSMC>2.0.CO;2

Stern, D. P. & Nolan, D. S. (2011). On the vertical decay rate of the maximum tangential winds in tropical cyclones. J. Atmos. Sci., 68, 9, 2073-2094. https://doi.org/10.1175/2011JAS3682.1.

Stern, D. P., Vigh, J. L., Nolan, D. S., & Zhang, F. (2015). Revisiting the relationship between eyewall contraction and intensification. J. Atmos. Sci., 72, 1283-1306. https://doi.org/10.1175/JAS-D-14-0261.1.

Stevenson, S. N., Corbosiero, K. L., & Molinari, J. (2014). The convective evolution and rapid intensification of Hurricane Earl (2010). Mon. Wea. Rev., 142, 4364-4380. doi:10.1175/MWR-D-14-00078.1.

Stevenson, S. N., Corbosiero, K. L., & Abarca, S. F. (2016): Lightning in eastern North Pacific tropical cyclones: A comparison to the North Atlantic. Mon. Wea. Rev., 144, 225-239. doi:10.1175/MWR-D-15-0276.1.

Stevenson, S. N., Corbosiero, K. L., DeMaria, M., & Vigh, J. L. (2018). A 10-year survey of tropical cyclone inner-core lightning bursts and their relationship to intensity change. Weather and Forecasting, 33, 23-36. https://doi.org/10.1175/WAF-D-17-0096.1.

Stewart, S. R. (2020). Hurricane Humberto (AL092019). Tropical Cyclone Report, National Hurricane Center. 44 pp.

Susca-Lopata, G., Zawislak, J., Zipser, E. J., & Rogers, R. F. (2015). The role of observed environmental conditions and precipitation evolution in the rapid intensification of Hurricane Earl (2010). Mon. Wea. Rev., 143, 2207-2223. https://doi.org/10.1175/MWR-D-14-00283.1.

Thomas, J. N. et al. (2004). Accuracy of the Lightning Mapping Array. J. Geophys. Res., 109, D14207. https://doi.org/10.1029/2004JD004549.

Thomas, J. N., Solorzano, N. N., Cummer, S. A., & Holzworth, R. H. (2010). Polarity and energetics of inner core lightning in three intense north Atlantic hurricanes. J. Geophys. Res., 115, A00E15. doi:10.1029/2009JA014777.

Vagasky, C. (2017). Enveloped eyewall lightning: The EEL signature in tropical cyclones. J. Oper. Meteor, 5, 171-179, https://doi.org/10.15191/nwajom.2017.0514.

Vigh, J. L. (2010). Formation of the hurricane eye. Ph.D. dissertation, Colorado State University, 538 pp.

Vigh, J. L. (2021). "About real-time guidance." Tropical Cyclone Guidance Project, National Center for Atmospheric Research. http://hurricanes.ral.ucar.edu/realtime/.

Willoughby, H . E., Clos, J. A., & Shoreibah, M. G. (1982). Concentric eye walls, secondary wind maxima, and the evolution of a hurricane vortex. J. Atmos. Sci., 39, 395-411. https://doi.org/10.1175/1520-0469(1982)039<0395: CEWSWM>2.0.CO;2.

Willoughby, H. E. (1990). Temporal changes of the primary circulation in tropical cyclones. J. Atmos. Sci., 47, 242-264, https://doi.org/10.1175/1520-0469(1990)047,0242:TCOTPC.2.0.CO;2.

Wood, K. M., & Ritchie, E. A. (2015). A definition for rapid weakening of north Atlantic and eastern north Pacific tropical cyclones. Geophys. Res. Lett., 42, 10091-10097. doi:10.1002/2015GL066697.

Xu, W., Rutledge, S. A., & Zhang, W. (2017). Relationships between total lightning, deep convection, and tropical cyclone intensity change. J. Geophys. Res. Atmos., 122, 7047-7063. doi:10.1002/2017JD027072.

Zawislak, J. et al. (2016). Observations of the structure and evolution of Hurricane Edouard (2014) during intensity change. Part I: Relationship between the thermodynamic structure and precipitation. Mon. Wea. Rev., 144, 9, 3333-3354. https://doi.org/10.1175/MWR-D-16-0018.1.

Zelinsky, D. A. (2020). Hurricane Kiko (EP132019). Tropical Cyclone Report, National Hurricane Center. 16 pp.

Zhang, D. & Cummins, K. L. (2020). Time evolution of satellite-based optical properties in lightning flashes, and its impact on GLM flash detection. J. Geophys. Res. Atmos., 125, e2019JD032024. https://doi.org/10.1029/2019JD032024.

Zhang, W., Zhang, Y., Zheng, D., Wang, F., & Xu, L. (2015). Relationship between lightning activity and tropical cyclone intensity over the northwest Pacific. J. Geophys. Res. Atmos., 120, 4072-4089. https://doi.org/10.1002/2014JD022334.

APPENDIX

For all 14 TCs considered in this dataset, three sets of plots are provided in this Appendix. In every set, each row of plots displays data for the same time period, and the text above it provides intensity change, time, date, RMW estimate, and flash count information. In the first set of plots, GLM flashes are shown as circles on axes of radial distance from the center in kilometers vs. time. The left column colors and sizes the flashes by AFA, the center column by FED, and the right column by TOE. Cyan squares indicate NOAA 42 flight derived RMW estimates, the dashed red lines and triangles represent ATCF b-deck RMW values, and the solid red lines show RMW multiples, where 1 RMW is an average estimate for that particular time period.

In both the second and third sets of plots, joint histograms are provided for the 2 km GLM pixels with AFA on the y-axis and another flash parameter on the x-axis (FED in the second plot set, TOE in the third). Horizontal red lines are provided for reference at 272.25 and 1000 km2, where 272.25 km2 is the square of the separation threshold used in the GLM flash clustering algorithm (Goodman et al. 2010). The left column contains flashes interior to the estimated period RMW, and the right column contains flashes exterior to the RMW out to a limit, usually 150 km, but larger when the RMW itself is O(150 km).

Dorian has two entries in the Appendix (six plots total): one using the NHC Best Track and one using the higher precision track created with inspection of satellite imagery.

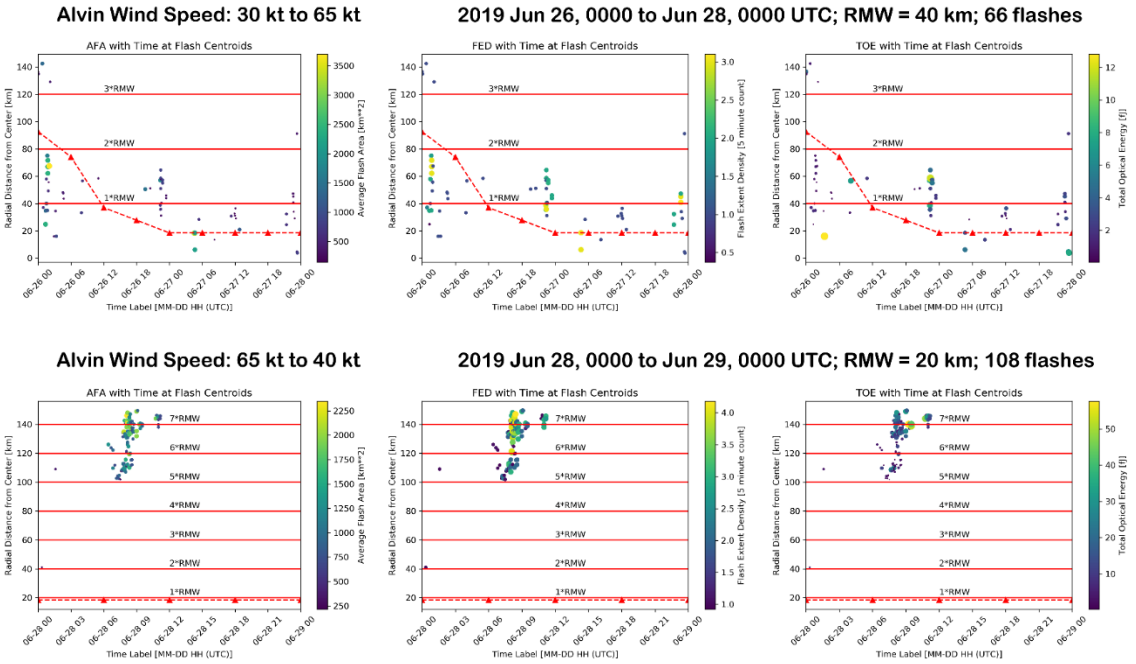

Figure A. 1 Alvin Flashes, Distance from Center vs. Time

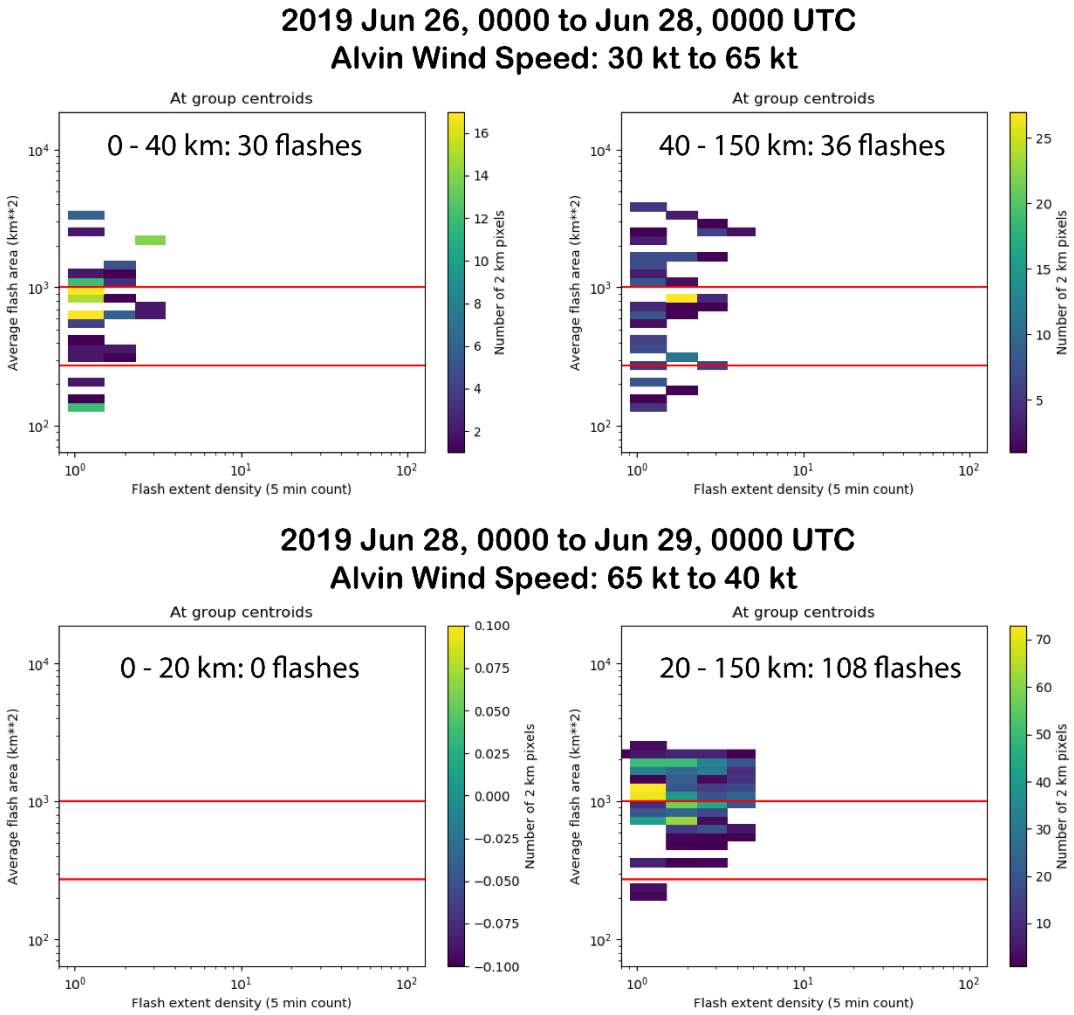

Figure A. 2 Alvin Joint Histogram, AFA vs. FED

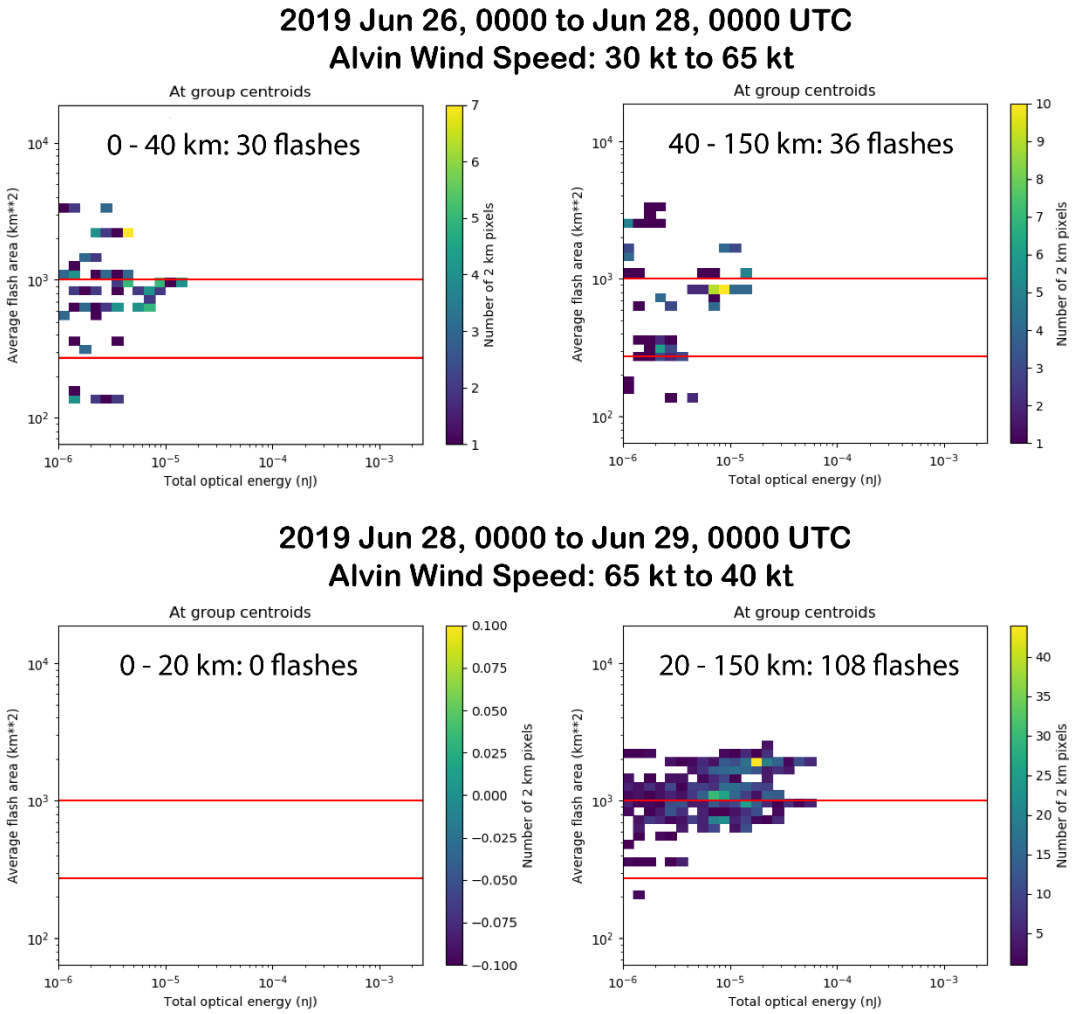

Figure A. 3 Alvin Joint Histogram, AFA vs. TOE

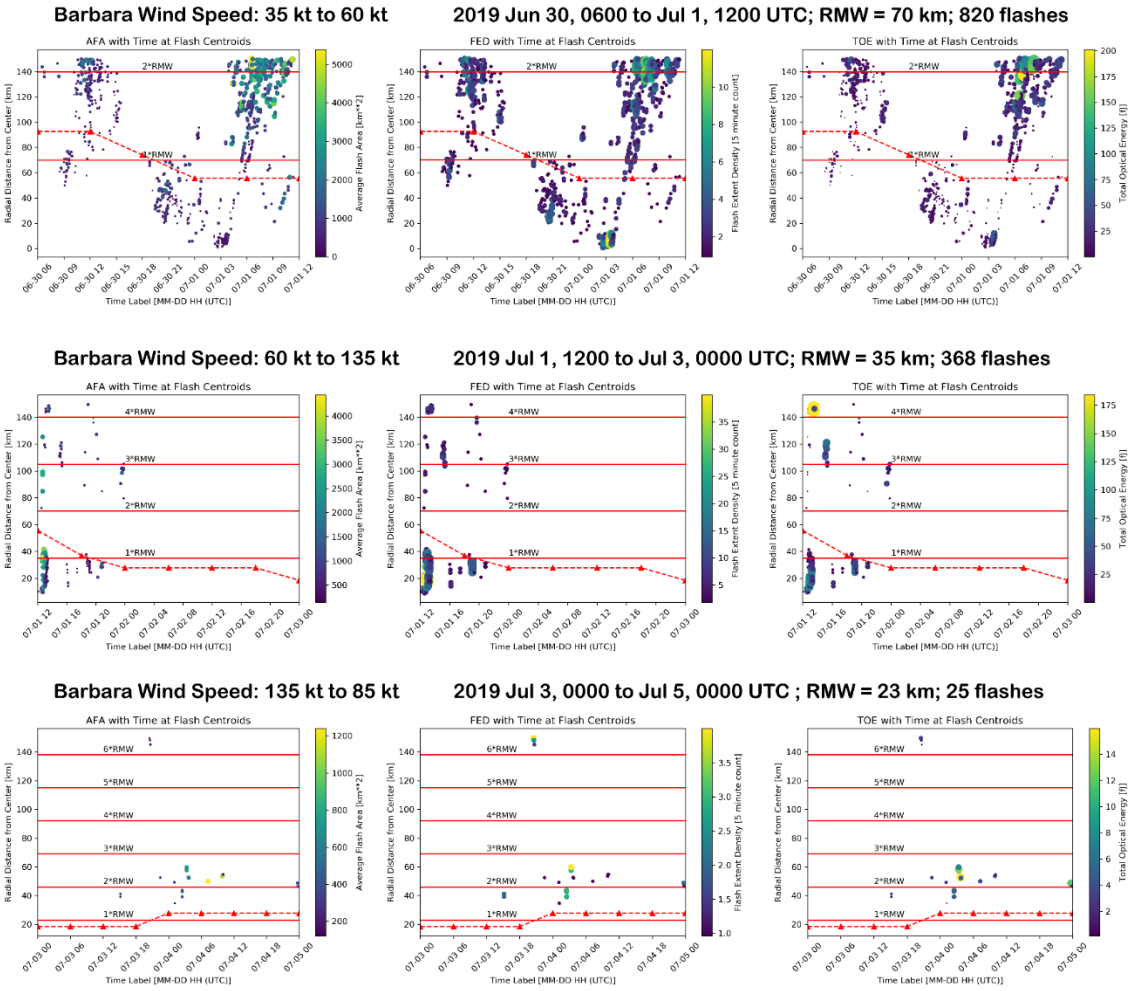

Figure A. 4 Barbara Flashes, Distance from Center vs. Time

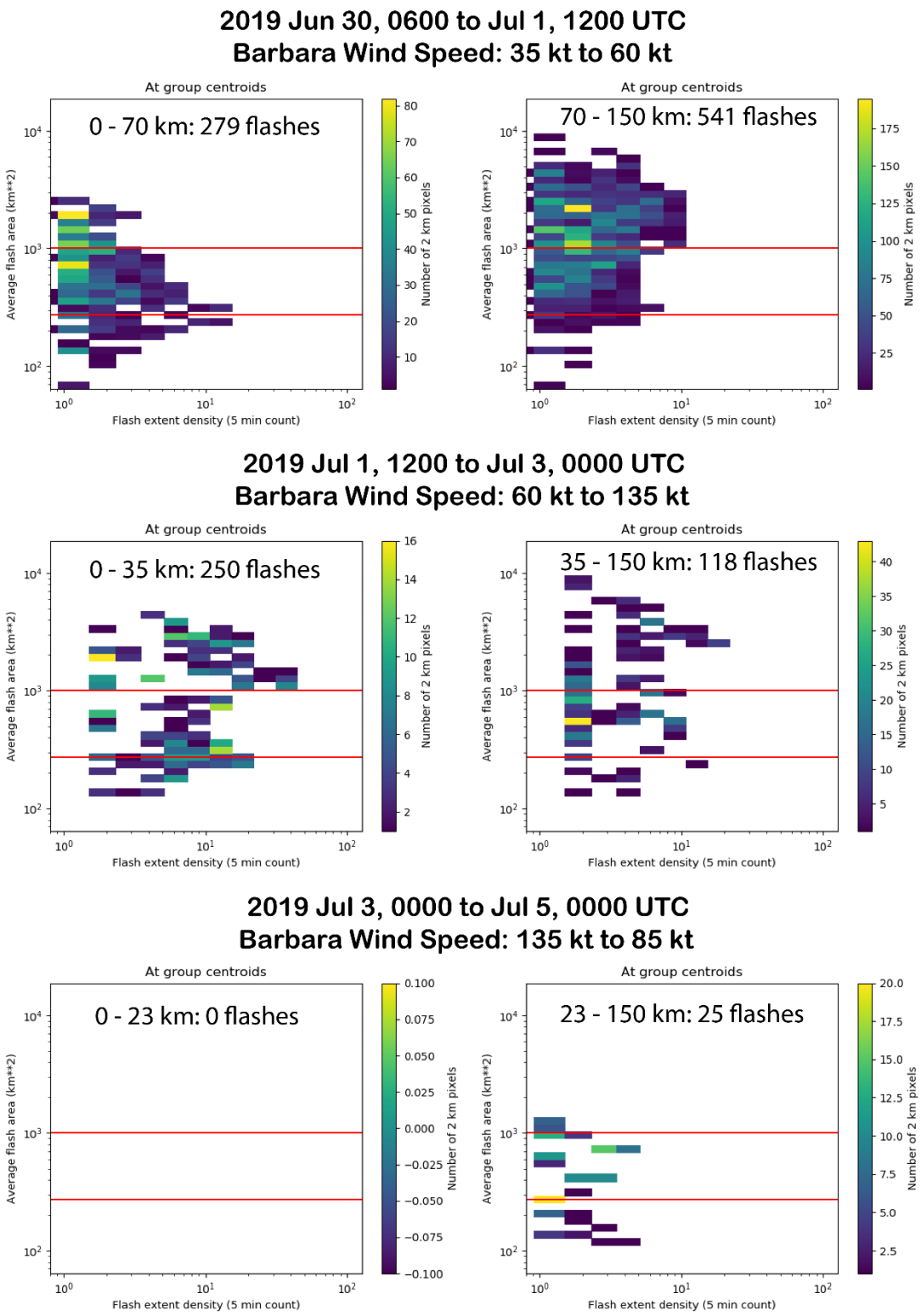

Figure A. 5 Barbara Joint Histogram, AFA vs. FED

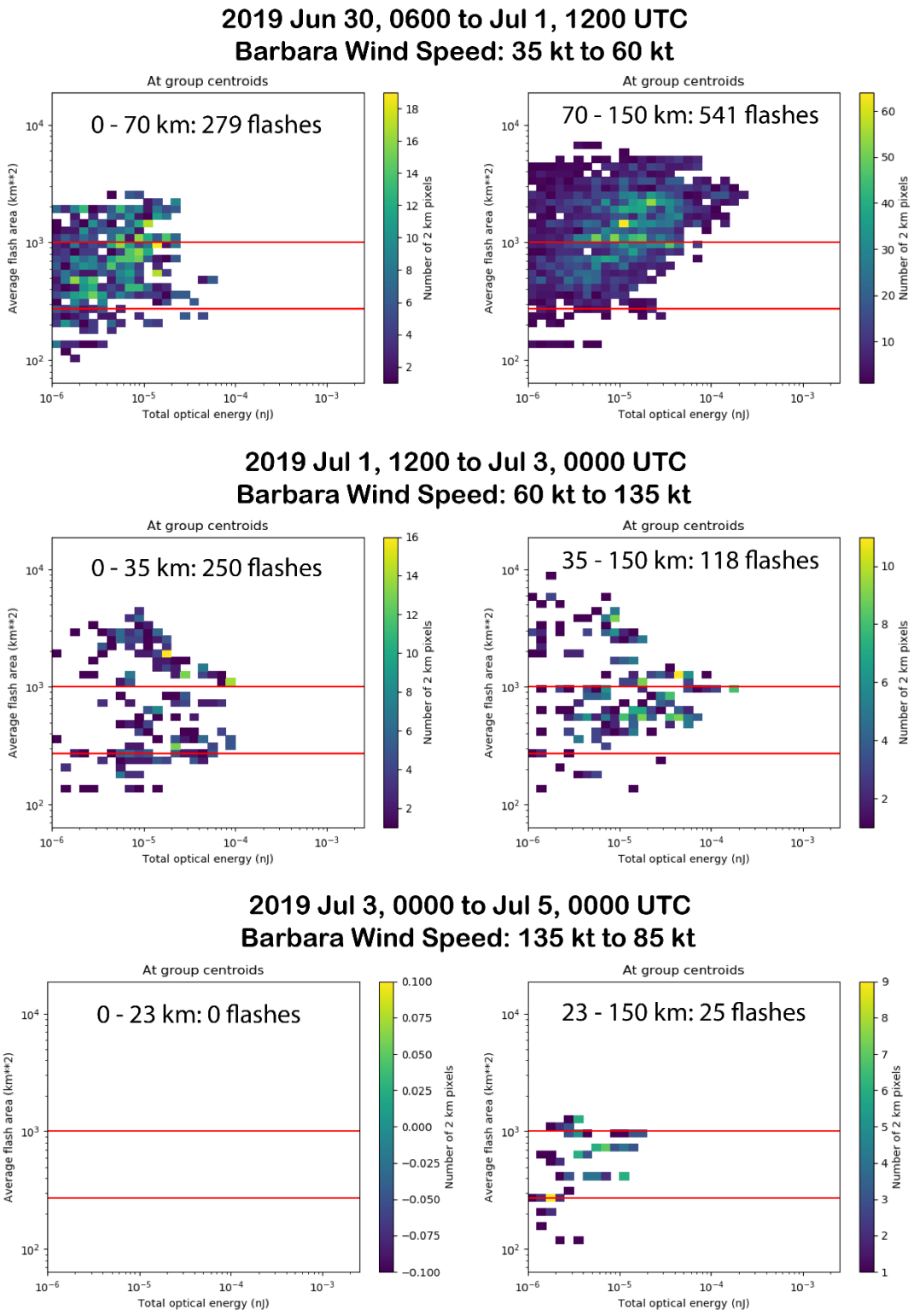

Figure A. 6 Barbara Joint Histogram, AFA vs. TOE

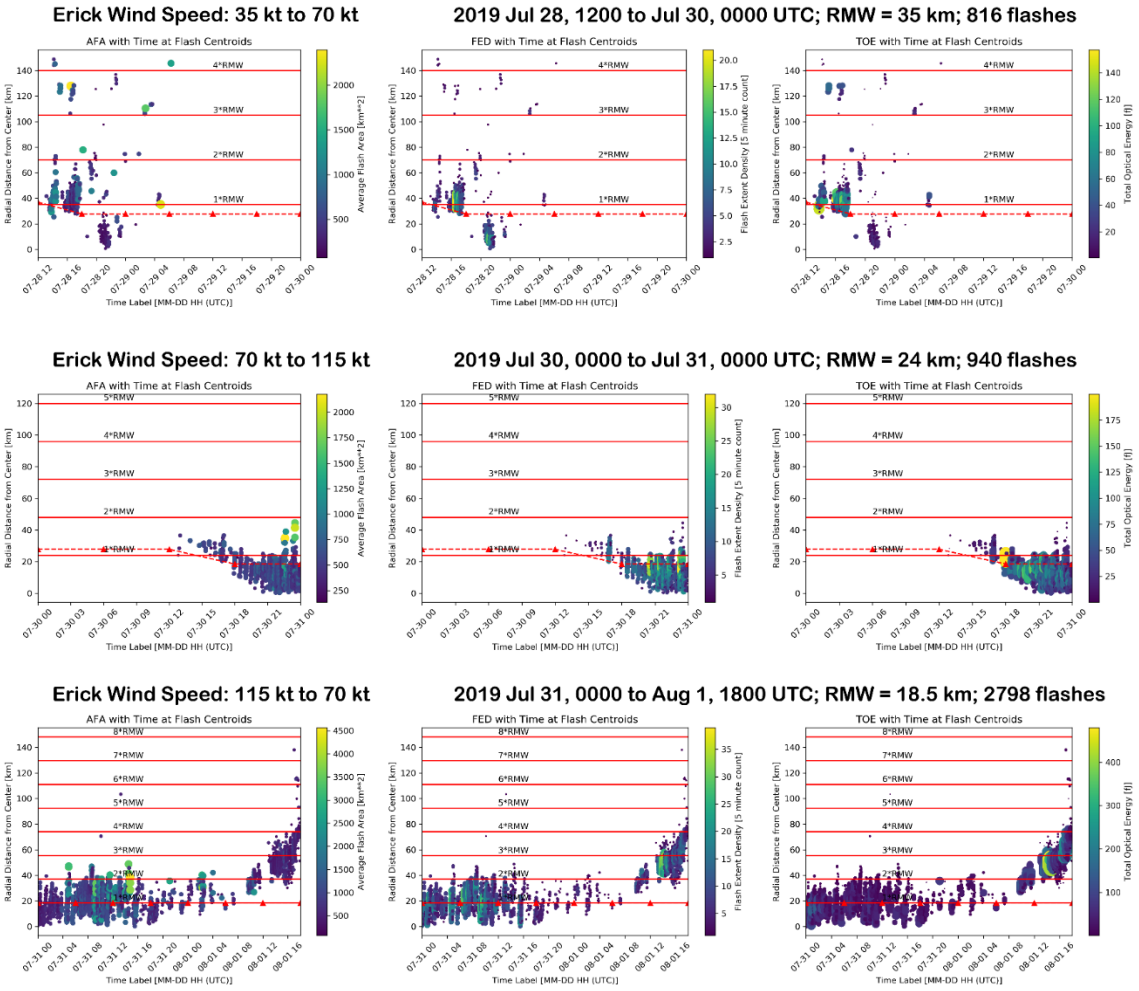

Figure A. 7 Erick Flashes, Distance from Center vs. Time

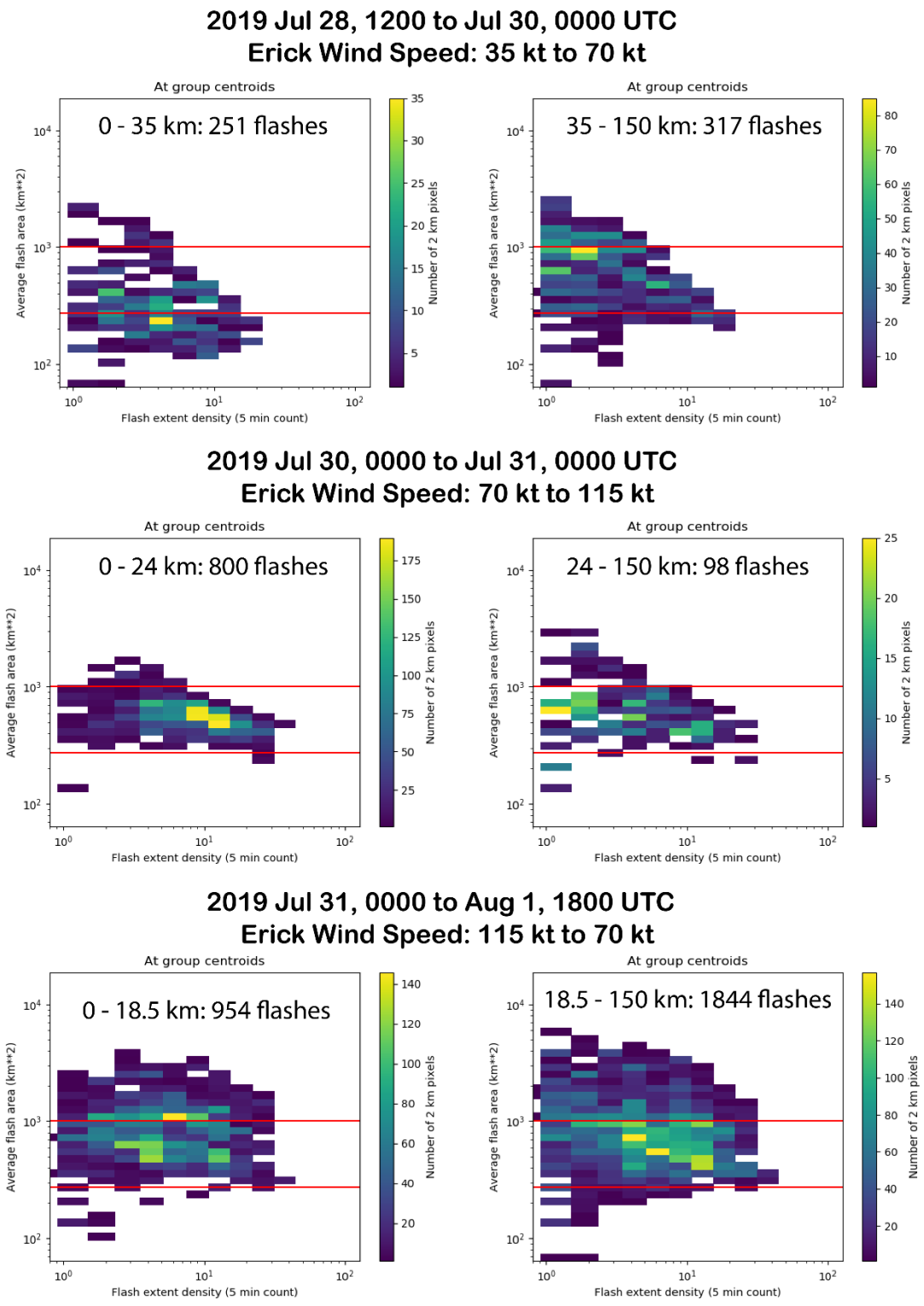

Figure A. 8 Erick Joint Histogram, AFA vs. FED

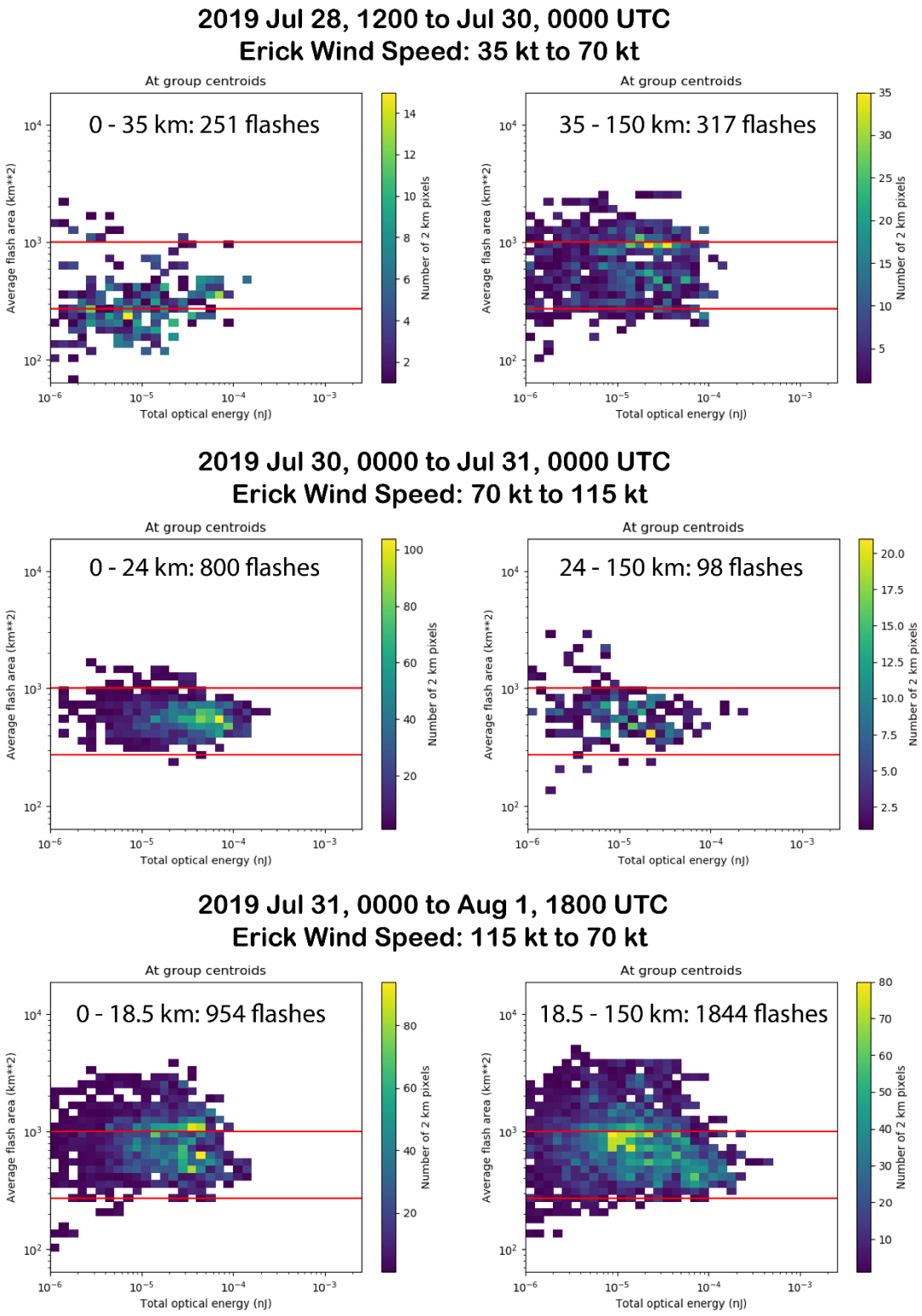

Figure A. 9 Erick Joint Histogram, AFA vs. TOE

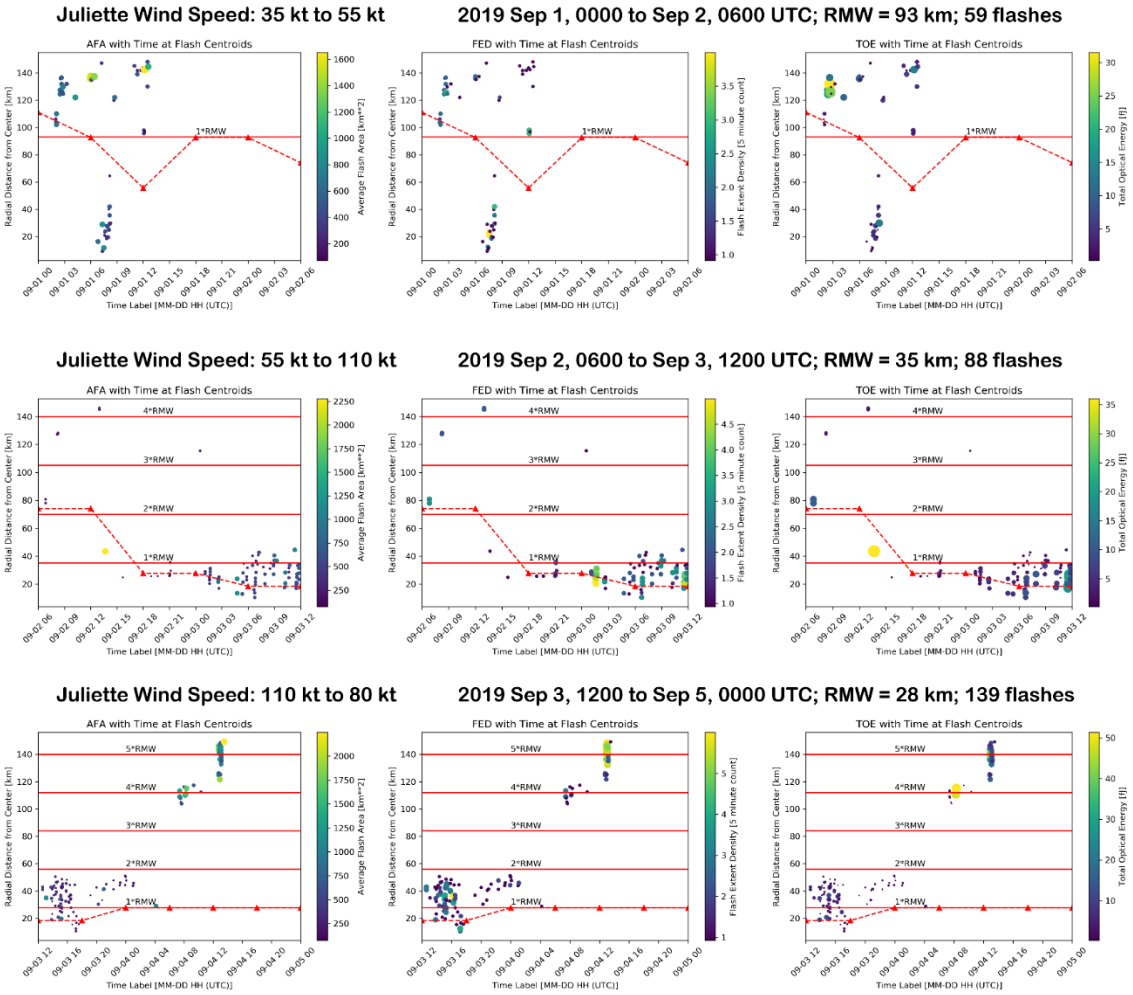

Figure A. 10 Juliette Flashes, Distance from Center vs. Time

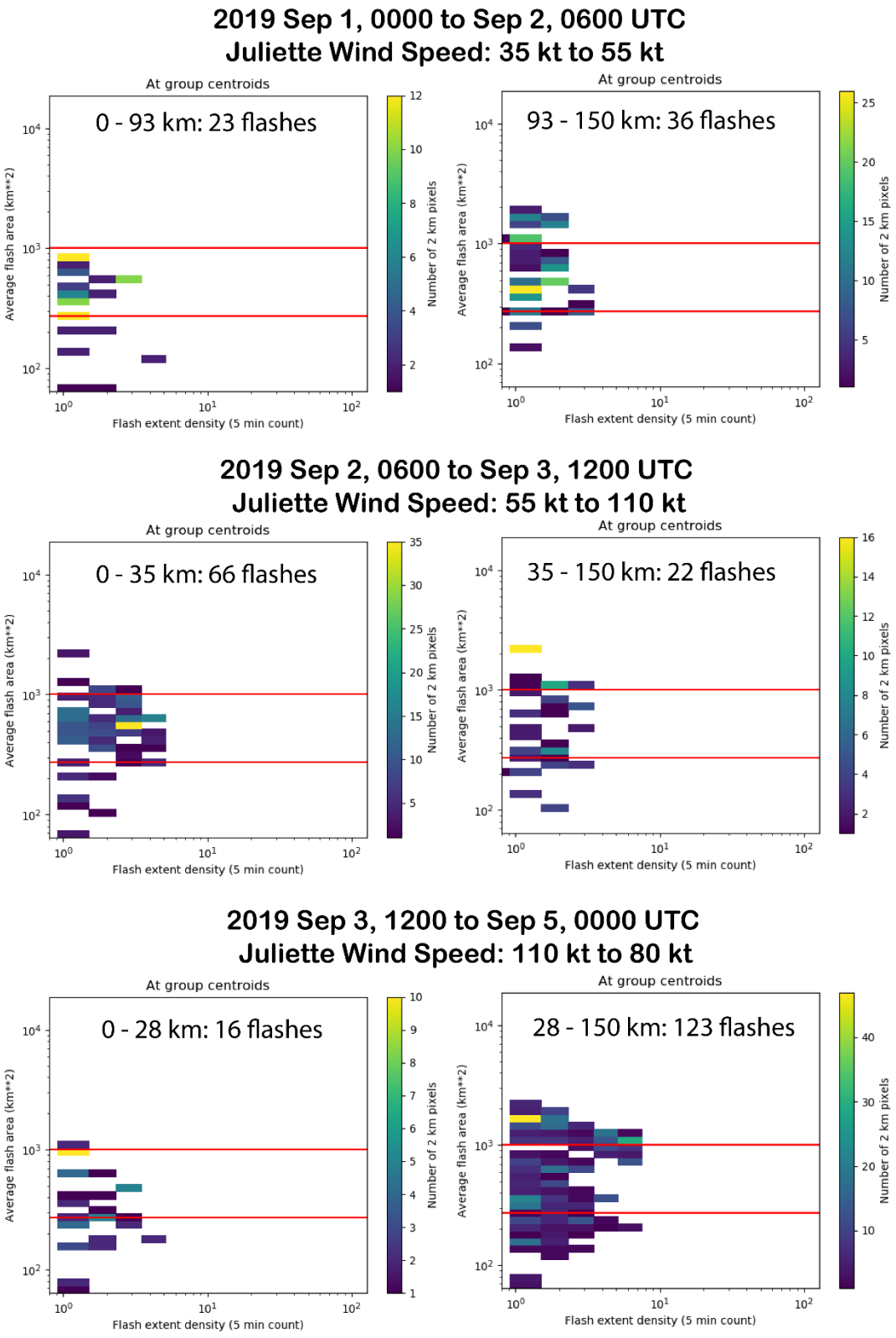

Figure A. 11 Juliette Joint Histogram, AFA vs. FED

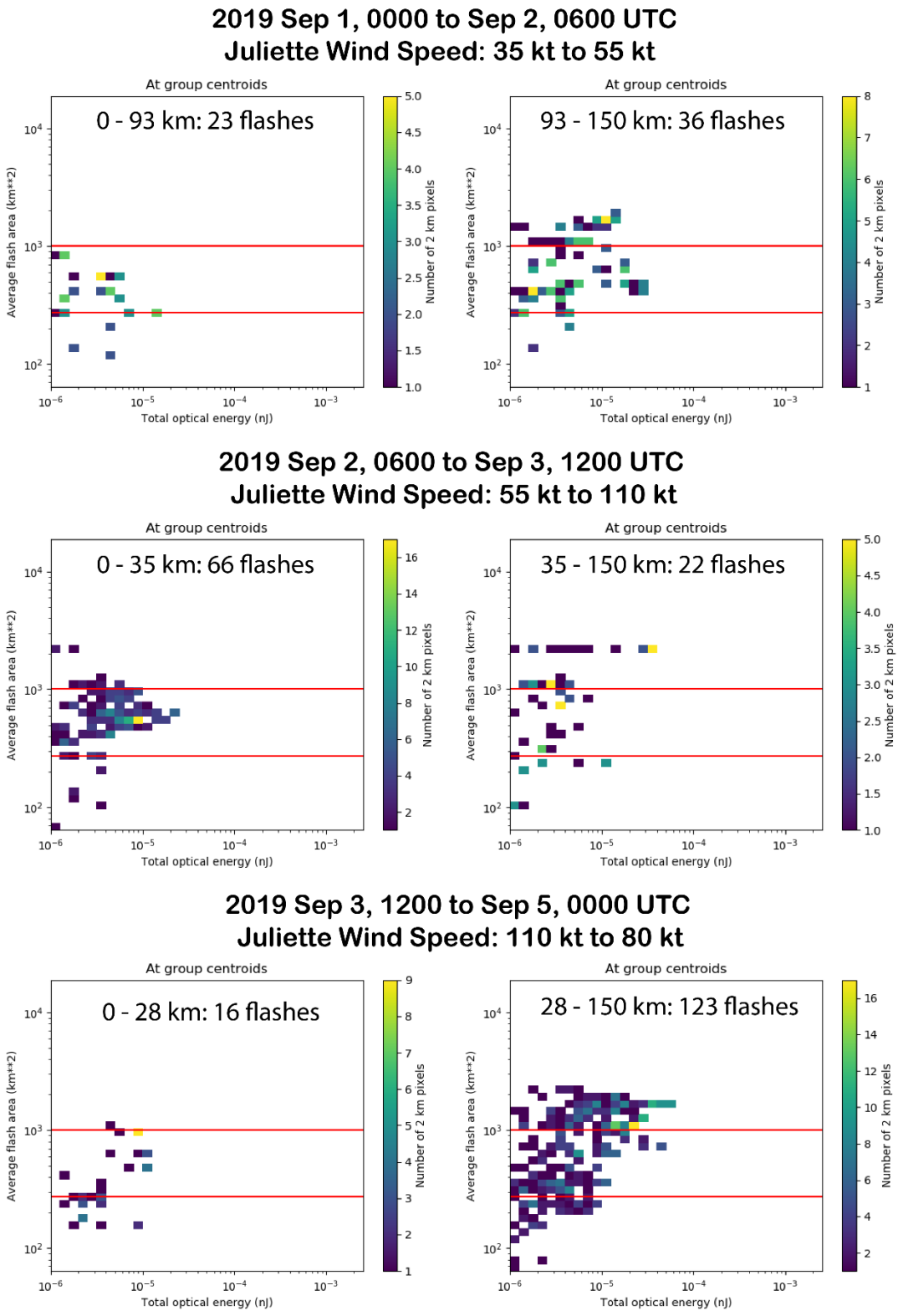

Figure A. 12 Juliette Joint Histogram, AFA vs. TOE

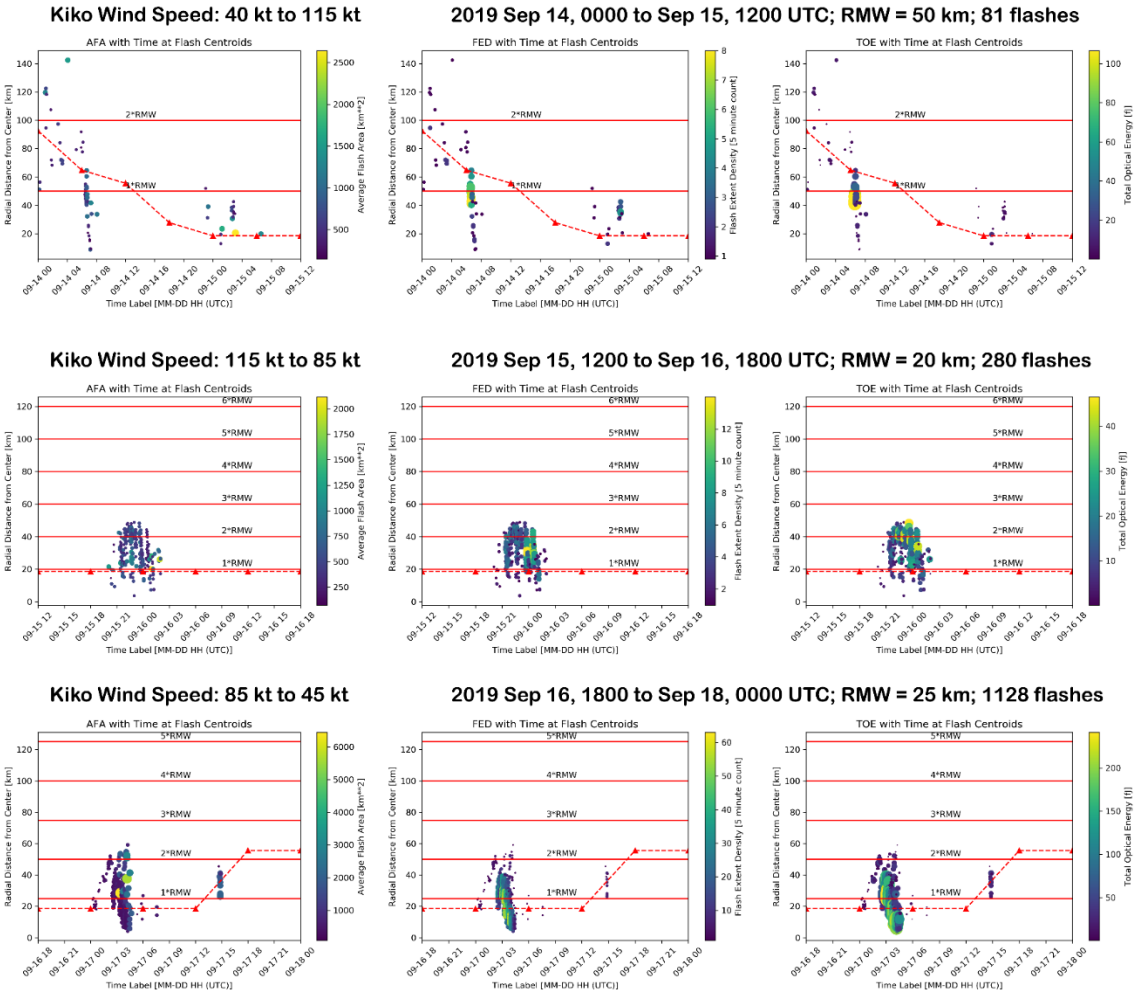

Figure A. 13 Kiko Flashes, Distance from Center vs. Time

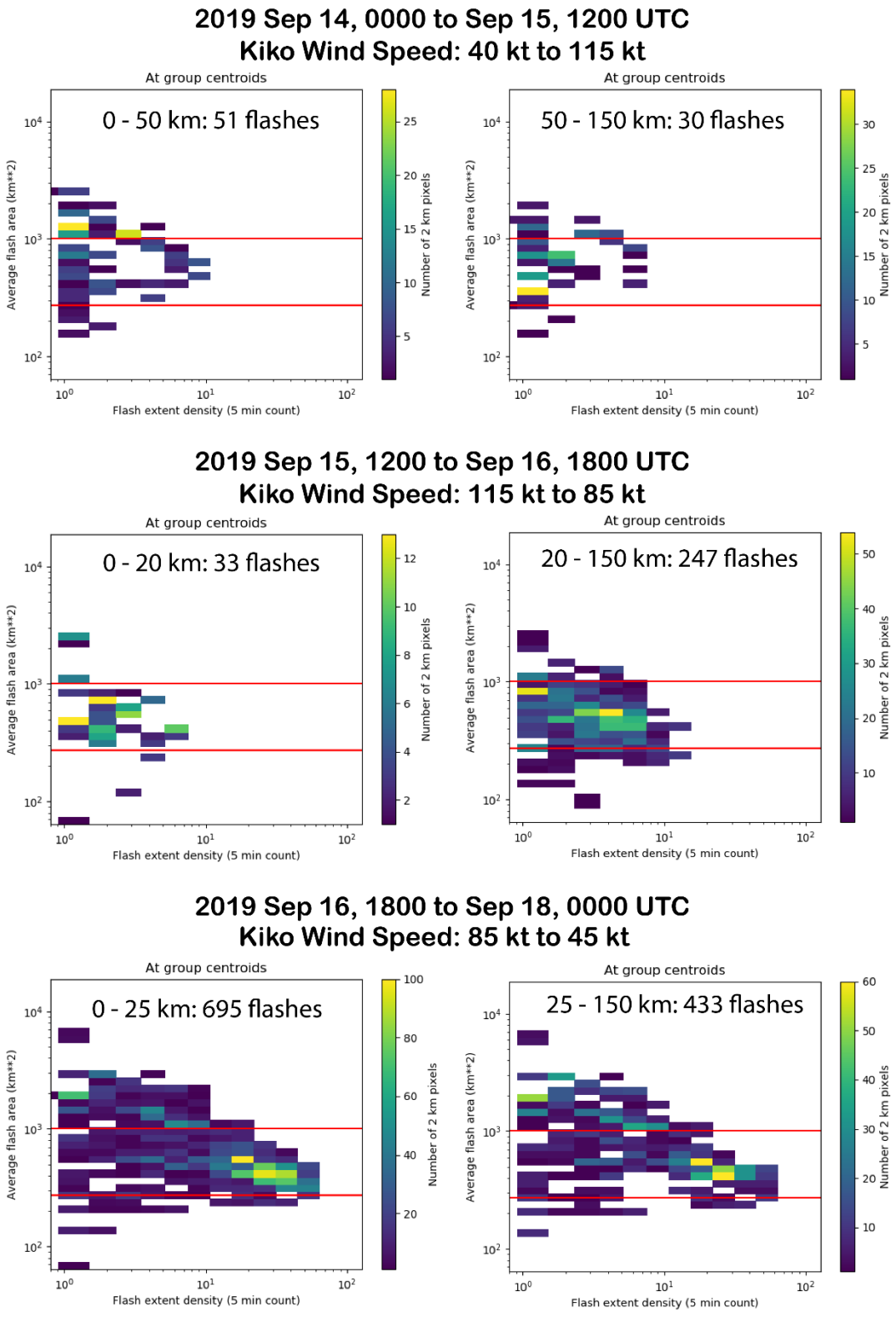

Figure A. 14 Kiko Joint Histogram, AFA vs. FED

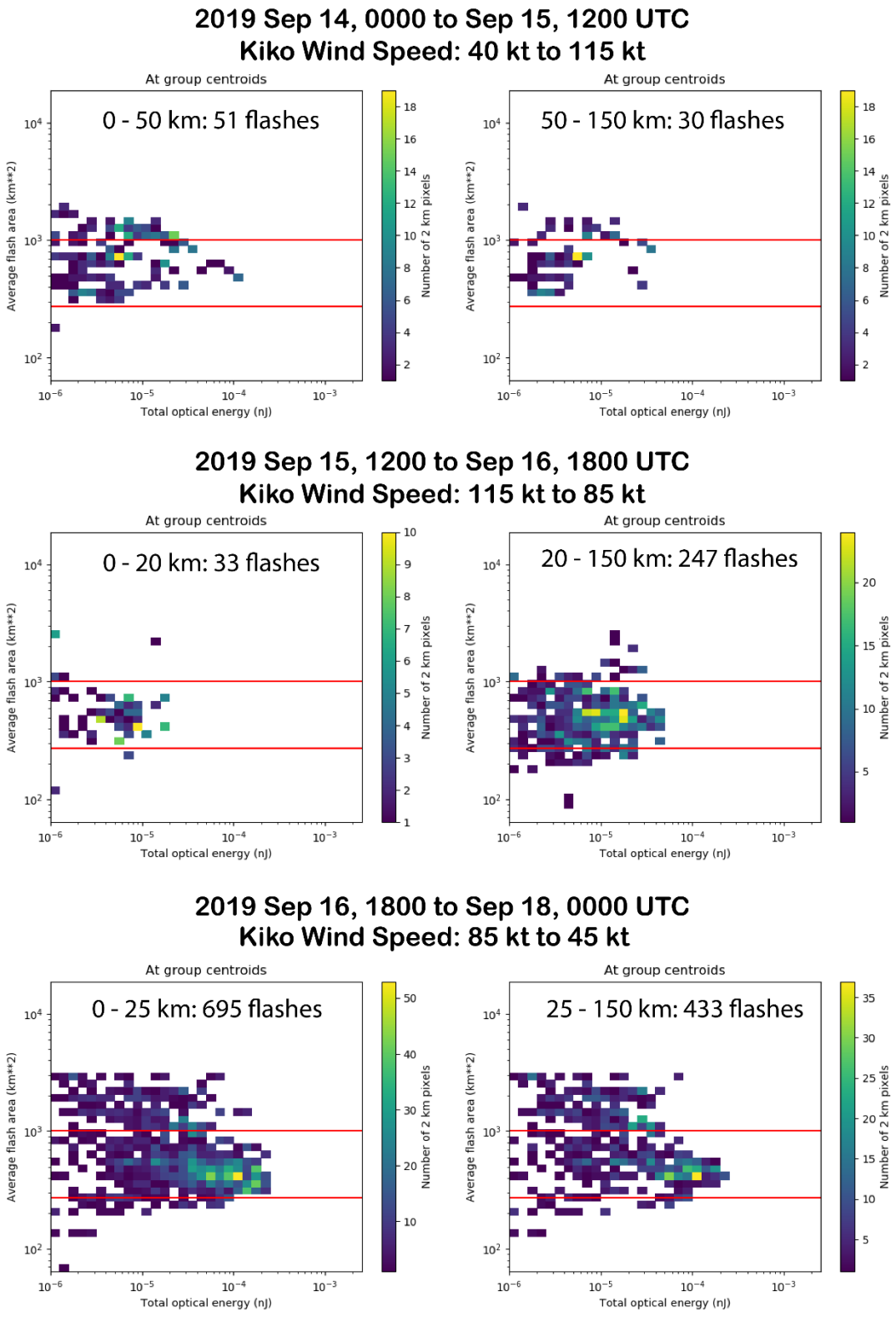

Figure A. 15 Kiko Joint Histogram, AFA vs. TOE

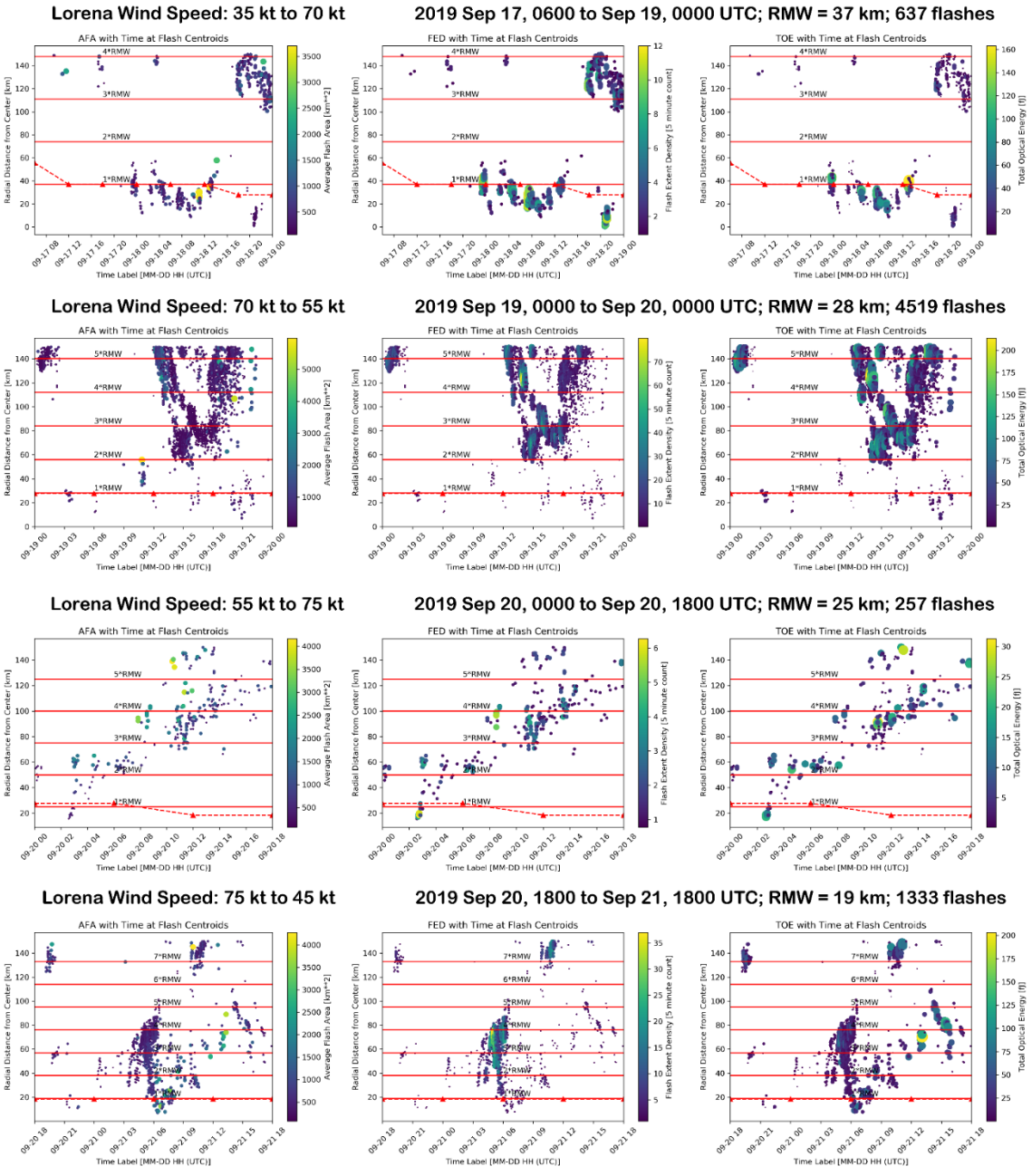

Figure A. 16 Lorena Flashes, Distance from Center vs. Time

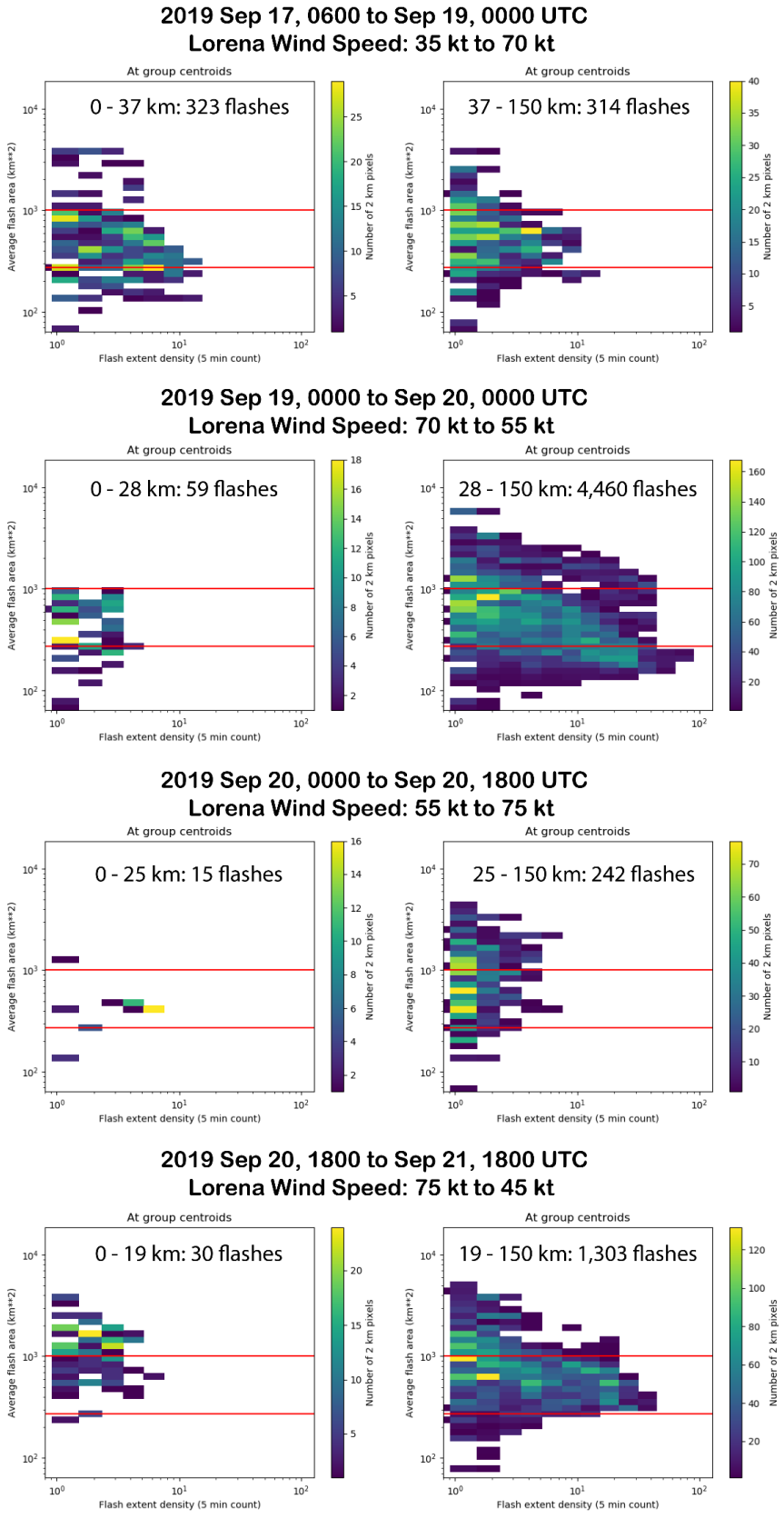

Figure A. 17 Lorena Joint Histogram, AFA vs. FED

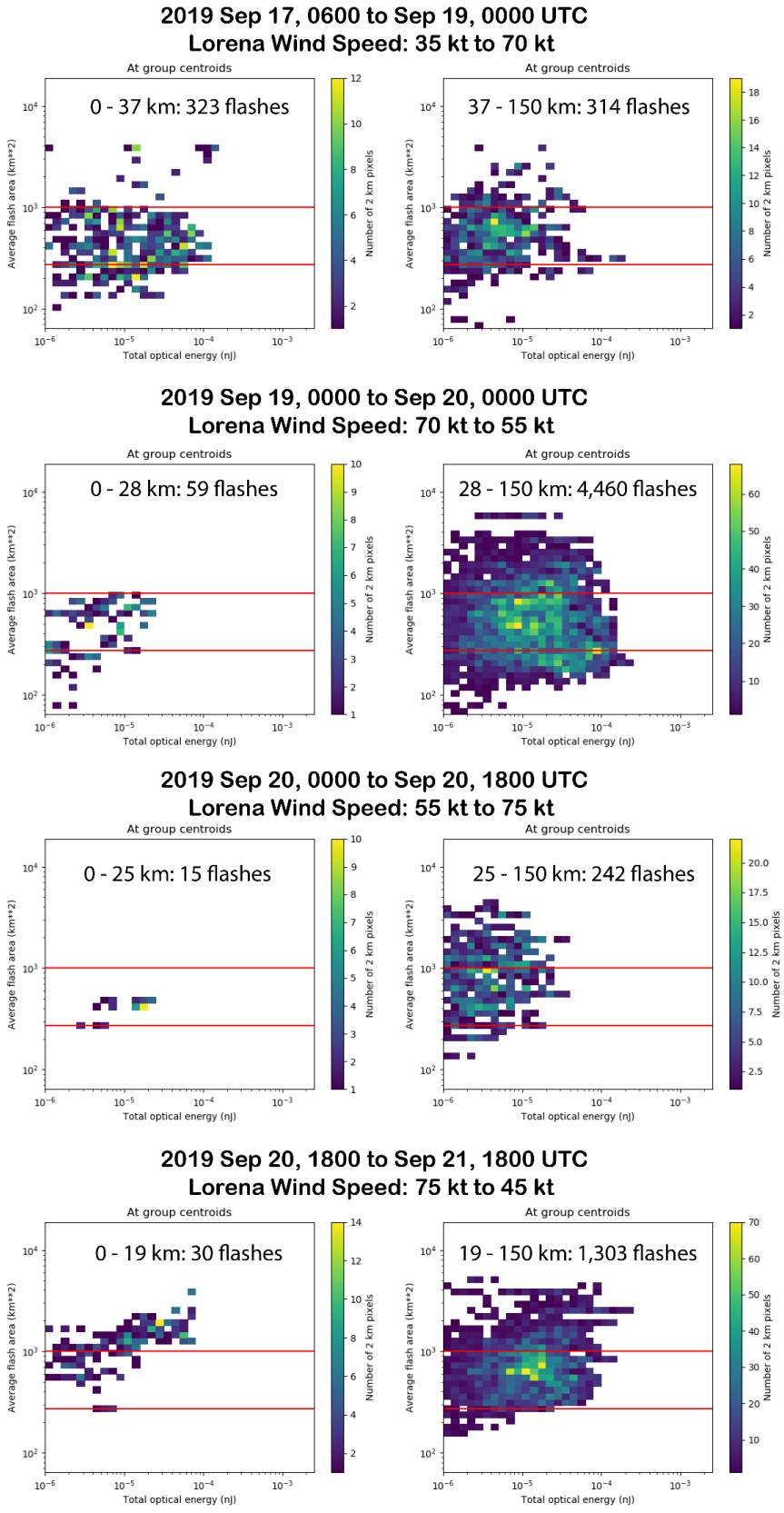

Figure A. 18 Lorena Joint Histogram, AFA vs. TOE

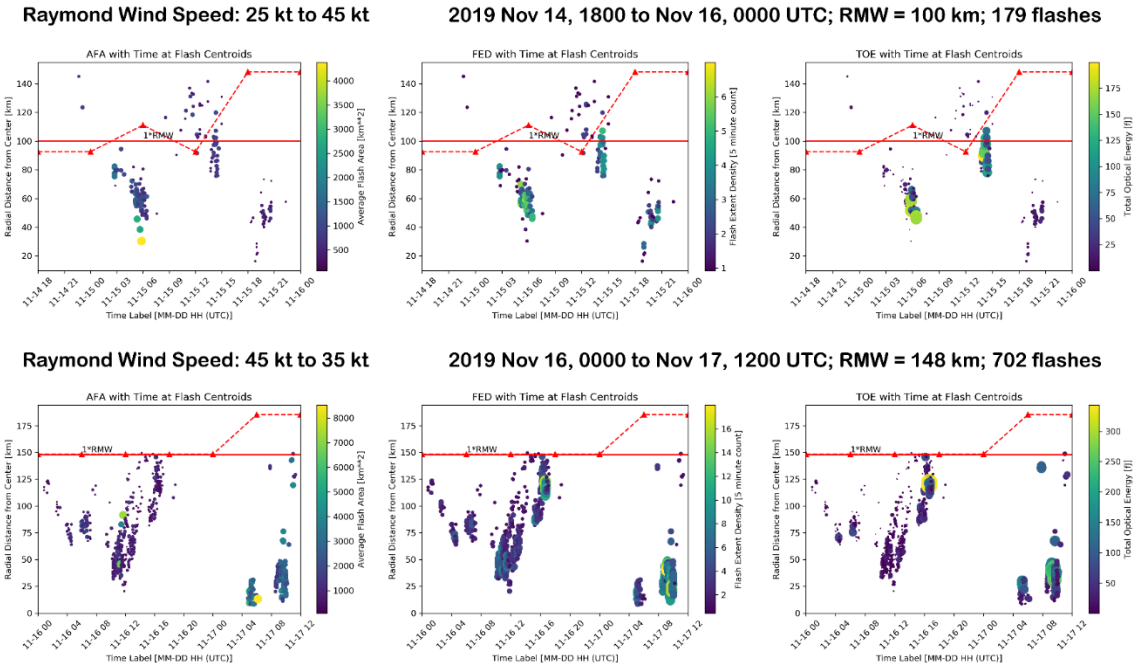

Figure A. 19 Raymond Flashes, Distance from Center vs. Time

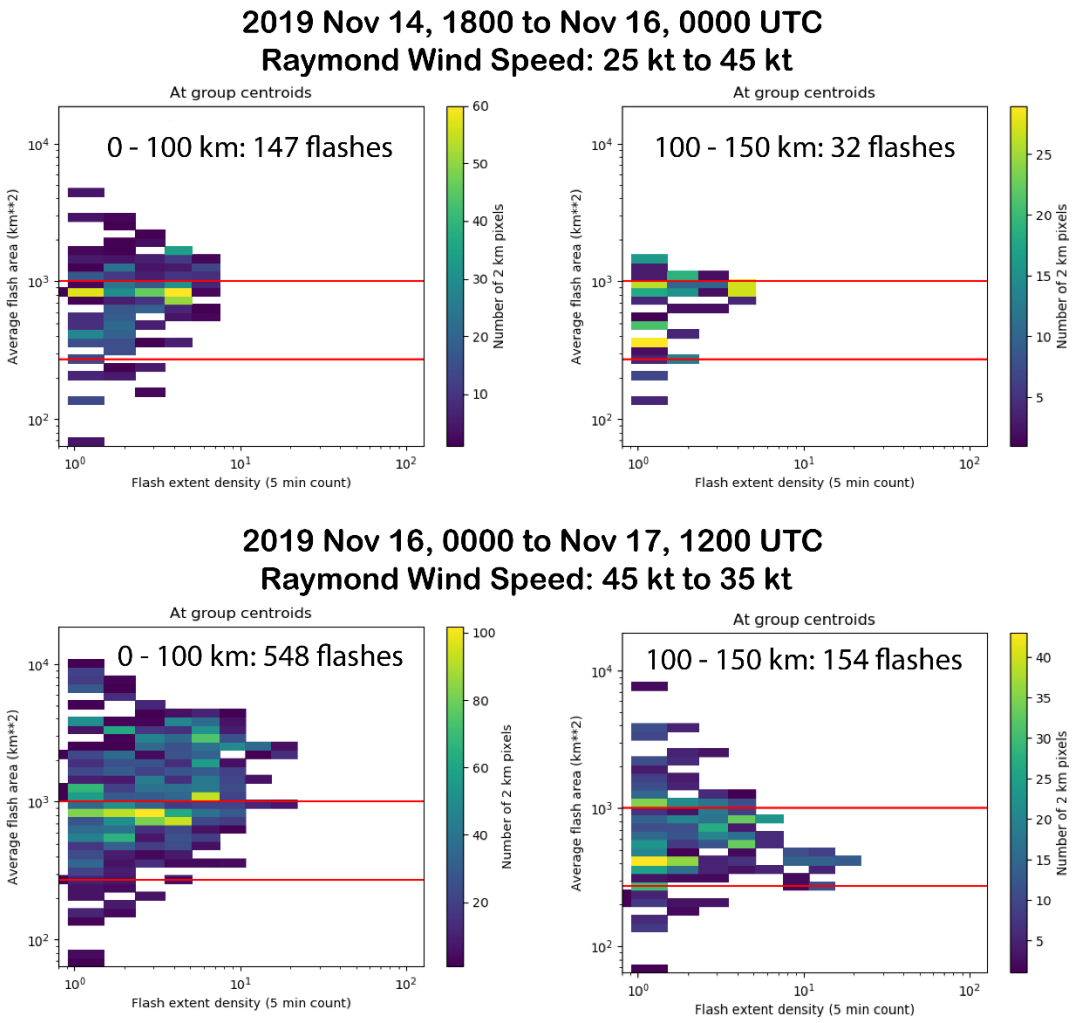

Figure A. 20 Raymond Joint Histogram, AFA vs. FED

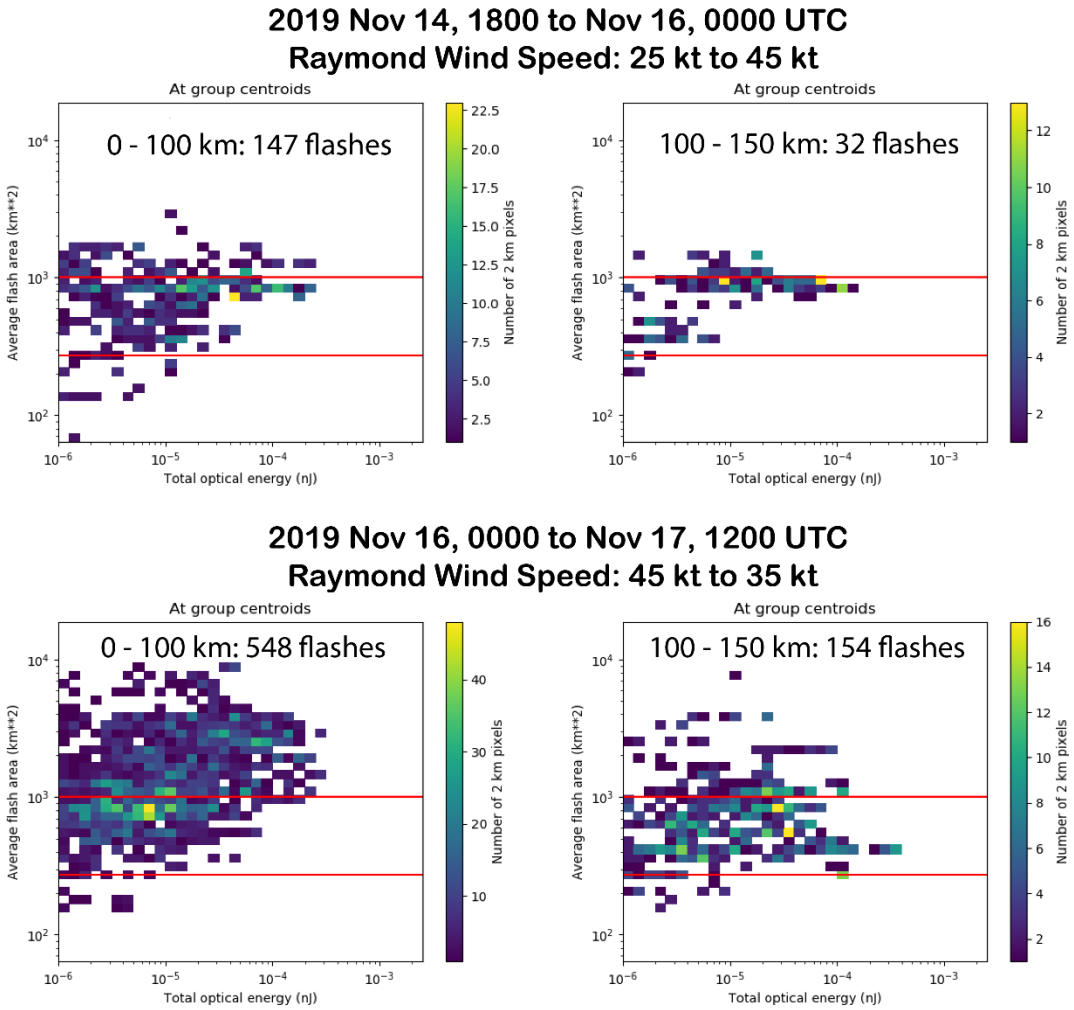

Figure A. 21 Raymond Joint Histogram, AFA vs. TOE

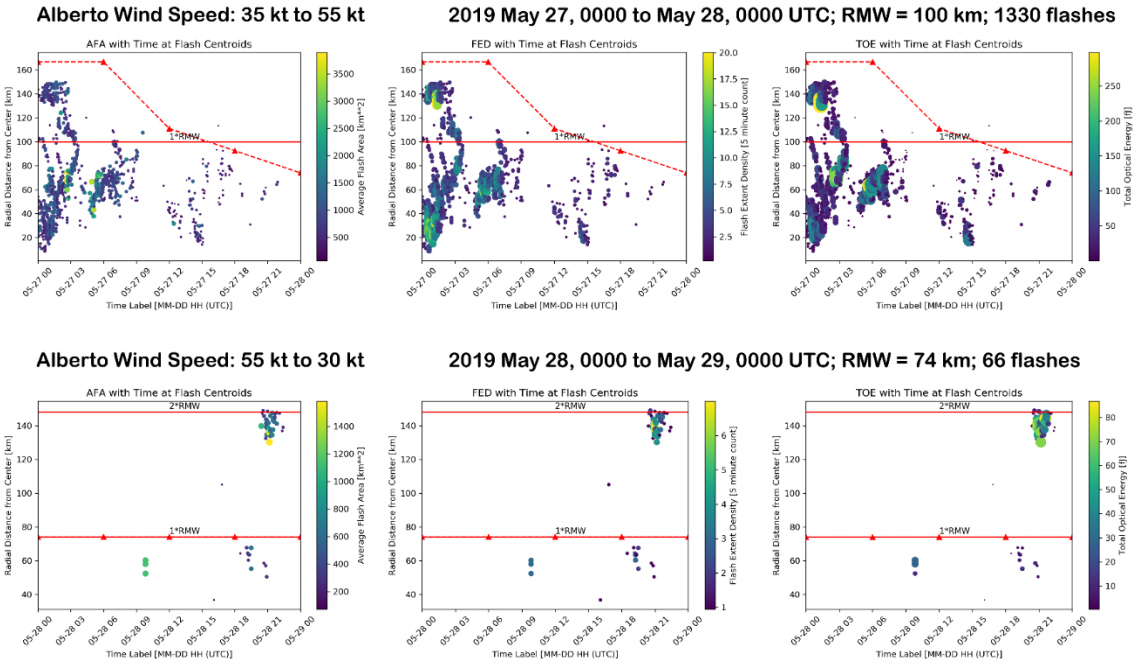

Figure A. 22 Alberto Flashes, Distance from Center vs. Time

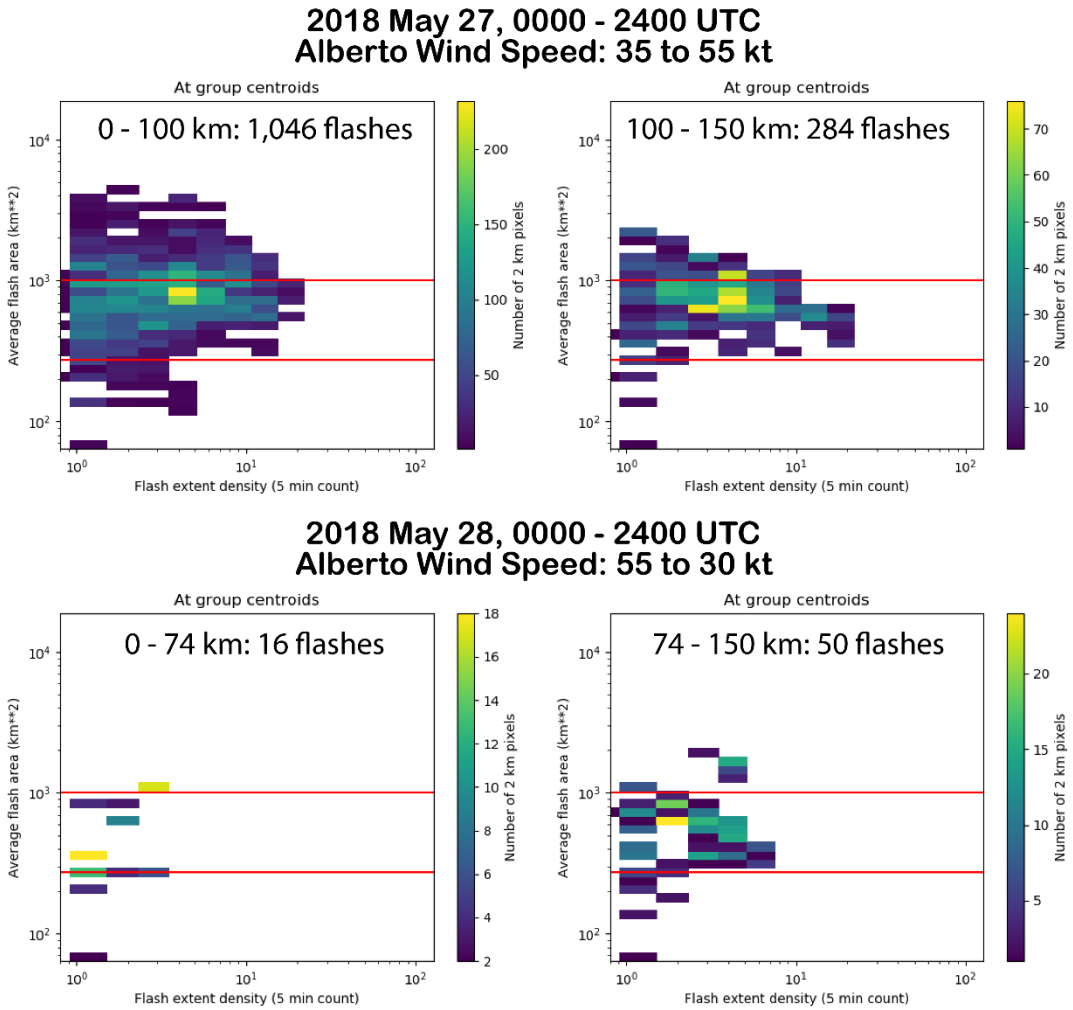

Figure A. 23 Alberto Joint Histogram, AFA vs. FED

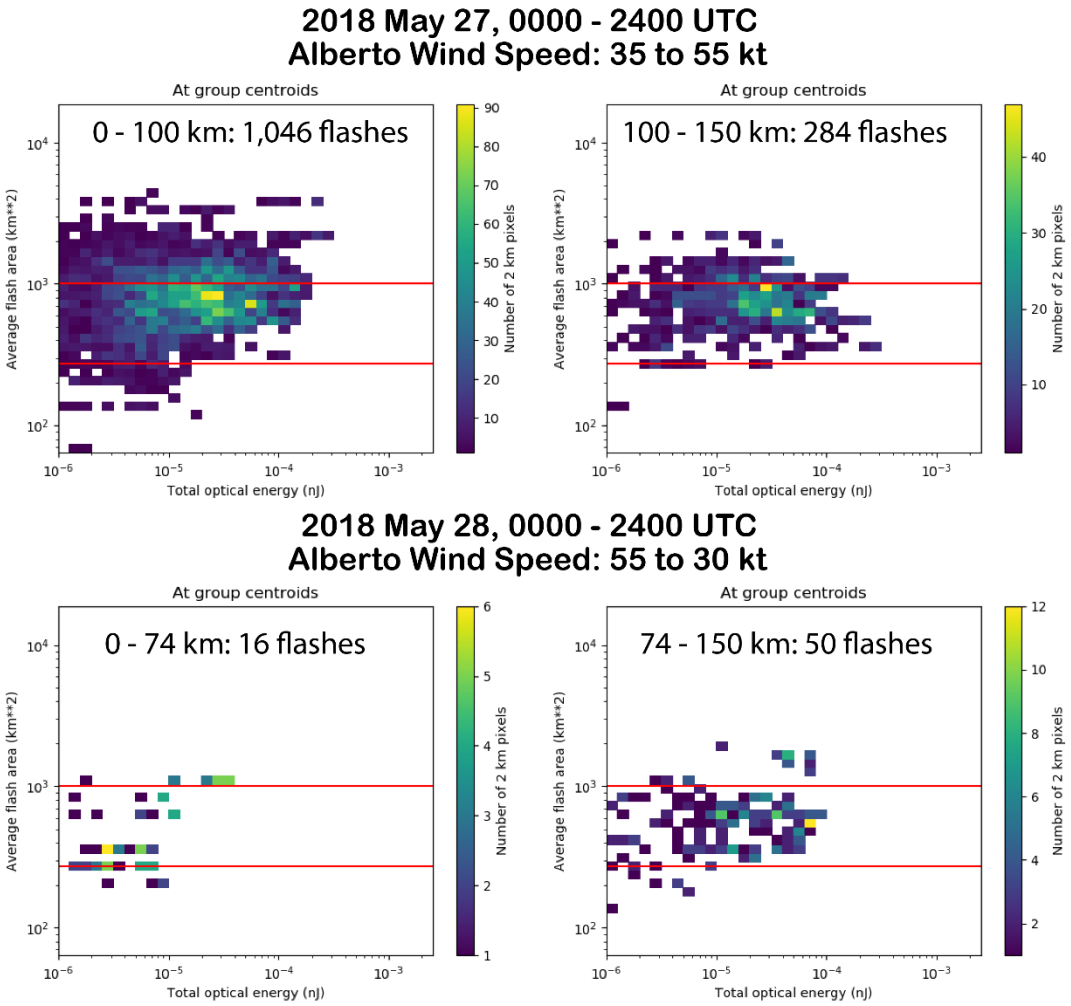

Figure A. 24 Alberto Joint Histogram, AFA vs. TOE

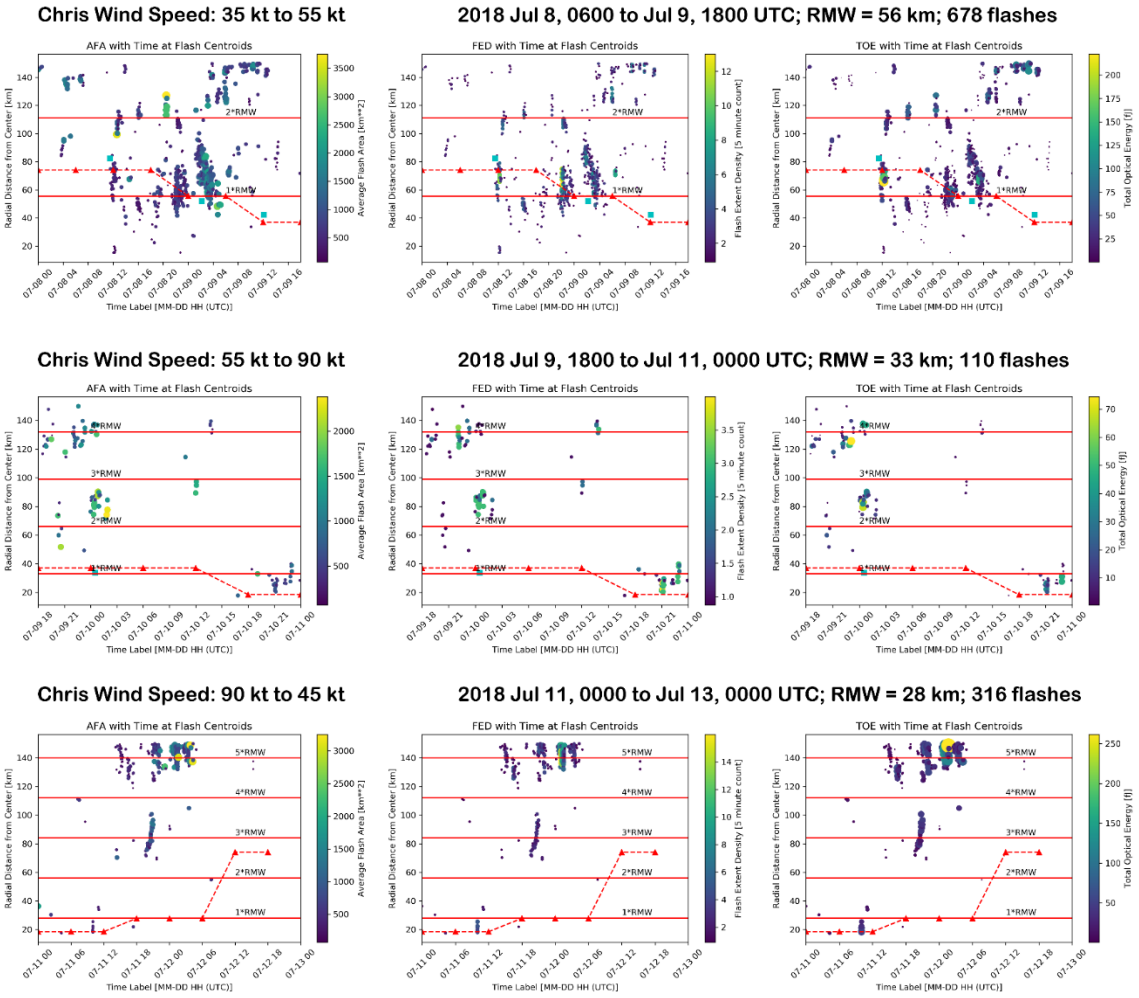

Figure A. 25 Chris Flashes, Distance from Center vs. Time

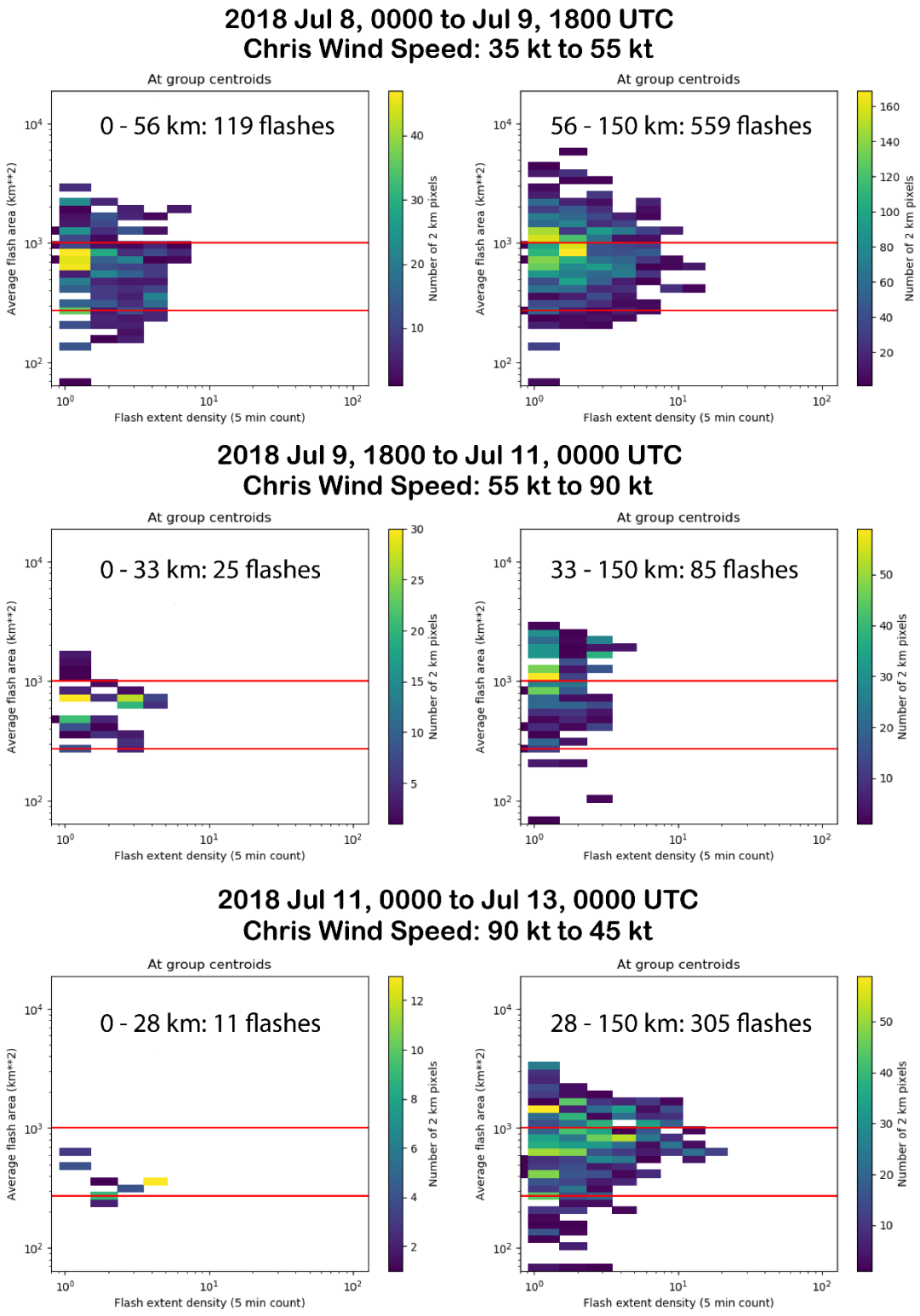

Figure A. 26 Chris Joint Histogram, AFA vs. FED

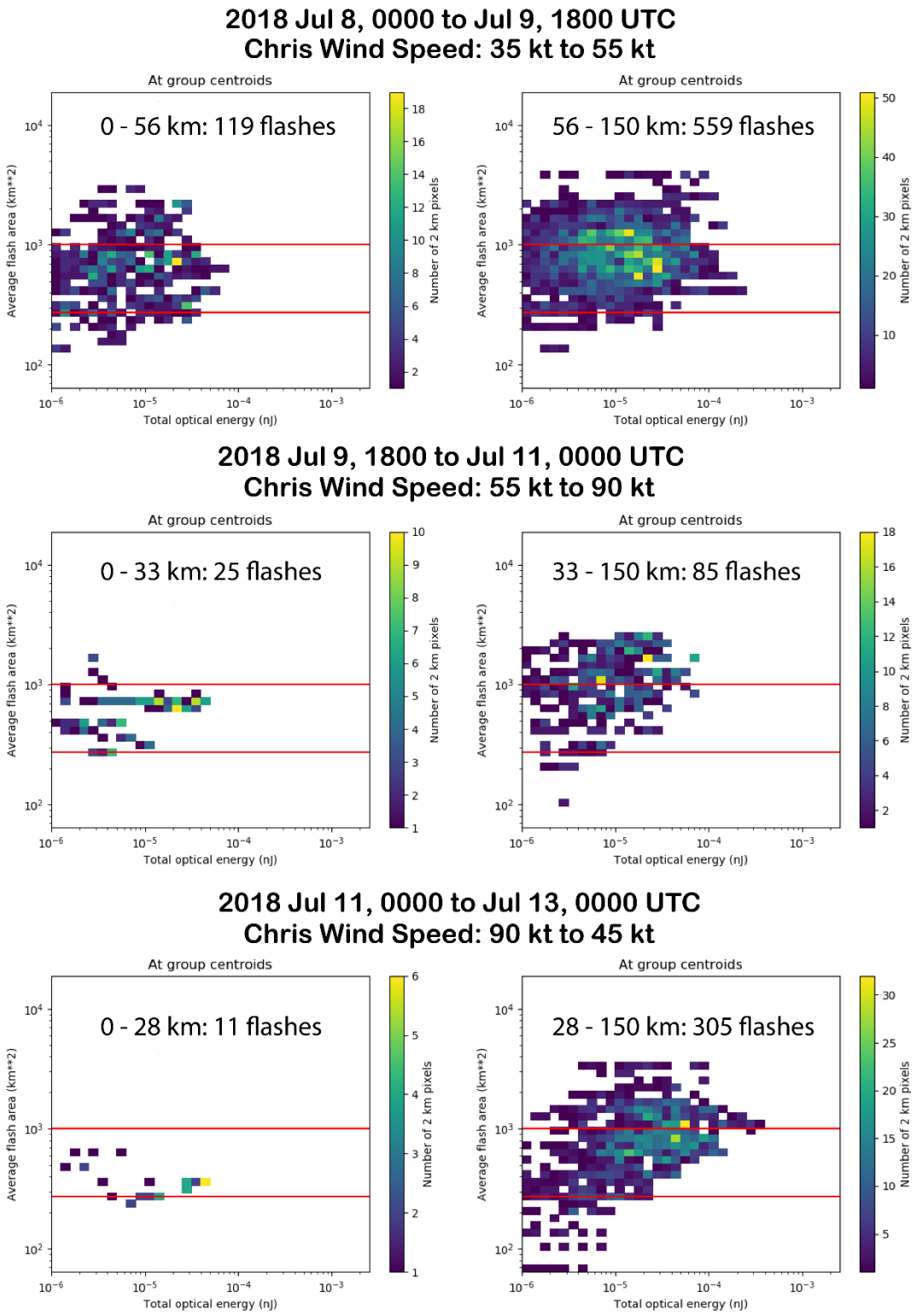

Figure A. 27 Chris Joint Histogram, AFA vs. TOE

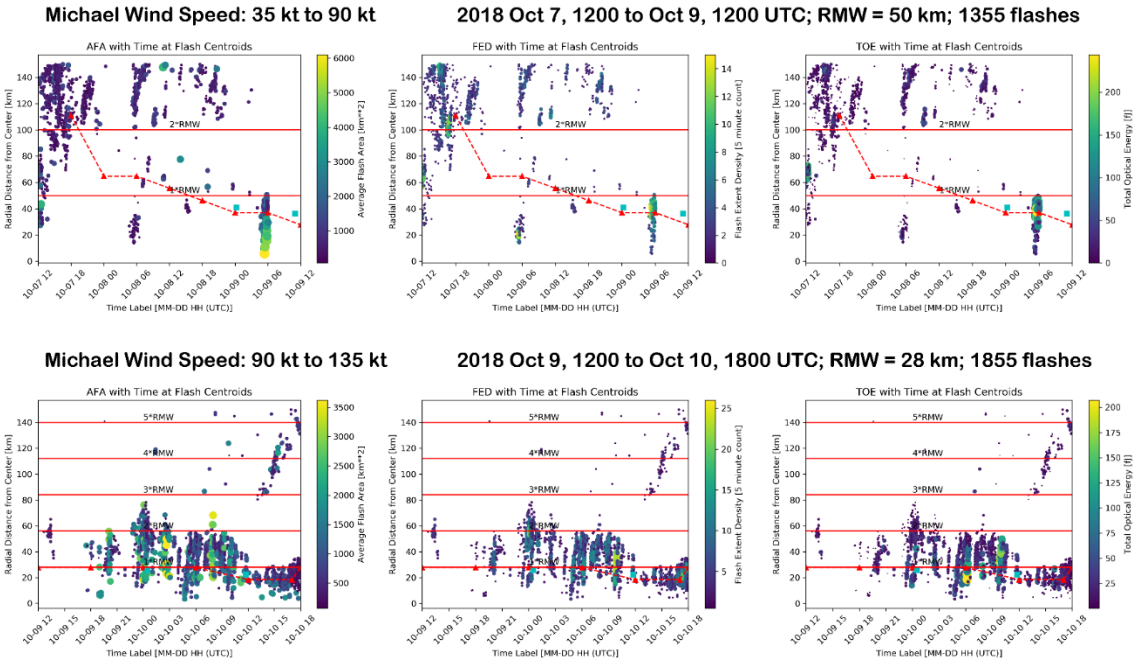

Figure A. 28 Michael Flashes, Distance from Center vs. Time

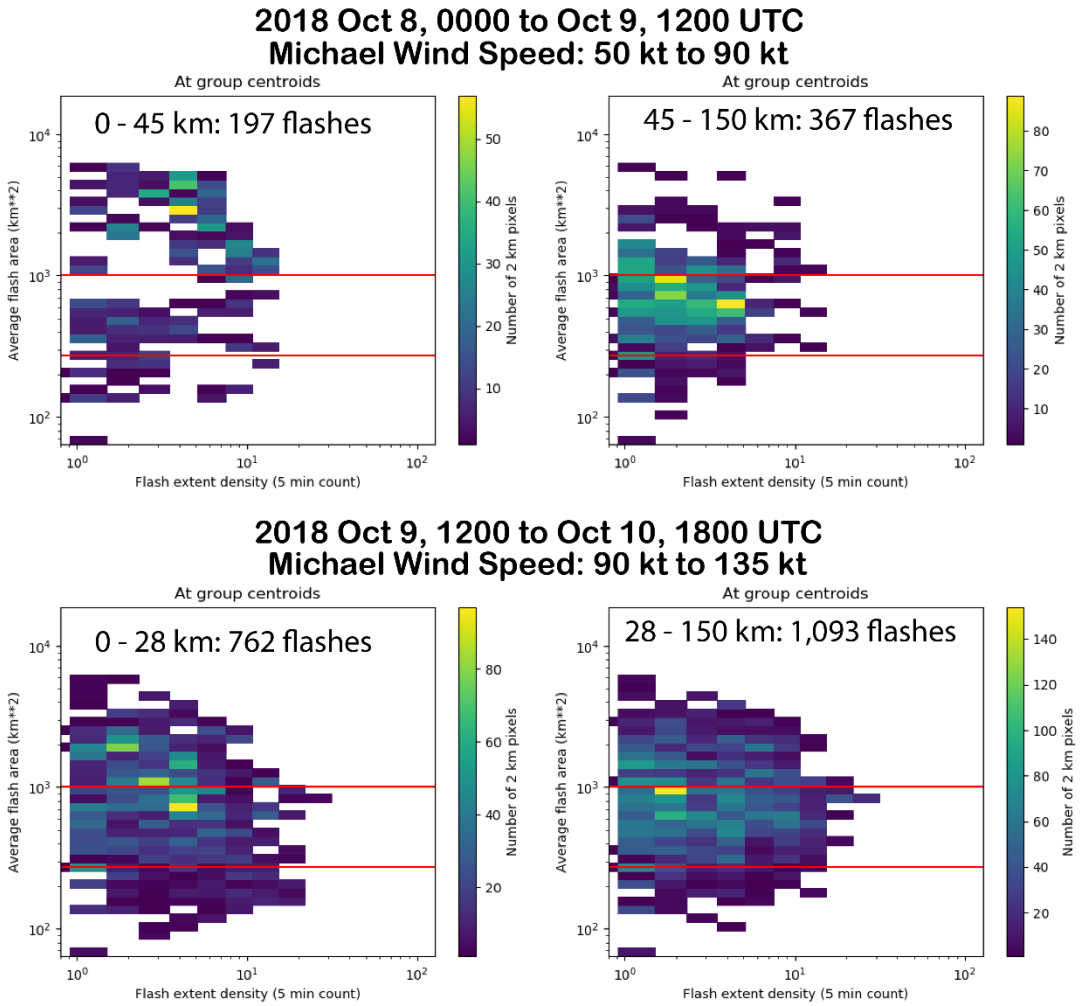

Figure A. 29 Michael Joint Histogram, AFA vs. FED

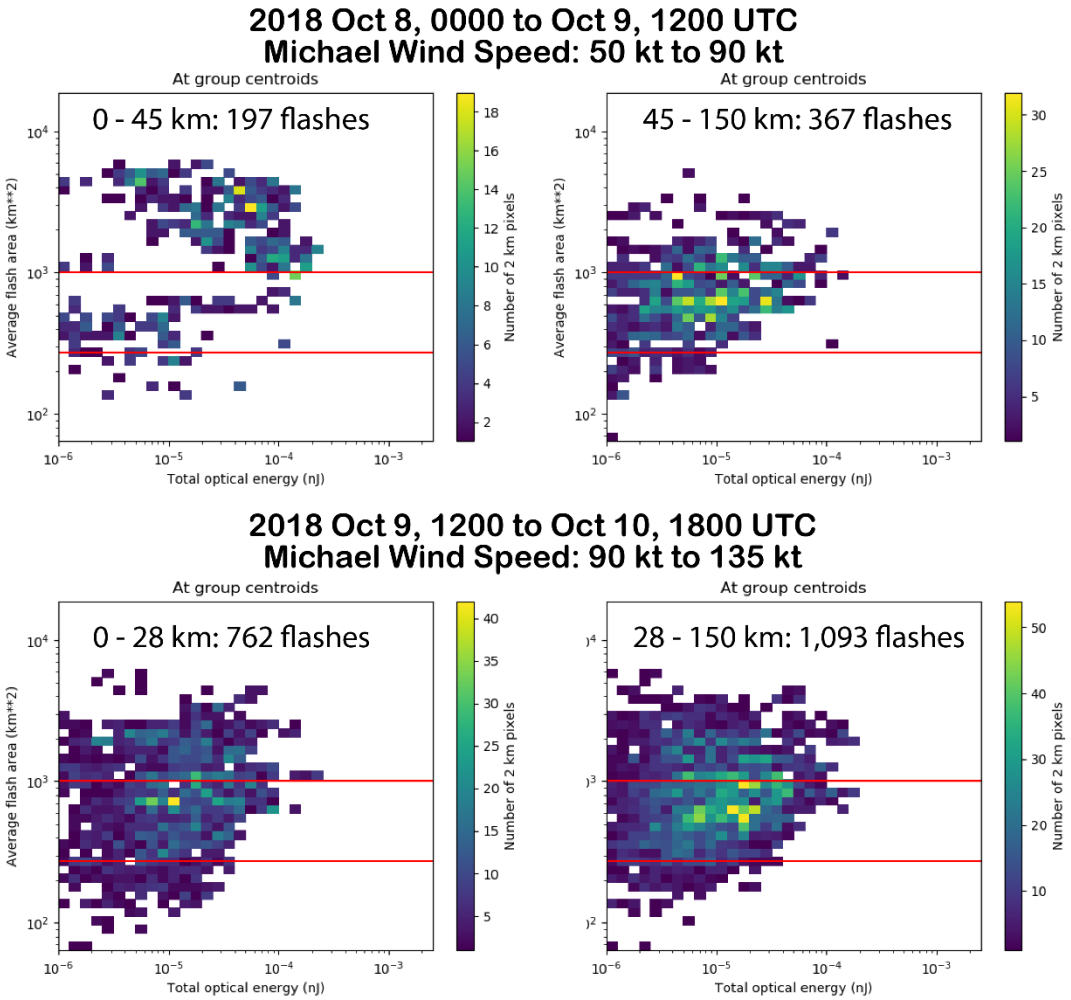

Figure A. 30 Michael Joint Histogram, AFA vs. TOE

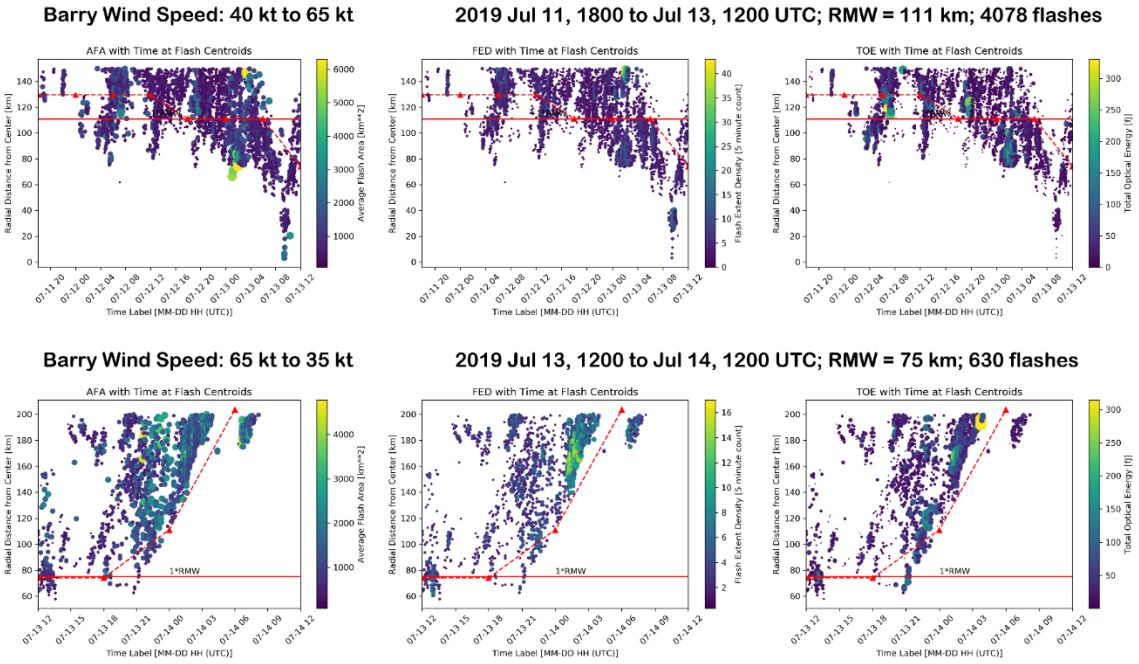

Figure A. 31 Barry Flashes, Distance from Center vs. Time

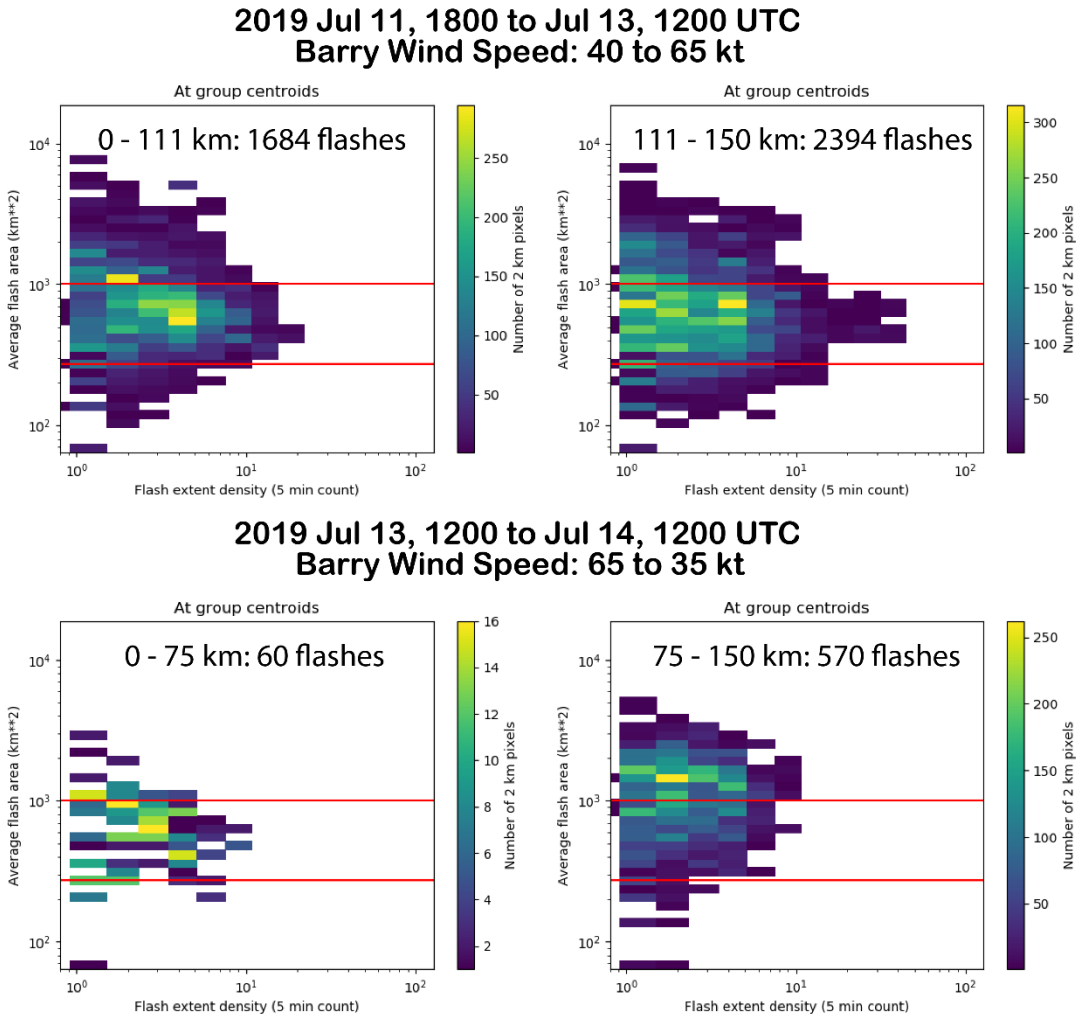

Figure A. 32 Barry Joint Histogram, AFA vs. FED

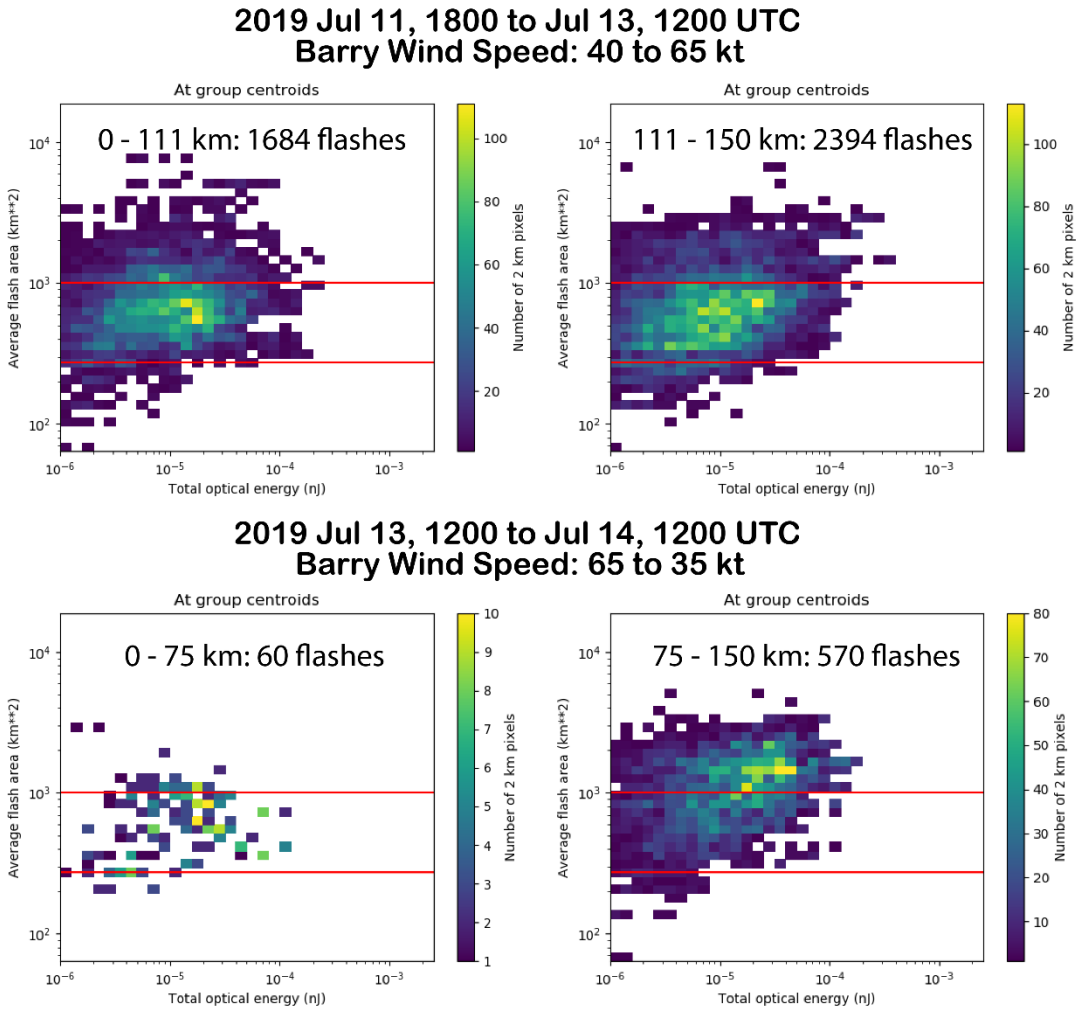

Figure A. 33 Barry Joint Histogram, AFA vs. TOE

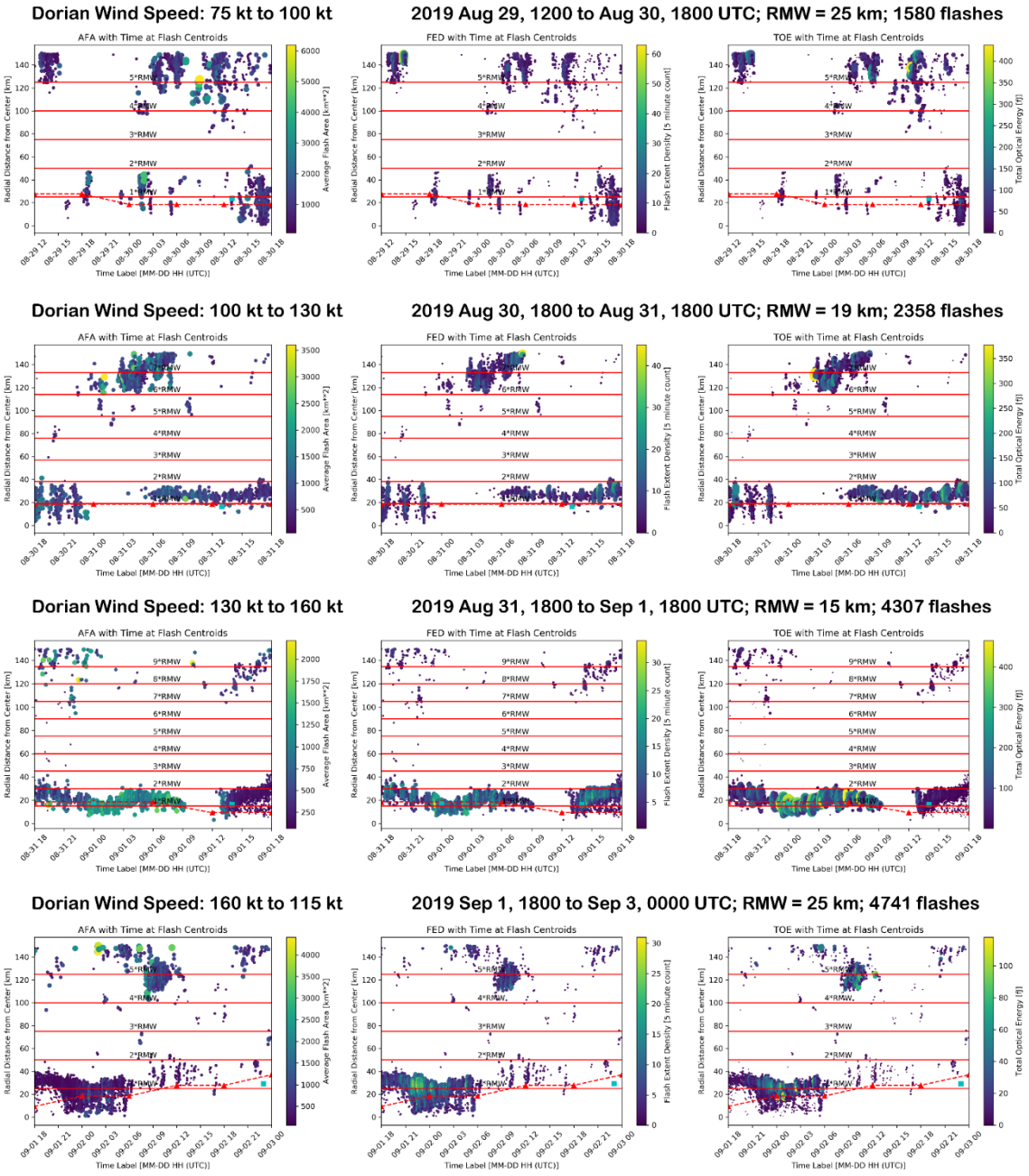

Figure A. 34 Dorian (NHC) Flashes, Distance from Center vs. Time

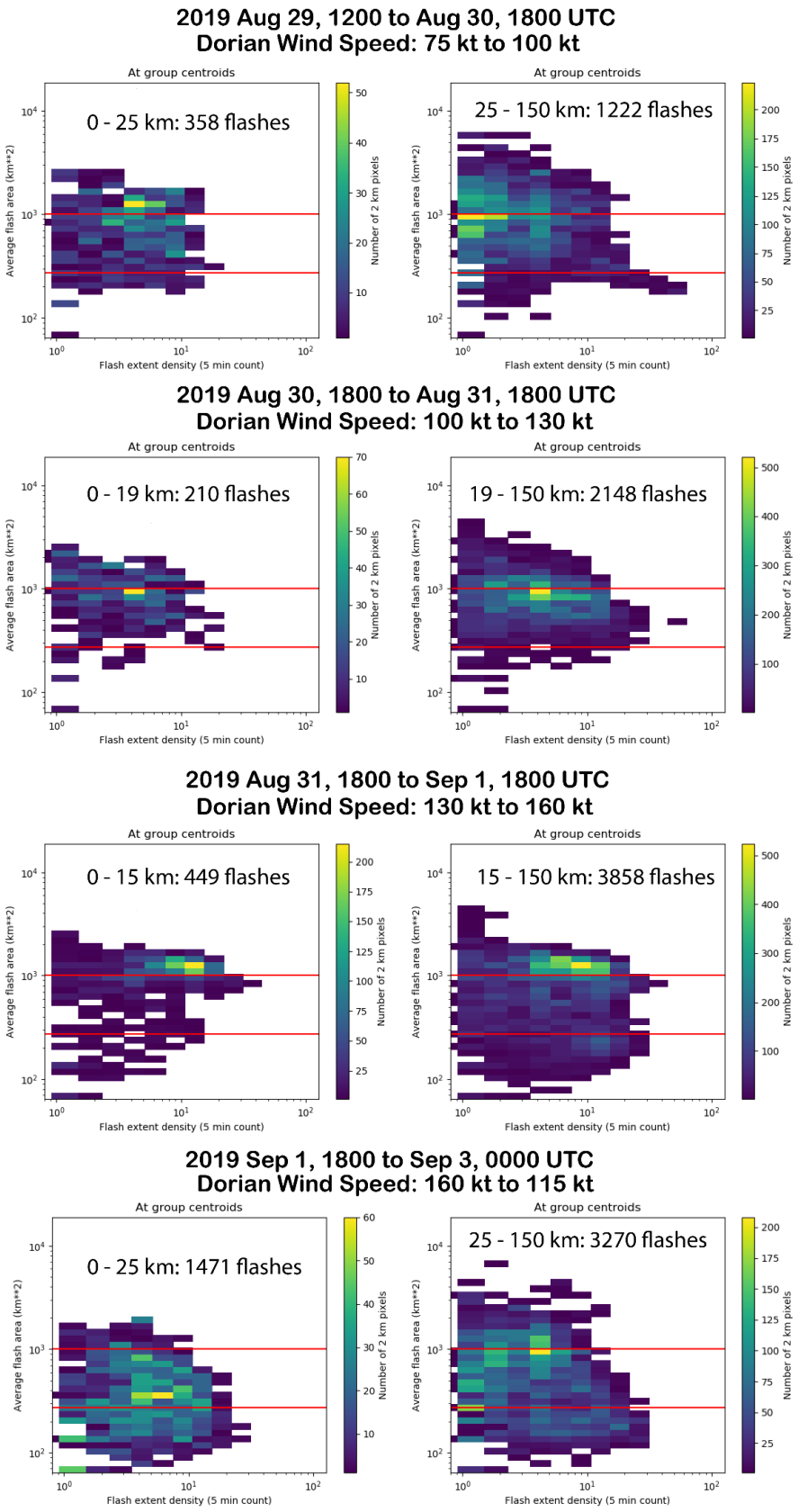

Figure A. 35 Dorian (NHC) Joint Histogram, AFA vs. FED

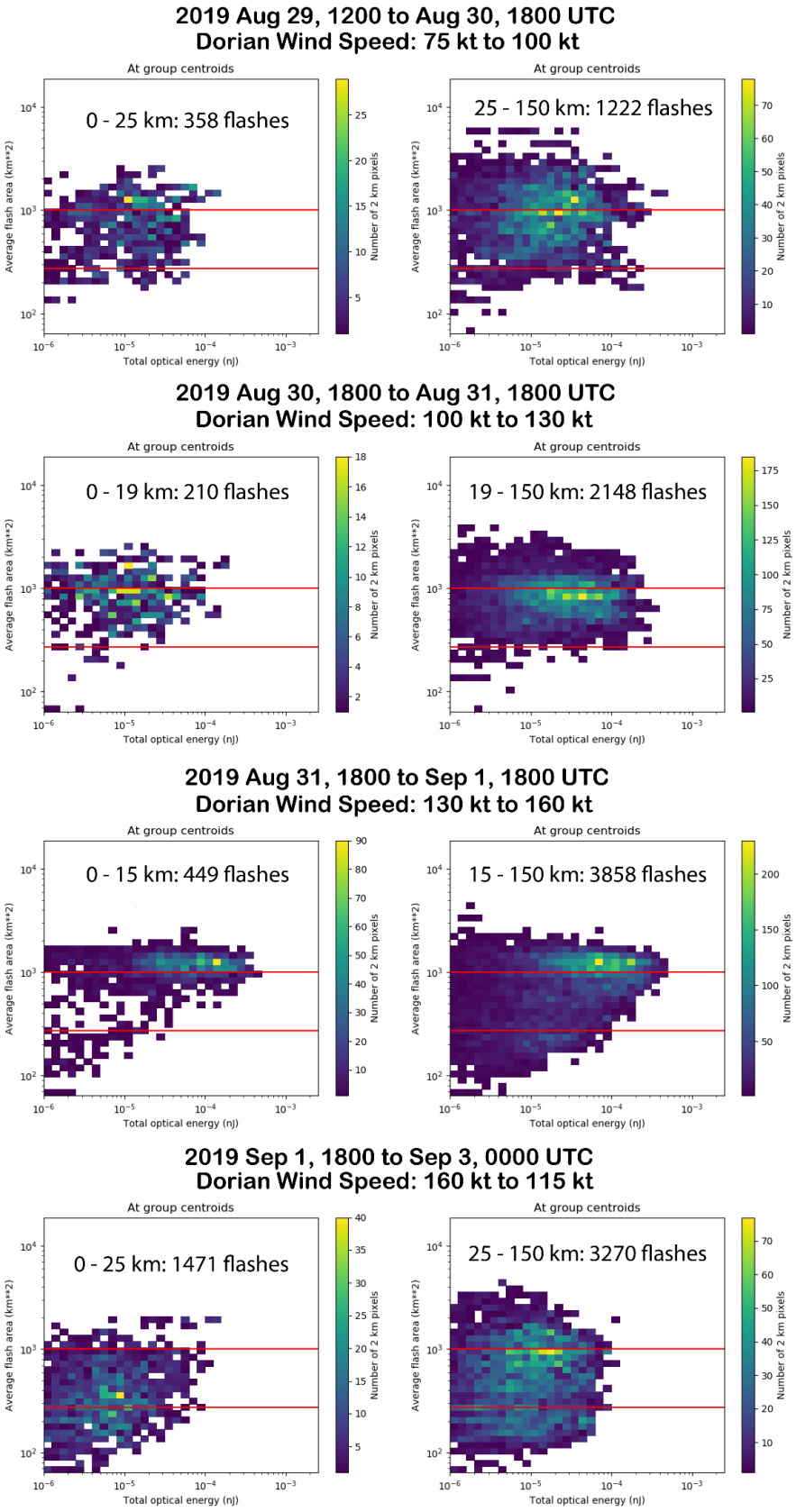

Figure A. 36 Dorian (NHC) Joint Histogram, AFA vs. TOE

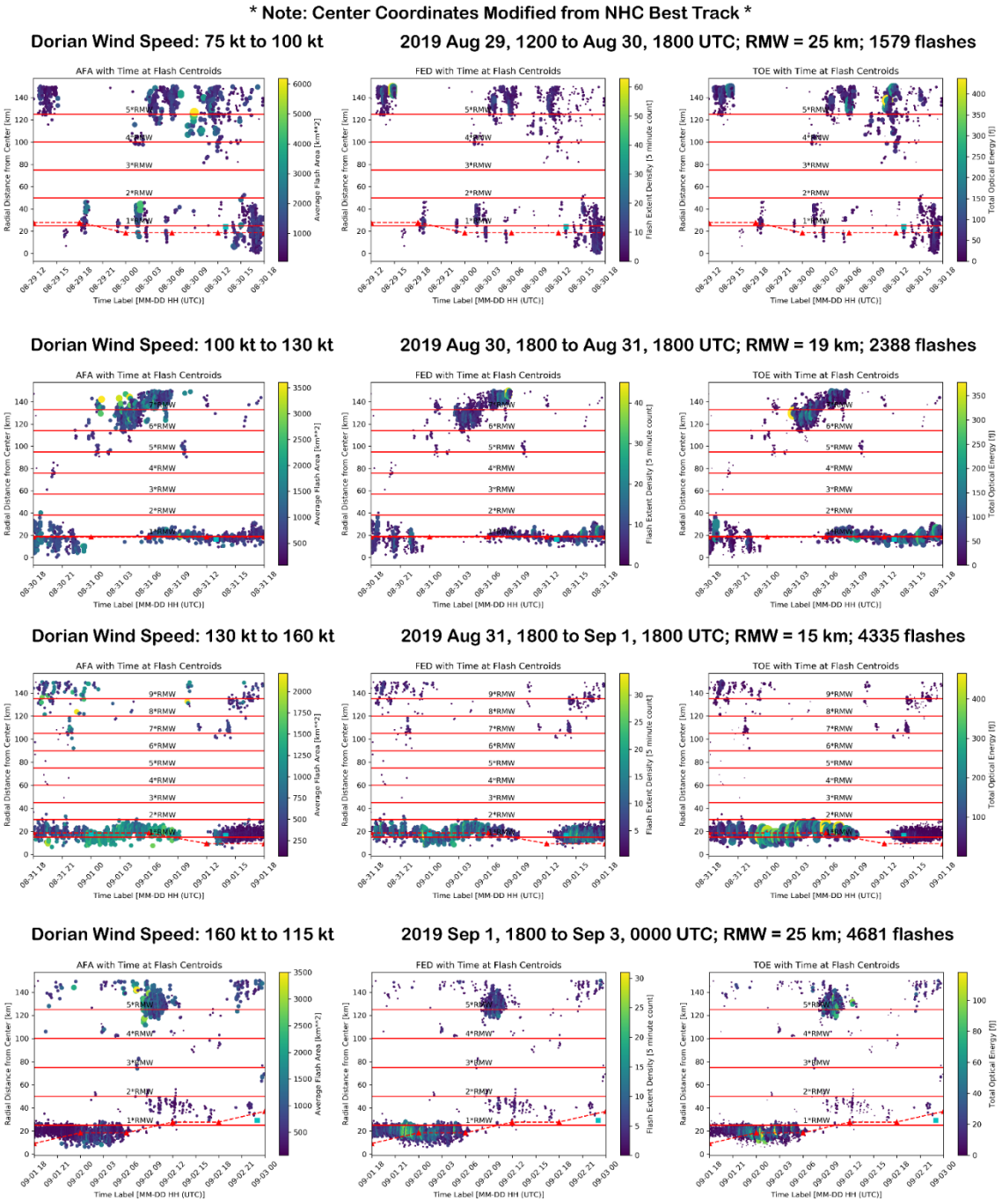

Figure A. 37 Dorian (Non-NHC) Flashes, Distance from Center vs. Time

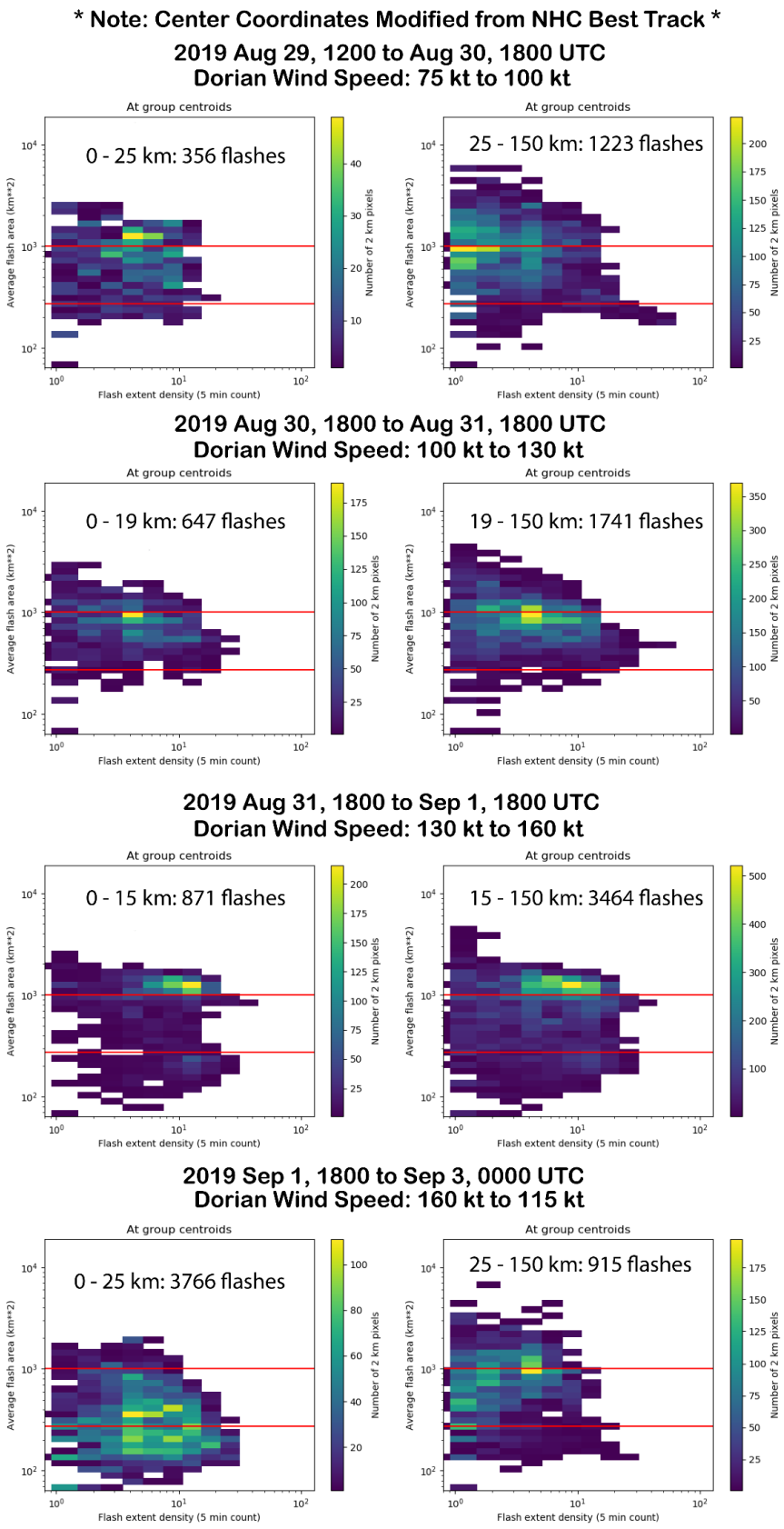

Figure A. 38 Dorian (Non-NHC) Joint Histogram, AFA vs. FED

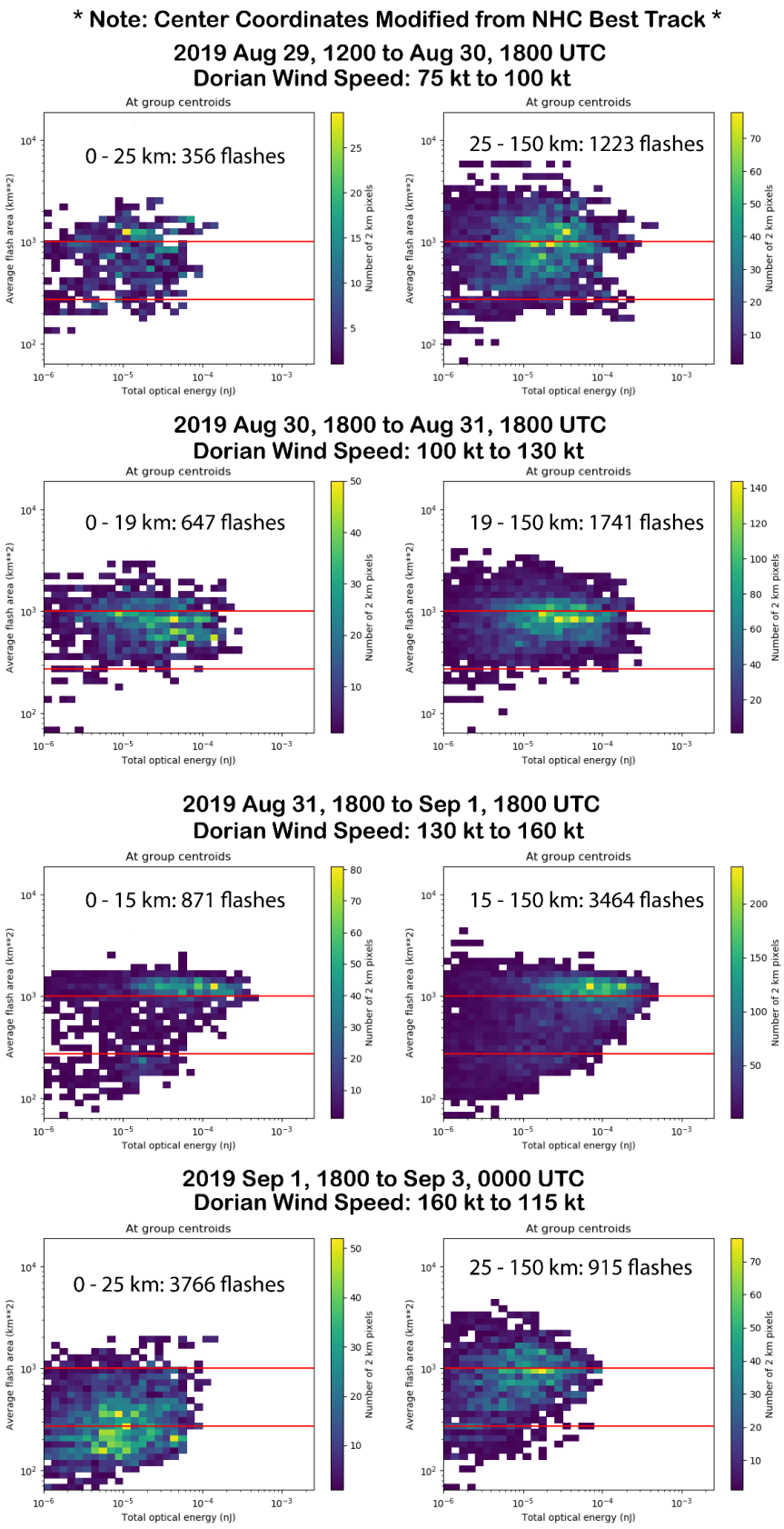

Figure A. 39 Dorian (Non-NHC) Joint Histogram, AFA vs. TOE

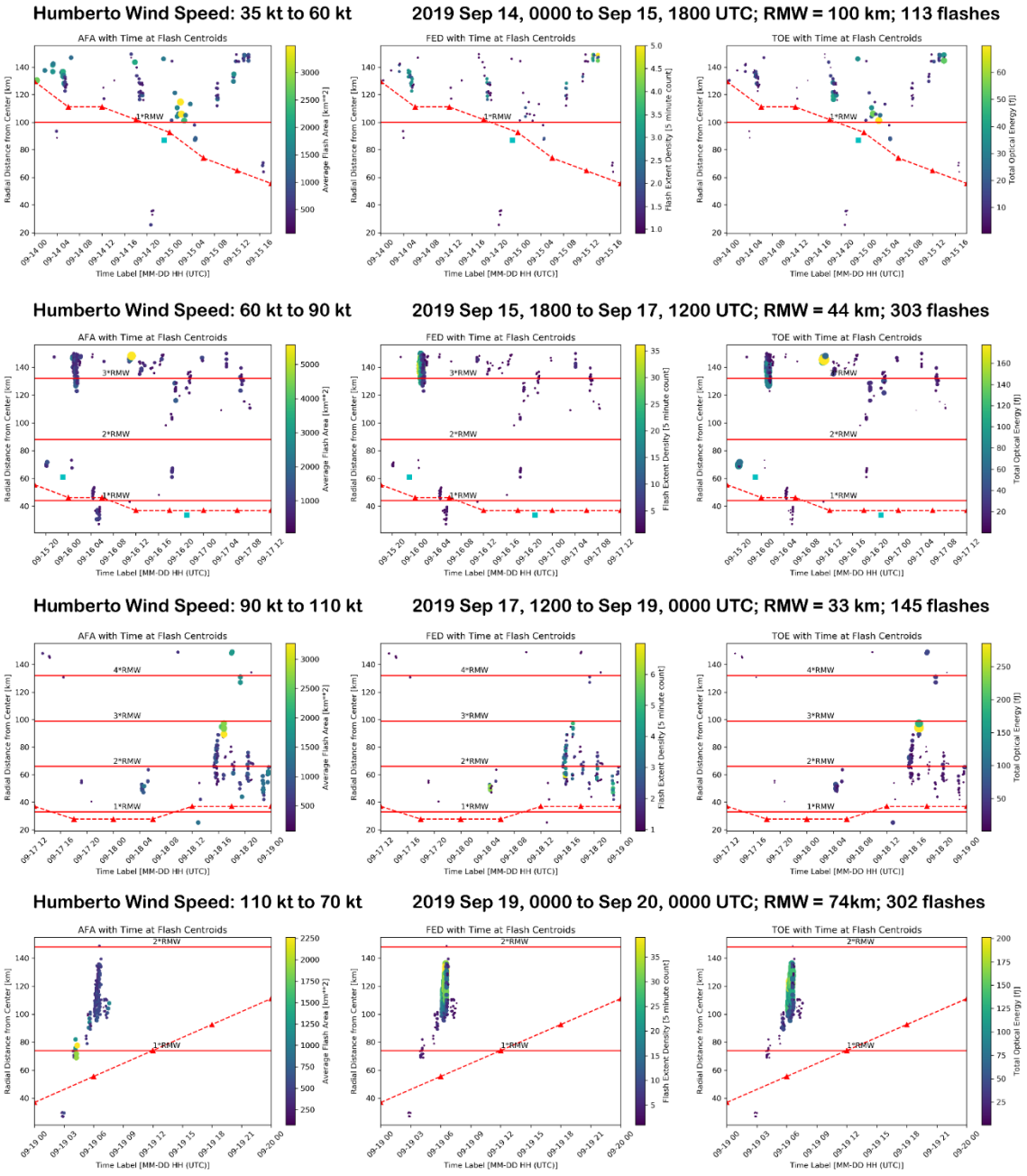

Figure A. 40 Humberto Flashes, Distance from Center vs. Time

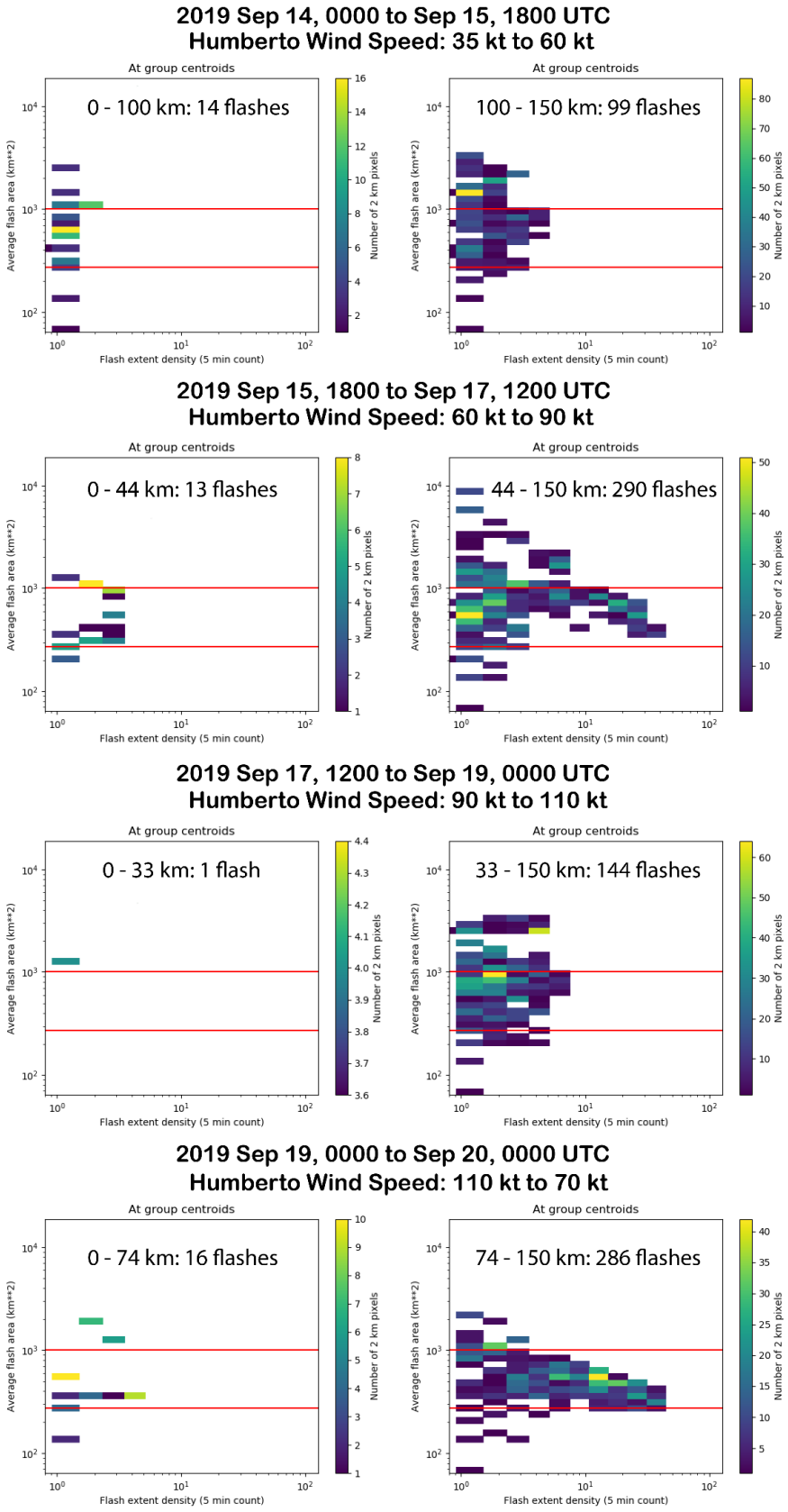

Figure A. 41 Humberto Joint Histogram, AFA vs. FED

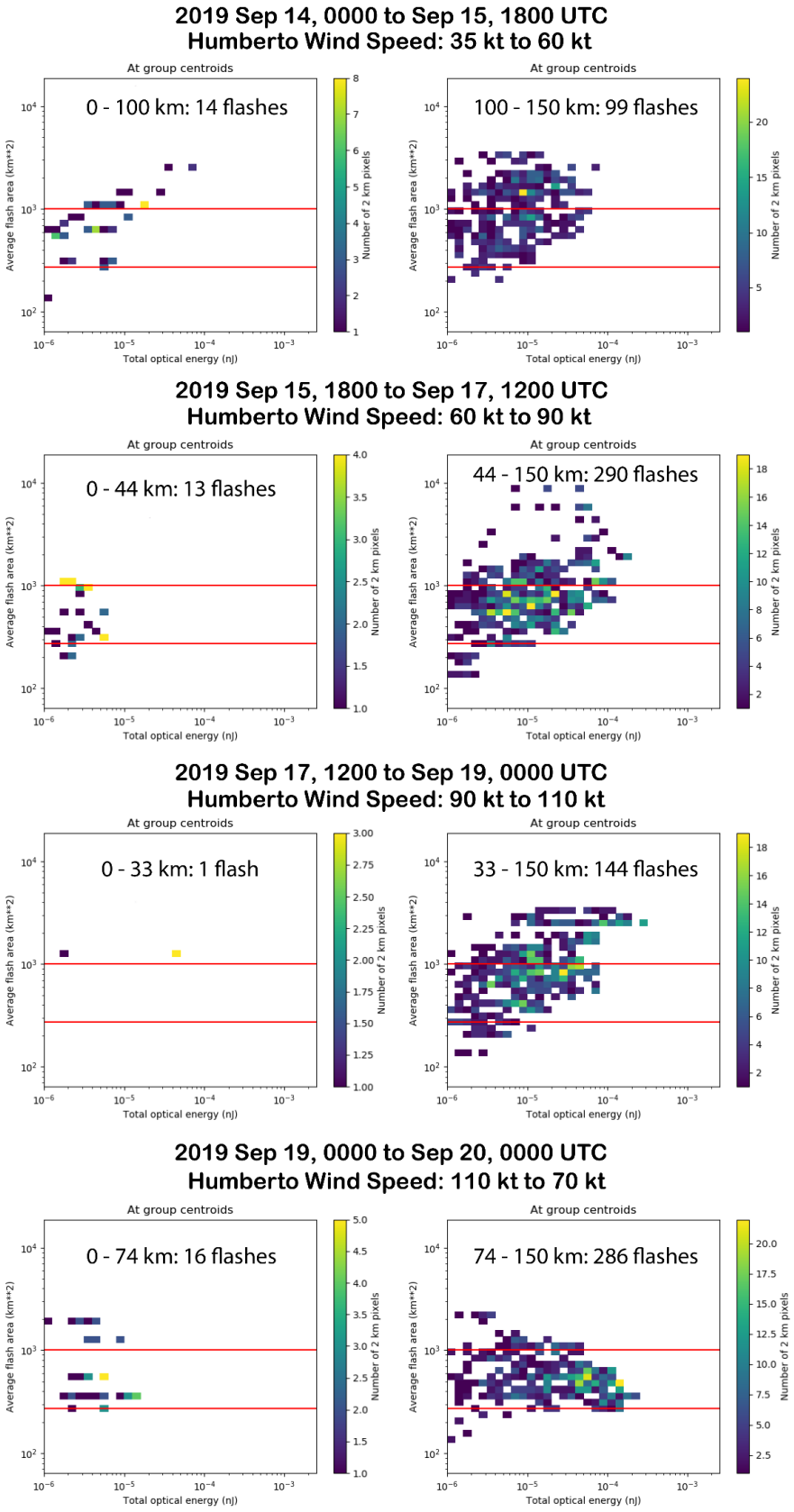

Figure A. 42 Humberto Joint Histogram, AFA vs. TOE

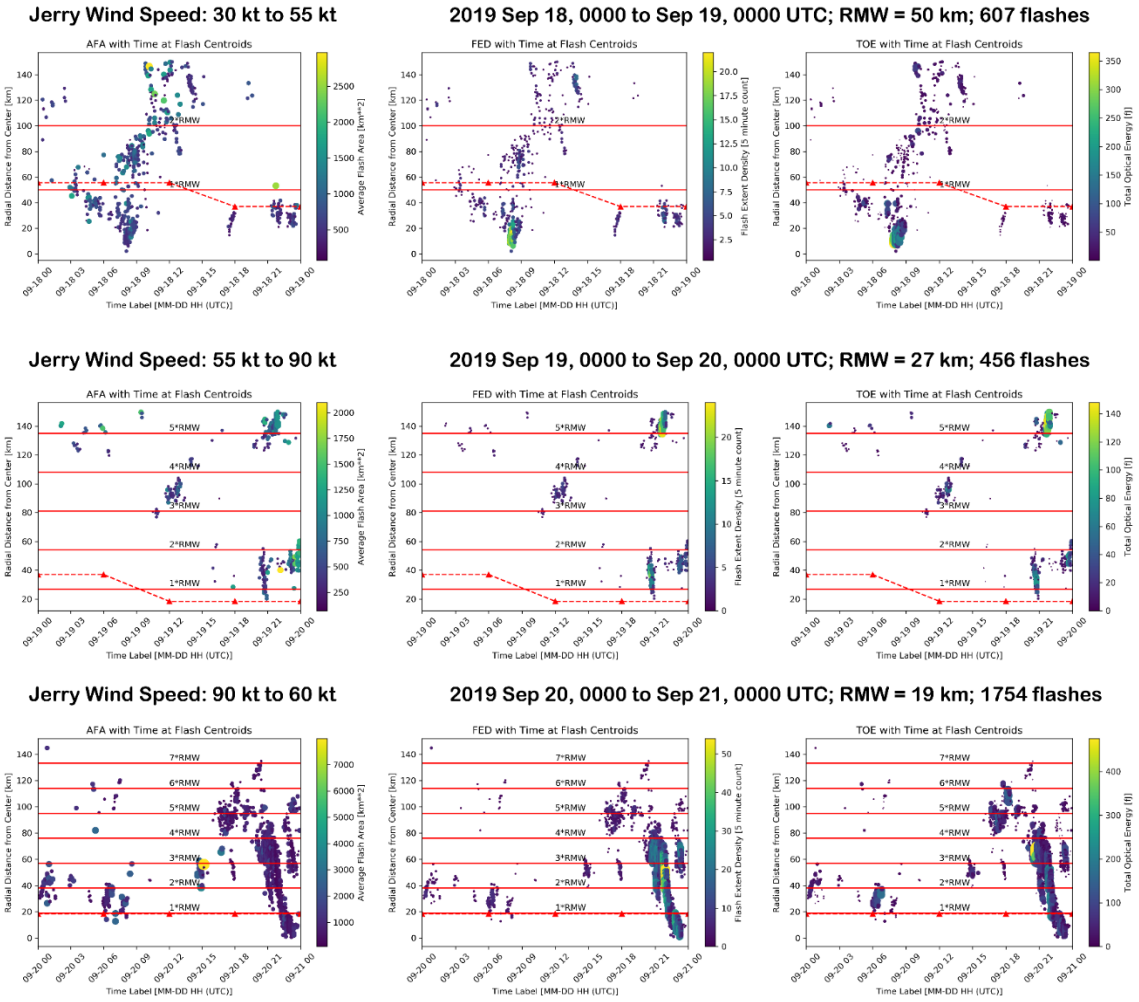

Figure A. 43 Jerry Flashes, Distance from Center vs. Time

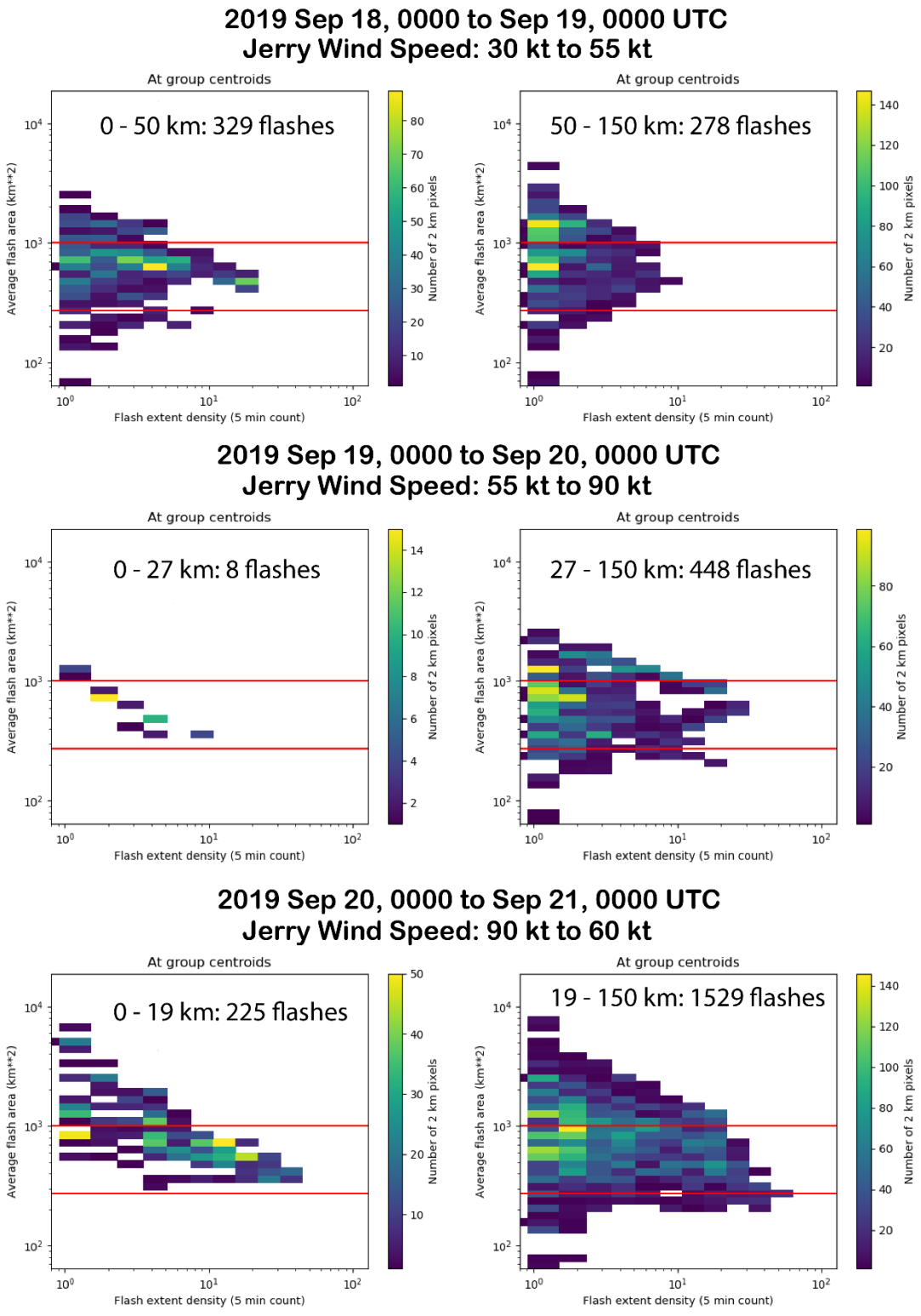

Figure A. 44 Jerry Joint Histogram, AFA vs. FED

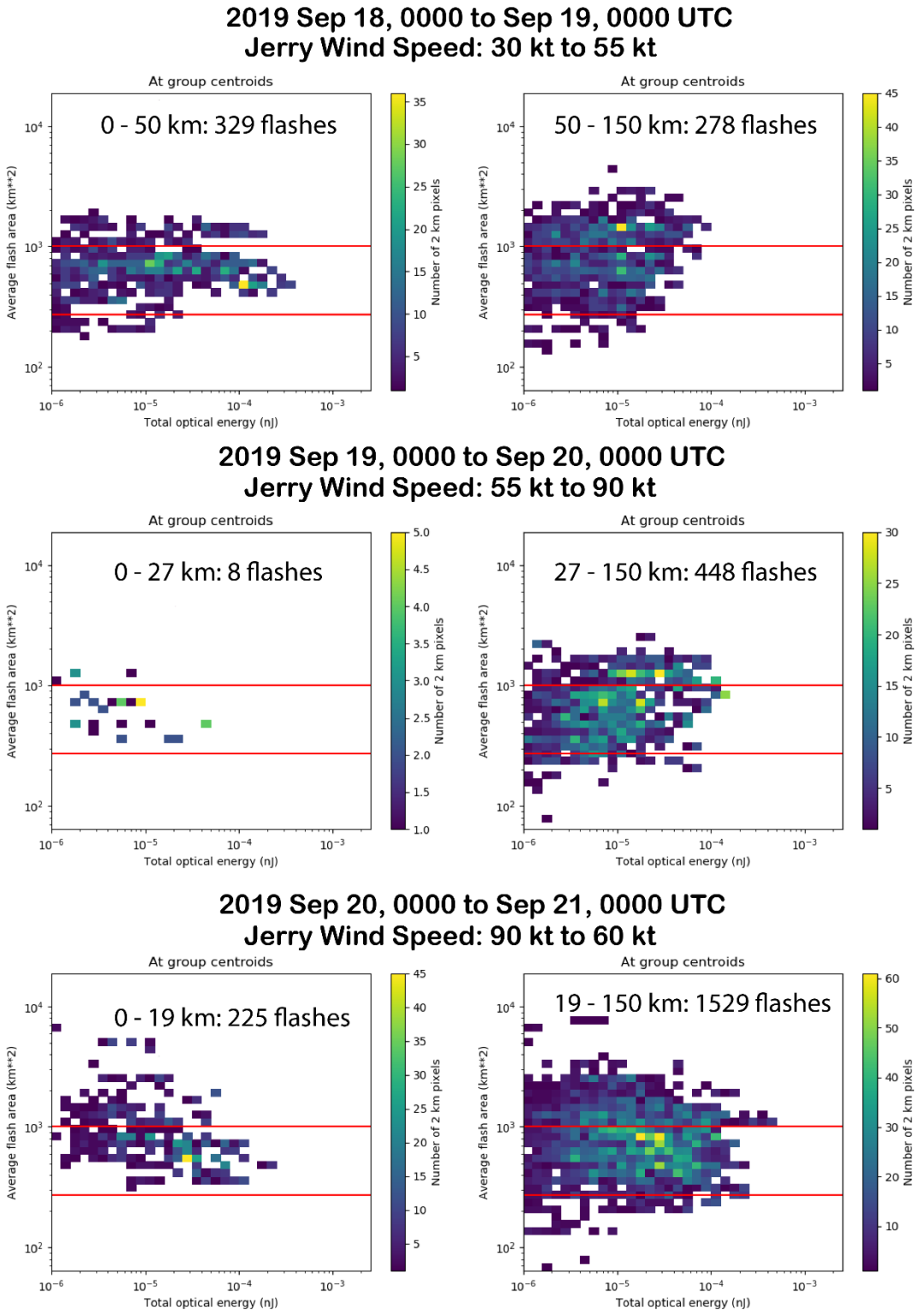

Figure A. 45 Jerry Joint Histogram, AFA vs. TOE